

Modelling and Simulating Twitching Bacteria and Phytoglycogen Nanoparticles

by

Michael Greenberg

A thesis submitted in partial fulfillment of the
requirements for the degree of

Master of Science

in

Applied Bioscience

University of Ontario Institute of Technology

Supervisor: Dr. Hendrick de Haan

August 2018

Copyright © Michael Greenberg, 2018

Abstract

This thesis covers work conducted on two projects. Each of these projects involve application in the field of biology, and both have been completed through the use of computer simulation techniques.

The first project is modelling and simulating the collective motion of twitching bacteria. This problem consists of hundreds of moving twitchers that can be modelled, tracked, and analysed easily through the use of computer simulation and visualization. Each twitcher was modelled as four spheres held into a rod-like configuration, and make use of two dummy spheres to guide twitching motility. Here, three different models of twitching motility were produced, and simulations confirmed the emergence of collective motion in each model.

The second project involves the use of atomistic simulations with the purpose of investigating the structure of phytoglycogen nanoparticles. Here, simulations allow us to analyse a reduced structure in atomistic detail. Simulations were conducted of a group of amylopectin branches solvated in water in order to study their interactions with each other, with water, and with beta-carotene. The interactions observed were a combination of hydrophobic and hydrophilic interactions, suggesting that phytoglycogen might be amphiphilic in nature.

Declaration

I, Michael Greenberg, declare that this thesis titled, Modelling and Simulating Twitching Bacteria and Phytoglycogen Nanoparticles and the work presented in it are my own. I confirm that:

- This work was done wholly or mainly while in candidature for a research degree at this University.
- Where any part of this thesis has previously been submitted for a degree or any other qualification at this University or any other institution, this has been clearly stated.
- Where I have consulted the published work of others, this is always clearly attributed.
- Where I have quoted from the work of others, the source is always given. With the exception of such quotations, this thesis is entirely my own work.
- I have acknowledged all main sources of help.
- Where the thesis is based on work done by myself jointly with others, I have made clear exactly what was done by others and what I have contributed myself.

Acknowledgements

I would like to thank Prof. Hendrick de Haan, my supervisor, for guiding me through my master's career, and for allowing me to work in his lab. I would also like to thank him for teaching me biophysics and for showing me ways that computers and computer simulations could be used to study biology. I would like to thank Prof. Janice Strap for her guidance and mentorship throughout my master's career, and for sitting as the external reviewer on my defense committee, Prof. Dario Bonetta for sitting as chair on my defense committee, and Prof. Sean Forrester for sitting on my advisory committee.

I would also like to thank all the current and past members of the cNAB.LAB and the CLEAN group for their friendship and support. In particular, I would like to thank Martin Magill for his friendship and mentorship, Mohammad-Hassan Khatami for his guidance on the subject of atomistic simulations, Konstantinos Kastratis for showing me how write more efficient code, and Andrew Nagel for collaborating with me on the Twitcher Project, and for allowing me to use one of his figures (permission form in page below). I would also like to thank John Dutcher and his lab group for their collaboration on the Twitcher Project.

Further thanks go to my friends and family for the support given to me throughout my education.

Andrew Nagel,

I am preparing my master thesis for submission to the Office of Graduate Studies at the University of Ontario Institute of Technology (UOIT) in Oshawa, Ontario, Canada. I am seeking your permission to include a figure that you have made in the thesis. This figure is figure 4.5 in my thesis.

Canadian graduate theses are reproduced by the Library and Archives of Canada (formerly National Library of Canada) through a non-exclusive, world-wide license to reproduce, loan, distribute, or sell theses. I am also seeking your permission for the material described above to be reproduced and distributed by the LAC(NLC). Further details about the LAC(NLC) thesis program are available on the LAC(NLC) website (www.nlc-bnc.ca).

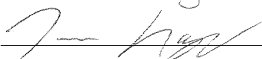
A copy of this permission letter will be included in the thesis.

Yours sincerely,
Michael Greenberg

Permission is granted for:

- a) the inclusion of the material described above in your thesis.
- b) for the material described above to be included in the copy of your thesis that is sent to the Library and Archives of Canada (formerly National Library of Canada) for reproduction and distribution.

Name: Andrew Nagel Title: Mr.

Signature:  Date: August 17, 2018

Contents

1	Introduction	17
1.1	Modelling and Simulating the Collective Motion of Twitching Bacteria	17
1.2	Atomistic Simulations of Phytoglycogen Nanoparticles	18
2	Literature Review	20
2.1	Twitching Bacteria	20
2.1.1	Type IV Pili	20
2.1.2	<i>Pseudomonas aeruginosa</i>	20
2.1.3	Bacterial Biofilms	21
2.1.4	Previous Simulation Work	22
2.1.4.1	Vicsek Model	22
2.1.4.2	Nematic Alignment	23
2.1.4.3	Twitcher Simulations	23
2.1.5	What Makes Our Model Different?	24
2.1.5.1	Quorum Sensing - Cell-to-Cell Communication	25
2.1.5.2	Reversals in Direction of Motion	26
2.1.5.3	Extracellular Polysaccharide Trail	27
2.1.5.4	Chemotaxis	27

2.2	Phytoglycogen Nanoparticles	28
2.2.1	PhytoSpherix™	28
2.2.1.1	Properties	28
2.2.1.2	Biological Function of Phytoglycogen	29
2.2.1.3	Applications of PhytoSpherix™	30
2.2.1.4	Questions Regarding PhytoSpherix™	30
2.2.2	Previous Simulation Work on Carbohydrates	31
3	Objectives	33
3.1	Modelling and Simulating the Collective Motion of Twitching Bacteria	33
3.1.1	Constructed a minimalistic model of rod-like twitchers and determined that collective motion emerged	33
3.1.2	Determined the effect of twitcher attachment on collective behaviour	34
3.1.3	Constructed and compared a model that more closely re- sembles rod-like swimmers.	34
3.2	Atomistic Simulations of Phytoglycogen Nanoparticles	35
3.2.1	Qualitatively analysed the interactions between indepen- dent glycan chains	35
3.2.2	Qualitatively and quantitatively analysed the interactions between glycan chains and water	36
3.2.3	Qualitatively analysed the interactions between glycan chains and beta-carotene	36
4	Methods	38
4.1	Twitching Bacteria and Phytoglycogen Nanoparticles	38
4.2	Molecular Dynamics (MD) Simulations	39

4.2.1	Velocity Verlet	40
4.3	Twitching Bacteria Simulations	41
4.3.1	Simulations - HOOMD	41
4.3.2	Molecular Dynamics for Twitching Bacteria	41
4.3.3	Langevin Dynamics	46
4.3.4	Twitching Motility Cycle	46
4.3.5	2D Environment - Taking Advantage of 3D	47
4.3.6	Comparing Between 3 Models of Twitching Bacteria	48
4.3.6.1	Surface Attachment Model (SAM) Twitchers	48
4.3.6.2	Twitcher Attachment Model (TAM) Twitchers	50
4.3.6.3	Jetpack Model (JPM) Twitchers	51
4.3.7	Analysis of Collective Motion	53
4.3.7.1	Mean Squared Displacement (MSD) and Diffusion	53
4.3.7.2	Velocity Autocorrelation (VAC)	55
4.4	Phytoglycogen Nanoparticles	56
4.4.1	AMBER MD	56
4.4.2	The Repeatable Branching Unit	57
4.4.3	Water	58
4.4.4	Simulation and Analysis of RBUs	58
4.4.5	Adding Beta-Carotene to RBU Simulations	65
5	Results - Twitching Bacteria	66
5.1	Collective Motion of SAM Twitchers	66
5.1.1	Mean Squared Displacement	68
5.1.1.1	Interpreting MSD	68
5.1.1.2	Analysing MSD	69
5.1.2	Diffusion	74
5.1.3	Velocity Autocorrelation	76

5.1.3.1	Interpreting VAC	76
5.1.3.2	Analysing VAC	79
5.1.4	Characteristic Decay Time	81
5.2	Comparing Models	82
5.2.1	Mean Squared Displacement Between Models	85
5.2.2	Diffusion Between Models	89
5.2.3	Velocity Autocorrelation of TAM and JPM Twitchers	94
5.2.4	Characteristic Decay Time	97
5.3	Summary	99
6	Results - Phytoglycogen Nanoparticles	101
6.1	Interactions between Amylopectin Chains	101
6.2	Hydration of 9 RBU System	104
6.3	Beta-Carotene - Interactions Within a 9 RBU System	109
7	Discussion	111
7.1	Twitching Bacteria	111
7.2	Phytoglycogen Nanoparticles	112
8	Conclusion	114
8.1	Summary - Twitching Bacteria	114
8.2	Summary - Phytoglycogen Nanoparticles	115
8.3	Future Work	116

List of Tables

4.1	List of Twitcher Variables. While all of these can be modified, the following variables have been set to the following for the content of this document	53
4.2	Number of Atoms in a 9 RBU and 50 RBU system	58

List of Figures

4.1	Schematic of an individual twitcher.	42
4.2	Potentials used to form a twitcher cell. Top left: Weeks-Chandler Anderson Potential (blue) and Lennard-Jones Potential (red). WCA is used to prevent body particles from passing through each other. WCA is a truncated and shifted version of the LJ potential. Top right: FENE potential (green) is used to hold body particles together. Each twitcher makes use of 3 of these potentials in order to form a polymer of 4 body particles. FENE potential is a stronger and more rigid interaction compared with the SHO potential (yellow) with the same spring constant and reference length. Bottom left: Combining the WCA and FENE potentials (purple) forms a potential well that keeps particles at a specific distance from each other. This combination is used to prevent bond crossing. Bottom right: SHO potential (yellow) with respect to angular configuration. SHO potential is used to keep twitchers rigid at $180 \text{ degrees}/\pi$ radians. Each twitcher makes use of two SHO interactions, one between the first 3 body particles, and one between the last 3 body particles.	44

4.3	A red, green, and blue particle are held in a rod-like configuration by the angular SHO potential. The blue particle should be in the position outlined in dotted purple. As θ increases, the restoring force increases, pushing the blue particle into the correct position.	45
4.4	Motility Phase of SAM, TAM, and JPM Twitchers over two STUs. Time increases from bottom to top. Red outlines show where the twitcher was during the previous STU	49
4.5	Twitching motility cycle of a single Surface Attachment Model (SAM) Twitcher - made by Andrew Nagel	50
4.6	Twitching motility cycle of a single Twitcher Attachment Model (TAM) Twitcher	52
4.7	Twitching motility cycle of a single Jetpack Model (JPM) Twitcher	54
4.8	Initial configuration of 1 RBU - amylopectin	59
4.9	Initial configuration of 9 RBUs	61
4.10	Initial configuration of 50 RBUs	62
4.11	Surface structure of the initial configuration of 9 RBUs	63
4.12	Surface structure of the initial configuration of 50 RBUs	64
5.1	500 and 2000 surface attachment twitchers in an area of 100 by 100 squared spatial units	67
5.2	Mean Squared Displacement of 500 SAM Twitchers	69

5.3	A particle moving across a surface. left: the particle progresses a short distance in a direction that is consistent with the direction it moved in the prior step. Small arrows show the progress that the particle makes over time. right: by following the red particles, it is possible to measure the displacement of a particle over a longer time window. Displacement over a long time window is considerably greater than displacement over a shorter time window. It is also less consistent in magnitude and directionality. While the particle is not moving diffusively, there is an appearance of random behaviour as the time scale increases . . .	70
5.4	Mean Squared Displacement of 500, 1000, 1500, and 2000 SAM Twitchers. Density of twitchers increases following graph lines from top to bottom.	71
5.5	Relative Mean Squared Displacement of 500, 1000, 1500, and 2000 SAM Twitchers	72
5.6	Relative Mean Squared Displacement of 500, 1000, 1500, and 2000 SAM Twitchers between Timescales of 10^1 and 10^2 . Density increases following graph lines from top to bottom.	73
5.7	Relative Mean Squared Displacement of SAM Twitchers at time scale from 10^3 to 10^5	75
5.8	Relative Diffusion Coefficients of SAM Twitchers	77
5.9	Example of Velocity Autocorrelation Plot - 500 SAM twitchers .	78
5.10	Relative velocity autocorrelation of SAM twitchers	80
5.11	Characteristic decay times of SAM twitchers	82
5.12	500 and 2000 twitcher attachment twitchers in an area of 100 by 100 squared spatial units	83

5.13	500 and 2000 jetpack twitchers in an area of 100 by 100 squared spatial units	84
5.14	Relative mean squared displacement of TAM twitchers. Density increases from top to bottom.	86
5.15	Relative mean squared displacement of TAM twitchers between timescales of $5 \cdot 10^0$ and $5 \cdot 10^2$. Density increases from top to bottom.	87
5.16	Relative mean squared displacement of TAM twitchers at time scale from 10^3 to 10^5 . Density increases from top to bottom. . .	88
5.17	Relative mean squared displacement of JPM twitchers. Density increases from bottom to top.	90
5.18	Relative mean squared displacement of JPM twitchers between timescales of $5 \cdot 10^0$ and $5 \cdot 10^2$. Density increases from bottom to top.	91
5.19	Relative mean squared displacement of JPM twitchers at time scale from 10^3 to 10^5 . Density increases from bottom to top. . .	92
5.20	Relative diffusion coefficients of SAM twitchers, TAM twitchers, and JPM twitchers	93
5.21	Relative Velocity Autocorrelation of TAM Twitchers	95
5.22	Relative velocity autocorrelation of JPM twitchers. Density increases from bottom to top.	96
5.23	Characteristic decay times of SAM twitchers (green), TAM twitchers (blue), and JPM twitchers (orange)	98
6.1	Surface plot of 9 RBUs after 20 nanoseconds	102
6.2	Surface plot of 50 RBUs after 20 nanoseconds	102
6.3	Potential Energy of the 50 RBU system over time	103
6.4	Snapshot of 50 RBU system after 20 nanoseconds	105

6.5	Snapshot of two chains interacting with each other - isolated from a 9 RBU system	106
6.6	Snapshot of fragments of two chains forming a water pocket - 9 RBU system	106
6.7	Final configuration of a 9 RBU system with visible water	107
6.8	Water molecules per glucose molecule for a 9 RBU system	108
6.9	Final configuration of 9 RBUs in the presence of beta-carotene (orange)	110

List of Abbreviations

CF	- Cystic Fibrosis
<i>chp</i>	- Chemosensory system gene cluster
CPU	- Central Processing Unit
FENE	- Finitely Extensible Non-linear Elastic
<i>frz</i>	- Frizzy gene cluster
GPU	- Graphical Processing Unit
JPM	- Jetpack Model
LJ	- Lennard-Jones
MD	- Molecular Dynamics
MSD	- Mean Squared Displacement
PDB	- Protein Databank
PSL	- Polysaccharide Synthesis Locus
RBU	- Repeatable Branching Unit
<i>rhlI</i>	- Acyl Homoserine Lactone Synthase
SAM	- Surface Attachment Model
SHO	- Simple Harmonic Oscillator
STU	- Simulation Time Unit
T4P	- Type 4 Pilus / Type 4 Pili
TAM	- Twitcher Attachment Model
TIP3P	- Transferable Intermolecular Potential 3P
VAC	- Velocity Autocorrelation
VDW	- Van der Waal's
WCA	- Weeks-Chandler-Anderson

Chapter 1

Introduction

1.1 Modelling and Simulating the Collective Motion of Twitching Bacteria

Twitching bacteria undergo twitching motility through the use of structures called type iv pili (T4P). These pili are hair-like structures that the bacteria use like grappling hooks to pull themselves across a surface [1].

Twitching motility is a social behaviour. In small groups, twitching bacteria do not tend to undergo twitching motility. However, in large numbers, twitching bacteria move collectively in order to explore their environment and form a biofilm [15].

Bacterial biofilms are structures consisting of a combination of bacteria, polysaccharides, proteins, and nucleic acids [12]. The exact composition of the biofilm depends upon the bacteria. These structures provide protection from the external environment, and allow the bacteria to filter resources from the environment and expel waste [12].

Bacteria that are capable of twitching motility depend on the use of T4P in

order to form a biofilm. For example, *Pseudomonas aeruginosa* requires T4P in order to form a microcolony, which later matures into a biofilm [15]. These T4P and twitching motility facilitates aggregation of cells [15]. This suggests that the role that T4P plays in microcolony formation comes from collective motion facilitated by twitching motility.

Computer simulations were conducted with a simple model of minimalistic, rod-like twitchers in order to study the collective behaviour of twitching bacteria. The use of computer simulations allows for the testing of complex problems that involve multiple moving components. It also allows for easy extraction of data.

1.2 Atomistic Simulations of Phytoglycogen Nanoparticles

Mirexus is a biotechnology company that focuses on the application of the PhytoSpherixTM compound. PhytoSpherixTM is a phytoglycogen compound that comes from sweet corn. Since it is chemically identical to animal derived glycogen - which consists of glucose - it can be safely used for a variety of nanotechnological applications. Currently it is used in cosmetics [38], but based on its ability to interact with other compounds, it may be possible to use this compound to deliver medicine. This possibility is being studied by GlysantisTM, which is a spinoff company of Mirexus.

While many things are understood about PhytoSpherixTM, there remain many questions about the structure of this compound. There are details about the size and structure of the compound that remain unknown.

As such, our lab has conducted various simulations at many different scales in order to better understand the PhytoSpherixTM compound. This thesis outlines simulations at the atomistic scale in order to better understand the interactions

that occur between phytoglycogen branches. Rather than simulating an entire PhytoSpherixTM compound in atomistic detail, simulations of a reduced system have been conducted in order to understand the way that phytoglycogen branches interact with each other. Simulations consist of multiple amylopectin branches, with the idea that interactions involving these branches would be similar to interactions that occur at the surface of the phytoglycogen nanoparticle.

Chapter 2

Literature Review

2.1 Twitching Bacteria

2.1.1 Type IV Pili

Some bacteria are capable of undergoing twitching motility through the use of structures called type iv pili (T4P). These hair-like structures consist of a compound called pilin. T4P extend and retract based on the addition and removal of these pilin subunits [1]. Twitching bacteria use these structures like grappling hooks to move across a surface - extending their pili outward, attaching to a surface, and pulling themselves across the surface with forces exceeding 100pN [2].

2.1.2 *Pseudomonas aeruginosa*

Pseudomonas aeruginosa is a species of bacteria that is capable of twitching motility. It is gram-negative, rod-shaped, and aerobic, and is able to grow in a variety of environments including along the edge of rivers and fresh water coasts [3].

Pseudomonas aeruginosa is of particular interest for study because they serve as a model organism for the study of biofilms. They are also of interest in the medical community because of their ability to grow in hospital environments. Keith Poole [4] reviews a list of compounds for which *Pseudomonas aeruginosa* is resistant. These compounds include beta-lactams [5] such as penicillin, fluoroquinolones [6], aminoglycosides [7], and polycationic antimicrobials such as polymyxin B [8] and colistin [9].

Pseudomonas aeruginosa is an opportunistic pathogen, and is known to be associated with cystic fibrosis [10]. Cystic Fibrosis (CF) is a state of chronic lung infection [11]. Lungs infected with CF are particularly vulnerable to infection by *Pseudomonas aeruginosa*, which infects 81.3% of CF patients between the ages of 26-30 [10]. While CF is caused by a genetic mutation, its mortality is connected to infection by *Pseudomonas aeruginosa* [11]. Mortality from CF is the result of the *Pseudomonas aeruginosa* biofilm, which partially consists of alginate [14]. Alginate is a particularly mucoid exopolysaccharide, and its presence in CF infected lungs is associated with poor lung function and increased risk of death [14].

2.1.3 Bacterial Biofilms

Biofilms are surface-imbedded structures consisting of bacteria and compounds such as carbohydrates, proteins, or nucleic acid [12]. Bacteria colonize a surface and form a biofilm in order to protect themselves from the external environment. Biofilms are also useful because they allow for bacteria to filter resources from the environment [12]. The exact composition of a biofilm depends on the bacteria that generates it.

Twitching motility is an important aspect of biofilm formation for twitching bacteria. *Pseudomonas aeruginosa* requires T4P in order to form micro-

colonies, which later mature into biofilms [15]. It is believed that *Pseudomonas aeruginosa* use T4P in order to aggregate and form a thin monolayer into a microcolony [15]. Once microcolonies are formed, T4P mediated motion causes these microcolonies to merge into larger single colonies [16].

Twitching bacteria undergo twitching motility when in large groups. In this situation, twitching bacteria form complex collective networks. In understanding this behaviour, it is possible to learn how they are able to undergo collective motility.

2.1.4 Previous Simulation Work

Simulations that model collective behaviour focus on the study of rod-like swimmers [17] [18] [19]. Most of these simulations make use of nematic effects (discussed in section 2.1.4.2) in order to simulate collective behaviour. Vicsek's Model is another technique that can be used to simulate collective behaviour, and will be discussed below.

2.1.4.1 Vicsek Model

In Vicsek's model, the direction of a particle's movement is based on the average direction of neighbouring particles in the system [20]. The direction of a particle is defined by the following formula [20]:

$$\theta(t + 1) = \langle \theta(t) \rangle_r + \Delta\theta \quad (2.1)$$

where $\theta(t + 1)$ is the direction that the particle will move at timestep $t+1$ measured as an angle, $\langle \theta(t) \rangle_r$ is the average direction of all of the particles within radius r of the particle of interest at timestep t , and $\Delta\theta$ is a noise factor that modifies the direction of a particles - a random value ranging from $[-\eta/2, \eta/2]$, and η is a variable. $\Delta\theta$ is randomly generated for each particle at

each moment in time.

Vicsek particles base their direction of motion on their neighbours. At each moment in time, a Vicsek particle determines the direction of motion of its neighbours. The particle then moves in the average direction of its neighbours. As a result, collective motion is a built-in feature of the system. However, when η is above zero, a random value between $-\eta/2$ and $\eta/2$ is added as a modifier to the direction of the Vicsek particle. This noise factor disrupts the collective behaviour that is coded into Vicsek particles, and as η increases, these disruptions become more pronounced.

2.1.4.2 Nematic Alignment

Nematic alignment refers to the way that rod-like particles interact with and align with each other. Alignment occurs because each particle has excluded volume [18], meaning that the space that a particle takes up cannot be occupied by another particle.

Work conducted by Peruani et al. (2006) [21] demonstrates that self-propelled rods can aggregate into clusters. Aggregation occurs from the combination of rod-like geometry and short-range repulsion due to excluded volume. The rods simulated by Peruani et al. (2006) [21] are propelled forward along the long axis of the rod. Since twitching motility is characterized by a cycle of motion and rest, these models cannot be used to characterize the collective motion of twitching bacteria - at least not in their current state. Rod-like swimmers are in a constant state of motion, where as twitchers pause cyclically.

2.1.4.3 Twitcher Simulations

There are some simulations that model twitching bacteria. These simulations are highly specific to particular phylotypes and particular behaviours. For example, work conducted by Zachreson et al. (2017) [22] is specific to *Pseudomonas*

aeruginosa. Zachreson et al. (2017) [22] study the influence of the surface on the collective motion of *Pseudomonas aeruginosa*. They note that the thickness of agar is important in the formation of collective behaviour. Thicker agar results in the formation of protruding structures formed by the bacterial collective.

Work conducted by Ponisch et al. (2017) [23] focuses on the merging of *Neisseria gonorrhoea* microcolonies as a result of twitching motility. These simulations are tuned to *Neisseria gonorrhoea*, which are diplococci as opposed to rods like *Pseudomonas aeruginosa*. *Neisseria gonorrhoea* are also capable of generating as many as 15 T4P [23], compared to 12 used by *Pseudomonas aeruginosa* [24]. Ponisch's group studied the formation of clusters by *Neisseria gonorrhoea*, as well as what happens when multiple smaller colonies merge into a single, larger colony. In doing so, they highlight the importance of twitching motility in the formation of microcolonies.

Work conducted by Brill-Karniely et al (2017) [24] focused on the mechanics of surface attachment. Rather than simulating collective motion, this group focused on single twitcher dynamics. Brill-Karniely's group studied the number of surface bound pili and the distribution of surface bound pili. Both of these characteristics have an effect on a twitcher's ability to move across a surface. When multiple pili are attached to the surface, they must be attached in a polarized configuration for the twitchers to progress. If the pili are uniformly distributed across the surface, the pili will pull in competing directions, resulting in little progress.

2.1.5 What Makes Our Model Different?

The model outlined in this thesis focuses on the fundamental physics of twitching motility and collective behaviour. It removes several biological features (discussed next page) that are a part of real bacteria and that are included in

the other models outlined above. The simplicity of this model means that it can be used to answer a more fundamental question - can simple, rod-like twitchers achieve collective motion on their own? If so, why is it that bacteria have all of these other features, and how do these features affect collective behaviour? If not, then what else is necessary for collective motion to occur?

Our model begins from the ground up. While research is inspired by *Pseudomonas aeruginosa*, it is not of *Pseudomonas aeruginosa*. The twitchers modelled and simulated here are generic and can be modified to apply to any sort of twitching bacteria. Once the fundamental physics is understood, new features could be added to the system to increase its applicability to living bacteria. Each new addition could be studied independently to determine their effects on collective behaviour. Later these effects could be studied together, allowing for potential synergies to be discovered.

A list of biological features is included below. While excluded from simulations outlined in this thesis, each feature should be studied in conjunction with this model.

2.1.5.1 Quorum Sensing - Cell-to-Cell Communication

Living bacteria use a process called quorum sensing as a form of cell-to-cell communication [25]. This method of bacterial communication is known to be associated with biofilm formation in various forms of bacteria, including *Vibrio cholerae* [26] and *Pseudomonas aeruginosa* [29].

Bacteria initiate quorum sensing by producing compounds known as autoinducers [25]. Each bacteria produces a unique form of autoinducer, and is equipped with receptors that are sensitive to the presence of its own autoinducer. Each bacteria produces autoinducer compounds, meaning that as more bacteria are present, more autoinducers are present. After a certain threshold, the bacteria undergo changes in gene expression to facilitate the formation of a

biofilm. These modifications to gene expression also lead to reduced motility. Work by Caizanna et al. (2007) [31] shows that there is an inverse regulation between swarming motility (flagellated motion) and biofilm formation. Work by Ueda and Wood (2009) [29] shows that quorum sensing is involved in the inverse regulation of swarming motility and biofilm formation.

Patriquin et al. (2008) [30] suggests a relationship between quorum sensing and twitching motility in *Pseudomonas aeruginosa*. They found a mutant that was deficient in low-iron stimulated twitching motility, and discovered that this was due to a mutation in the *rhlI* gene - a gene responsible for the production of N-butanoyl homoserine lactone (the autoinducer for *Pseudomonas aeruginosa* [30]). Their work suggests that twitching motility depends on the presence of autoinducer compounds [30].

Cell-to-Cell communication is excluded from the model conducted in this thesis. Twitchers covered in this thesis have a cycle of motion that is independent of other twitchers, but this would not be the case if cell-to-cell communication were included.

2.1.5.2 Reversals in Direction of Motion

Living bacteria capable of twitching motility are able to generate T4P on both poles [27]. In *Myxococcus xanthus*, reversal frequency is controlled by the frizzy (*frz*) gene cluster, while in *Pseudomonas aeruginosa*, reversal frequency is controlled by the *Chp* chemosensory system [27].

Reversals in the direction of motion are not just possible in twitching bacteria. Be'er et al. (2013) [28] outlines that *Paenibacillus dendritiformis* reversals occur once every $20 \pm 11 \mu s$. These reversals occur independently of external factors, as if these bacteria were operating on an internal clock [28].

Reversals in the direction of motion are beyond the scope of this thesis. Twitchers in this thesis are modelled with the ability to reverse direction, but

this ability has been disabled for now.

2.1.5.3 Extracellular Polysaccharide Trail

During microcolony formation, *Pseudomonas aeruginosa* leaves behind a trail of polysaccharides generated by the polysaccharide synthesis locus (psl) [32]. This polysaccharide is rich in galactose and mannose, and serves as a component of the *Pseudomonas aeruginosa* biofilm [13]. This saccharide trail facilitates collective behaviour in twitchers, as T4P more easily associates with the psl trail [32]. This makes it easier for new twitchers to follow those that are exploring unexplored surfaces, and facilitates biofilm formation as twitchers follow each other and group up.

This feature could be simulated by implementing a probability of surface attachment; this probability would be higher if the pilus lands on psl-coated surface. The simple implementation for this is as follows: if a pilus lands on unexplored surface, there is a chance that the twitcher will select a different place to attach to up to a maximum number of attempts. If the pilus lands on explored surface, it is more likely to undergo twitching motility. Zachreson et al. (2016) [22] conducted simulations of *Pseudomonas aeruginosa*, and have determined a maximum probability of attachment of 0.3 and a minimum probability of attachment of 0.1 based on the presence or absence of psl. A probability of 0.1 is consistent with the probability a rod-like twitcher outlined in this thesis has to exit the rest phase and begin twitching motility (this will be explained in the Methods chapter). An implementation could involve an increased probability of leaving rest if the twitcher dummy particle lands on an explored surface.

2.1.5.4 Chemotaxis

Chemotaxis describes the way that bacteria move in response to the presence of extracellular chemicals [33]. Living bacteria have chemoreceptors. Bacteria ca-

pable of chemotaxis use these chemoreceptors to send information about their environment directly to their motility structures. The process of chemotaxis guides bacteria towards chemoattractive compounds, and away from chemorepellent compounds [33].

Jeong et al. (2010) [34] used microfluidic devices to study chemotaxis in *Pseudomonas aeruginosa*. Here they demonstrated with their device that *Pseudomonas aeruginosa* is attracted to peptone and repulsed by trichloroethylene. Jeong et al. (2010) also demonstrate that *Pseudomonas aeruginosa* is attracted to the 20 amino acids at varied concentrations. *Pseudomonas aeruginosa* seek alanine, cysteine, aspartic acid, lysine, methionine, asparagine, and histidine at concentrations approaching 10 mM, while arginine, leucine, proline, and threonine were sensed at concentrations approaching 4 mM [34].

2.2 Phytyglycogen Nanoparticles

2.2.1 PhytoSpherixTM

2.2.1.1 Properties

The PhytoSpherixTM nanoparticle is a phytyglycogen compound that is extracted from sweet corn. Phytyglycogen compounds consist of glucose, forming a vast, branching network through a combination of alpha 1-4 and alpha 1-6 bonds [35]. This structure is made up of linear chains of up to 12 glucose bound via alpha 1-4 bonds, after which two branches are formed via an alpha 1-4 linkage and an alpha 1-6 linkage [36].

This compound has received a lot of attention due to its ease of extraction and interesting properties. The method of extraction, as outlined by Nickels et al. (2016) [35] involves a series of filtrations and purifications, resulting in a phytyglycogen yield approximately equal to 0.2 times the mass of the sweet

corn kernels.

The PhytoSpherixTM nanoparticle has various properties that makes it useful for nanotechnological applications. Since it is extracted from sweet corn, it is an entirely natural compound - used for the purpose of storing energy in the plant. Since it consists entirely of glucose, it is not dangerous for human consumption.

Other properties of this compound include its high water retention. A PhytoSpherixTM is able to retain 22.5 molecules of water per molecule of glucose [35]. It is also capable of forming a film on a surface [38].

2.2.1.2 Biological Function of Phytoglycogen

Phytoglycogen is used in plants to store energy. Work conducted by Melendez et al. (1999) [39] suggests that phytoglycogen is particularly efficient at energy storage. Energy storage efficiency is due to the fractal properties of phytoglycogen [39]. While mathematically speaking fractal structures consist of infinite iterations, Melendez et al. (1999) suggest that phytoglycogen can be considered fractal within a limited system [39]. These properties lead to efficient energy storage and energy access. In any one phytoglycogen nanoparticle, 33% of the glucose stored is immediately accessible regardless of the size of the particle [39]. The fractal nature of the phytoglycogen nanoparticle also helps to stabilize the compound, as the distribution of glucose in the compound allows for the formation of an extensive network of interactions between glucose residues within the phytoglycogen compound.

Melendez et al. (1996) outline the ways that glycogen is evolutionarily optimized for energy storage [40], considering features such as chain length, number of branches per branch point, and number of generations of branches. The evolutionary path is of great importance to the evolution of glycogen, as disadvantageous paths would not be selected for. Frequent branches are considered

to be efficient, and can be achieved with branches occurring every 5-10 glucose units per branch. Two chains per branch is also considered to be favoured evolutionary speaking over three chains per branch, as three chains per branch would not be beneficial enough at early branching generations to be worthwhile later [40].

2.2.1.3 Applications of PhytoSpherix™

Currently, the biotechnology company Mirexus - which holds the trademark on PhytoSpherix™ - applies the compound in the field of cosmetics [41]. PhytoSpherix™ has a variety of properties that make it effective as a moisturizer, including high water retention and rheological properties [37]. The rheological properties of PhytoSpherix™ are the result of its interactions with water and its monodispersed structure [37]. This results in a compound with high stability and low viscosity [37]. The combination of these properties makes it possible for PhytoSpherix™ to hydrate the skin, while its rheological properties result in a pleasant texture.

Experiments conducted directly by Mirexus suggests that PhytoSpherix™ interacts tightly with a variety of compounds, but the nature of these interactions is unknown. Mirexus believes that medicinal compounds could be stored inside of a PhytoSpherix™ compound. When the phytoglycogen is broken down into glucose, medicine placed within the phytoglycogen compound is released.

2.2.1.4 Questions Regarding PhytoSpherix™

There remain many questions regarding PhytoSpherix™. Up until recently, the size of PhytoSpherix™ was in dispute, but work conducted by members of the cNAB.LAB helped to resolve this conflict. Results from previous experiments conducted by Nickels et al. (2016) [35] suggested that the compound has a radius of 17.4 ± 1.6 nm, and that the compound is of uniform density.

This measurement was collected through neutron scattering. These results were in conflict with results from [41], stating that these compounds have a radius of approximately 35 nm. These results were collected using dynamic light scattering. This data was collected from and given to us by Mirexus.

There remain other questions about the structure of the PhytoSpherixTM compound, and how it interacts with itself and other compounds - especially since these details are of great importance in the applications of this compound. Experiments conducted by Mirexus suggest that the PhytoSpherixTM compound interacts tightly with non-polar compounds such as beta-carotene. PhytoSpherixTM is also able to interact with polar compounds such as creatine, but the interactions between PhytoSpherixTM and beta-carotene is stronger in comparison. This suggests that PhytoSpherixTM may be amphiphilic.

This thesis outlines research conducted on the structure of phytoglycogen by simulating and analysing a reduced system in atomistic detail. The size of the PhytoSpherixTM compound makes it very difficult and time consuming to simulate the entire structure. However, simulating a reduced system will allow us to gain insight into the structure within a more reasonable timeframe. The reduced system simulated here is more comparable to the surface of a phytoglycogen compound, and it is likely that interactions involving loose chains will be shared with the interactions involving phytoglycogen chains at the surface of the molecule.

2.2.2 Previous Simulation Work on Carbohydrates

Up until now, most simulations involving carbohydrates have been of much smaller scale. For example, simulations conducted by Hansen et al. (2008) [42] are of trisaccharides. The largest carbohydrate structures to be simulated have been made by Sattelle and Almond [43], who have produced simulations

of amylose structures as long as 12 glucose molecules over a period of up to 20 microseconds.

The structures simulated in this thesis consist of amylopectin structures. These simulations involve as many as 50 branching chains of glucose with 30 glucose molecules per branching chain. The following chapter describes the methodology used to study these interacting chains, as well as the methodology used to study the collective motion of twitching bacteria.

Chapter 3

Objectives

3.1 Modelling and Simulating the Collective Motion of Twitching Bacteria

Below is a list of objectives that were completed over the course of this thesis:

1. Constructed a minimalistic model of rod-like twitchers and determined that collective motion emerged
2. Determined the effect of twitcher attachment on collective behaviour
3. Constructed and compared with a model that more closely resembles rod-like swimmers.

3.1.1 Constructed a minimalistic model of rod-like twitchers and determined that collective motion emerged

The first model covered in this thesis is referred to as the Surface Attachment Model (SAM). This model is a simple, physical model of rod-like twitchers, and while it takes inspiration from *Pseudomonas aeruginosa*, it is not of *Pseudomonas aeruginosa*. The construction of a minimalistic, simple model allowed

for the study of fundamental physical behaviour.

As will be covered in chapter 4, the body of a single twitcher is made of 4 spheres held into a rod-like configuration. The twitcher moves by making use of a dummy particle that exerts an attractive force on the twitcher head.

Modelling twitchers this way made it possible to ask and answer a fundamental question about the physics of the twitching-like motility of rod; can collective motion emerge naturally from simple, rod-like twitchers undergoing individualistic rules of motion? The results in this thesis suggest that this is the case, and that this is due to the effects of excluded volume. Collective motion arises as simulated twitchers interact with each other through collisions and nematic alignment, as each twitcher takes up space that another cannot occupy at the same time.

3.1.2 Determined the effect of twitcher attachment on collective behaviour

The twitcher attachment model (TAM) was constructed by modifying the surface attachment model and giving SAM twitchers the ability to attach to other twitchers. As more twitchers are present in the system, less free surface is available for surface attachment. Results from our experimental collaborators suggests that twitching bacteria are capable of attaching to each other with their pili, making the twitcher attachment model a natural evolution of the surface attachment model.

3.1.3 Constructed and compared a model that more closely resembles rod-like swimmers.

Most work analysing the collective motion of rods is not comparable to twitching bacteria. The cycle of motion and rest is an important aspect of twitch-

ing motility that distinguishes it from swimmers. However, it is important to make comparisons with rod-like swimmers, and to make sure that the results obtained here are consistent with the analysis of rod-like swimmers. By comparing rod-like twitchers with rod-like swimmers, it is possible to understand and differentiate effects that arise due to the cycle of motion and rest.

Rod-like swimmers move with respect to the direction they face - as if pushed by the force of a jetpack as opposed to being pulled by the force of a grappling-hook. The jetpack model (JPM) was constructed with this in mind. These twitchers move with respect to the direction they face, but cycle between motion and rest like a twitcher.

3.2 Atomistic Simulations of Phytoglycogen Nanoparticles

Below is a list of objectives that were completed over the course of this thesis:

1. Qualitatively analysed the interactions between independent glycan chains
2. Qualitatively and quantitatively analysed the interactions between glycan chains and water
3. Qualitatively analysed the interactions between glycan chains and beta-carotene

3.2.1 Qualitatively analysed the interactions between independent glycan chains

Simulations were conducted using amylopectin chains referred to as repeatable branching units (RBUs). Reducing a 20,000 glucose molecule into 9 to 50 RBUs has its limitations. The main limitation is that a few chains of glucose is not comparable to the entire structure, and many features of the entire structure

are lost by reducing the system this much. Despite this, a reduce system was useful in obtaining insight on the structure of phytoglycogen, as interactions between the 9 to 50 RBUs are likely to occur in a phytoglycogen nanoparticle.

3.2.2 Qualitatively and quantitatively analysed the interactions between glycan chains and water

Results from Mirexus show that the PhytoSpherix(TM) nanoparticle is highly water soluble, and that it retains approximately 20 water molecules per glucose molecule. Studying the interactions between the RBUs and water served in part as a confirmation of the applicability of the water. Quantifying the water retention of water molecules serves as the first step in understanding the overall structure, as the overall structure forms from a combination of RBU-RBU interactions, and RBU-water interactions.

In this thesis, it was determined that the 9 RBU system retained approximately 20 water molecules per glucose within 0.9 nm. These results are consistent with results obtained by Mirexus through experiment, but further analysis will be necessary to better analyse the interactions between water and RBUs. For example, counting the number of hydrogen bonds could be done by considering the orientation of water with respect to nearby RBUs.

3.2.3 Qualitatively analysed the interactions between glycan chains and beta-carotene

Mirexus is interested in using the PhytoSpherix(TM) molecule to transport medicinal and supplemental compounds. They believe that based on the way that PhytoSpherix(TM) interacts with other compounds, Phytospherix(TM) could be used to transfer these compounds safely into the body.

Beta-carotene is used as a supplement for vitamin A. Mirexus has taken

particular interest in beta-carotene because their experiments have shown that beta-carotene interacts strongly with PhytoSpherix(TM). Qualitative analysis conducted in this thesis confirmed these results, showing beta-carotene interacting hydrophobically with nearby RBUs.

Chapter 4

Methods

4.1 Twitching Bacteria and Phytoglycogen Nanoparticles

This thesis outlines work conducted at two different scales. Twitching bacteria are microscopic organisms and their motion occurs in seconds, while phyto-glycogen is a nanoparticle with motion occurring in nanoseconds. Both projects make use of molecular dynamics (MD), but each project uses MD differently.

Twitching bacteria simulations are conducted using coarse-graining techniques. Rather than simulating a fully detailed bacterial cell, the body of each twitcher is represented with 4 spheres held together into a stiff rod, with 2 additional dummy particles acting as the combined effect of multiple T4P. In these simulations, time progresses in time steps at a rate of $dt = 0.01$. Each integration (described in section 4.2.1) progresses the simulation by one timestep, or one dt . Analysis is conducted in simulation time units (STU) equivalent to 100 dt .

Phytoglycogen simulations are conducted using fully atomistic MD. Each

sphere represents a single atom. Simulations make use of multiple repeatable branching units (RBUs - outlined later), each consisting of 633 atoms. Each atom has a mass and charge, each bond is characterized by length and by strength, the relative position of three atoms is characterized by an angle, and the orientation of four atoms is characterized by a rotational configuration called torsional angle. Phytoglycogen simulations also include water in abundance. Here, time progresses at a rate of $dt = 0.002$ ps. Each STU is equivalent to 500 dt , and represents 1 picosecond of real time.

4.2 Molecular Dynamics (MD) Simulations

Simulations for both projects involve the use of molecular dynamics (MD). MD simulations use Newton's Second Law ($\vec{F} = m\vec{a}$) [44] to conduct simulations of biochemical systems:

$$m\vec{a} = \sum \vec{F} = \vec{F}_1 + \vec{F}_2 + \vec{F}_3 + \dots \quad (4.1)$$

This relationship between force and acceleration means that the acceleration of a simulated particle can be extracted by determining the net force on the particle. Each time step, the net force is calculated based on the position and velocity of the previous time step, as well as the influence of each individual force. Once the forces have been calculated, the acceleration can be calculated with Newton's Second Law. The velocity of a particle is then calculated by integrating the acceleration with respect to time, and the position of the particle is calculated by integrating the velocity with respect to time. These positions and velocities are written in a trajectory file and used to determine the velocity and positions of particles at the next time step. MD simulations can be conducted for millions of time steps. The Velocity Verlet integration used to calculate these trajectories

is outlined in the following section.

4.2.1 Velocity Verlet

At each integration step, the trajectories of each particle in the simulation is calculated using the Velocity Verlet integration technique. Velocity Verlet calculates the velocity of the particle in two half-steps.

The standard Euler approach to calculating the trajectory of particles is as follows:

$$m \vec{a}(t + \Delta t) = \sum \vec{F} \quad (4.2)$$

$$\vec{v}(t + \Delta t) = \vec{v}(t) + \vec{a}(t + \Delta t) \Delta t \quad (4.3)$$

$$\vec{r}(t + \Delta t) = \vec{x}(t) + \vec{v}(t + \Delta t) \Delta t \quad (4.4)$$

where m is the mass of a particle, $\vec{v}(t)$ is the velocity of a particle at integration step t , $\vec{a}(t)$ is the acceleration, $\vec{r}(t)$ is the position, t is a reference time, and Δt is an increment in time, such that $t + \Delta t$ is Δt integration steps after t .

The problem with using this method is that it does not correctly calculate conservation of energy. As time progresses, the energy of the particle in question increases. Velocity Verlet is used because it calculates trajectories without incorrectly disrupting the energy of particles. It is conducted through the following formulae:

$$\vec{v}\left(t + \frac{1}{2}\Delta t\right) = \vec{v}(t) + \frac{1}{2}\vec{a}(t) \Delta t \quad (4.5)$$

$$\vec{x}(t + \Delta t) = \vec{x}(t) + \vec{v}\left(t + \frac{1}{2}\Delta t\right) \Delta t \quad (4.6)$$

$$m \vec{a}(t + \Delta t) = \sum \vec{F} \quad (4.7)$$

$$\vec{v}(t + \Delta t) = \vec{v}\left(t + \frac{1}{2}\Delta t\right) + \vec{a}(t + \Delta t) \Delta t \quad (4.8)$$

This technique calculates the velocity after half of a timestep. After the half-

step is calculated, it is used to calculate an updated position and acceleration. The newly calculated acceleration and the half-step velocity are then used in order to calculate the full-step velocity.

4.3 Twitching Bacteria Simulations

4.3.1 Simulations - HOOMD

Simulations of twitching bacteria were simulated using a molecular simulation tool-kit called HOOMD-Blue [45] [46]. The HOOMD-Blue simulation package is used for conducting MD simulations of coarse-grained systems, and is optimized to make use of graphical processing units (GPUs) in the computer. GPU computing increases the production speed of these simulations, as GPUs are capable of conducting a significantly greater number of floating point operations per unit of time than the central processing unit (CPU) [45]. This means that more particles can be simulated at once while still maintaining good performance.

4.3.2 Molecular Dynamics for Twitching Bacteria

The sum of forces for particles in simulations of twitchers is described as follows:

$$\sum \vec{F} = m\vec{a} = \vec{F}_{WCA} + \vec{F}_{FENE} + \vec{F}_{SHO} + \vec{F}_{\text{pilus-retraction}} + \vec{F}_{\text{langevin}} \quad (4.9)$$

where \vec{F}_{FENE} and \vec{F}_{SHO} are internal forces that hold the twitcher together and keep the twitcher rod-like respectively, \vec{F}_{WCA} is an intermolecular force that prevents twitchers from passing through each other, $\vec{F}_{\text{retraction}}$ is the force of pilus retraction, and $\vec{F}_{\text{langevin}}$ is a combination of friction and thermal noise. These forces will be further outlined below.

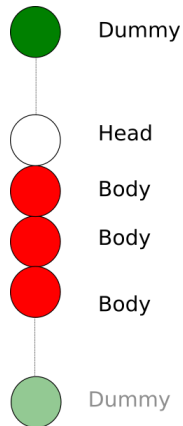


Figure 4.1: Schematic of an individual twitcher.

Each individual twitcher consists of four body spheres and two dummy spheres (Figure 4.1). Dummy spheres are used to facilitate twitching motility.

The four spheres that make up the body are held together via finitely-extensible-nonlinear-elastic (FENE) bonds [48]. The FENE Potential is described with the following formula:

$$V_{\text{FENE}} = -\frac{1}{2}kR_0 \ln \left(1 - \frac{r^2}{R_0^2} \right) \quad (4.10)$$

where k is the spring constant set to 50, r is the distance that a particle is away from a bonded particle, and R_0 is the maximum distance a particle can move from a bonded particle set to 1.5 spatial units. The FENE potential can be seen in Figure 4.2 on the top right, along with a comparison with the Simple Harmonic Oscillator (SHO) potential. The FENE potential is chosen over the SHO potential for the purpose of binding body spheres together because it sets $R_0 = 1.5$ as the maximum distance that bonded particles can separate from each other. This distance cap is important in order to prevent bond crossing.

To prevent twitchers from passing through each other, volume exclusion in-

teractions between body particles is defined by the Weeks-Chandler-Anderson (WCA) potential [49]. The WCA potential is described with the following formulae:

$$V(r) = \begin{cases} 4\epsilon\left[\left(\frac{\sigma}{r}\right)^{12} - \left(\frac{\sigma}{r}\right)^6\right] + \epsilon, & \text{if } r < r_c \\ 0, & r \geq r_c \end{cases} \quad (4.11)$$

Where ϵ is the strength of the potential set to 1, and σ is the diameter of a particle set to 1, \vec{r} is the distance two particles are away from each other. For simulations involving twitchers, spatial units are defined by σ . The WCA potential is a truncated and shifted version of the Lennard-Jones (LJ) potential. These modifications of the LJ potential are implemented in order to remove the attractive component. As a result, when twitchers come close to each other, they will not be attracted to each other. Combined with the FENE potential, the WCA potential prevents bond crossing. This potential is explained in Figure 4.2 on the top left.

In order to keep the twitcher stiff and rod-like, the first three and the last three body particles are held in a rod-like configuration by a simple harmonic oscillator (SHO) angular potential. The SHO angular potential can be described with this formula:

$$V(\theta) = \frac{1}{2}k(\theta - \theta_0)^2 \quad (4.12)$$

where θ is the angle of 3 particles, θ_0 is the default angle, and k is the strength of the potential set to 33. The SHO potential is displayed in Figure 4.2. This potential is dependant on the angular configuration of the twitcher as opposed to distance of two particles. An example of the angular SHO potential being used can be seen in Figure 4.3.

Dummy particles only interact with its twitcher's head. Dummy particles exert a constant force on the attached twitcher head, pulling the twitcher towards it so long as the distance between the twitcher and dummy is between

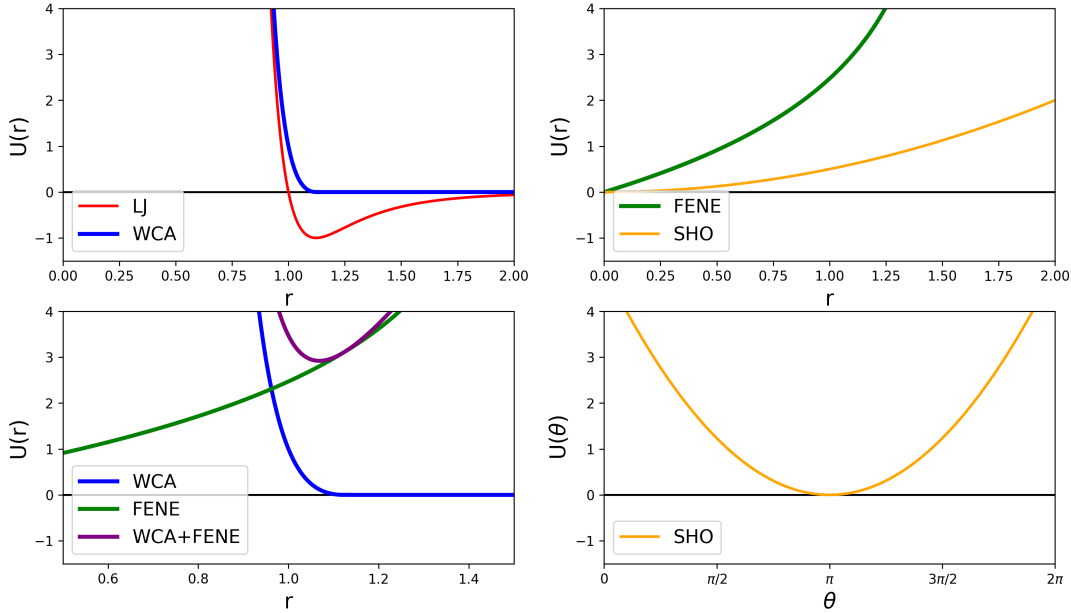


Figure 4.2: Potentials used to form a twitcher cell. **Top left:** Weeks-Chandler Anderson Potential (blue) and Lennard-Jones Potential (red). WCA is used to prevent body particles from passing through each other. WCA is a truncated and shifted version of the LJ potential. **Top right:** FENE potential (green) is used to hold body particles together. Each twitcher makes use of 3 of these potentials in order to form a polymer of 4 body particles. FENE potential is a stronger and more rigid interaction compared with the SHO potential (yellow) with the same spring constant and reference length. **Bottom left:** Combining the WCA and FENE potentials (purple) forms a potential well that keeps particles at a specific distance from each other. This combination is used to prevent bond crossing. **Bottom right:** SHO potential (yellow) with respect to angular configuration. SHO potential is used to keep twitchers rigid at 180 degrees/ π radians. Each twitcher makes use of two SHO interactions, one between the first 3 body particles, and one between the last 3 body particles.

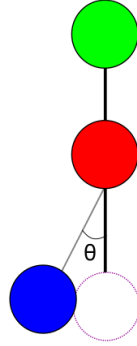


Figure 4.3: A red, green, and blue particle are held in a rod-like configuration by the angular SHO potential. The blue particle should be in the position outlined in dotted purple. As θ increases, the restoring force increases, pushing the blue particle into the correct position.

minimum distance $L_{reach} = 0.2$ and maximum distance $L_{snap} = 3.0$. The pilus attraction potential is described below:

$$V(r) = \begin{cases} -r, & \text{if } 0.2 < r < 3.0 \\ 0, & r \leq 0.2 \text{ or } r \geq 3.0 \end{cases} \quad (4.13)$$

This potential results in a constant attractive force of 1.

The minimum distance was selected to be 0.2 spatial units. Ideally this would be set to 0, but originally the simulation would crash when the head and dummy came this close. The minimum distance was set to 0.2 because 0.2 is still very close to reaching the dummy.

The maximum distance was selected to be 3.0. As will be explained later, a simulated twitcher undergoes twitching motility when the dummy is placed 2.4 units away from the head. If a twitcher is pushed beyond 2.4 spatial units

from its dummy by other twitchers, the twitcher will no longer move towards its dummy, even though the simulation assumes that the twitcher is moving.

4.3.3 Langevin Dynamics

Simulations of twitchers are conducted using Langevin Dynamics [47] in 2D. In most instances, Langevin Dynamics are used in order to simulate the presence of a solvent. This makes it easier to conduct simulations without having to simulate large numbers of particles.

In the simulations conducted for this thesis, the minimalistic nature of the model means that the use of Langevin Dynamics does not directly represent a solvent. Here, Langevin Dynamics is mainly used to apply friction to the model. However, bacterial twitchers undergo twitching motility across an surface of agar.

Langevin Dynamics can be described using the following formula.

$$m\ddot{\vec{r}} = -\zeta\vec{v}(t) + \vec{R}(t) \quad (4.14)$$

where \vec{F} is the total force of a particle, m is mass, $\ddot{\vec{r}}$ is acceleration, ζ is the coefficient of friction set to 1, $\vec{v}(t)$ is velocity, and $\vec{R}(t)$ is thermal noise. Normally, $R(t)$ represents thermal kicks in a system that occur as a fluid interacts with particles. In these simulations, the thermal noise term $R(t)$ is set to be very small (0.0000002 units). Twitching bacteria propel themselves through the use of their pili. Setting a low $R(t)$ means that almost all of the motion of simulated twitchers is due to twitching motility and collisions with other twitchers.

4.3.4 Twitching Motility Cycle

The twitching motility cycle consists of 3 phases - the rest phase, the extension phase, and the motility phase. A twitcher at the rest phase does not conduct

twitching motility, but it will be affected by other forces (see section 4.3.2). It has a 10% chance per STU to enter the extension phase. Should a twitcher enter the extension phase, it will stay still for extension time = 10 STUs. During this time, a twitcher selects an angle to move in. Twitchers select an angle up to 45 degrees from either side of the direction it is facing in a uniform distribution. The motility phase begins when the extension phase ends. The dummy particle is placed 2.4 spatial units ahead of the twitcher's head particle. Each twitcher model has its own set of conditions for when it will stop moving and return to the rest phase.

4.1 shows a list of variables used in the simulation of twitchers and in the implementation of the motility cycle. Also shown in Table 4.1 are the values used in the simulations outlined in this thesis.

4.3.5 2D Environment - Taking Advantage of 3D

Living bacteria are capable of undergoing reversals in their direction of motion. Twitching bacteria in particular have T4P on both poles. Twitchers in simulations outlined in this thesis do not conduct reversals. However, implementing twitchers with two poles is useful in providing randomness in the system. This is because the system is initiated in an ordered configuration with all twitchers facing the same direction for the sake of simplicity. In the future, this feature could be used to implement reversals in twitching directionality.

At the start of each simulation, each twitcher has a 50% chance to select one pole or the other. Once a twitcher selects its pole, it will consider the selected pole to be the head for the entirety of the simulation. This is done by setting the reversal probability to zero. While twitchers have one dummy for each pole, it will only ever use the one attached to its selected head.

A simulation trick is used to allow simulations to run in 2D while taking

advantage of the third dimension. Twitchers are confined between two walls in order to keep them in a 2D plane. Without these walls, the forces in the system can push twitchers along the z-axis. The tail dummy will stay 50 units below the twitchers' plane, which is well beyond the maximum distance of 3.0 spatial units. When the twitcher is conducting twitching motility, the head dummy is placed in the plane, 2.4 spatial units ahead of the twitcher. When the twitcher enters the rest phase, the dummy is moved 50 units below.

4.3.6 Comparing Between 3 Models of Twitching Bacteria

In this thesis document, 3 different models of twitching motility was analysed. These models are discussed below. Figure 4.4 shows the motility phase of all three models for easy comparison.

4.3.6.1 Surface Attachment Model (SAM) Twitchers

The first model is referred to as the Surface Attachment Model (SAM) 4.5. A SAM twitcher places its dummy pilus on the surface and moves toward it. SAM twitchers have 3 conditions under which it will return to the rest phase. The first condition is that the twitcher reaches its pilus. This occurs when the twitcher's head is within $L_{reach} = 0.2$ spatial units of its dummy. Once the twitcher reaches its pilus, it must extend it again in order to make more progress. The second condition is that it moves too far away from its pilus, which occurs when the twitcher's head is beyond $L_{snap} = 3.0$ spatial units of its dummy. A twitcher's pilus can only be extended so far. If a twitcher moves beyond this point, the pilus is considered to have snapped, at which point, the twitcher returns to rest and the cycle begins again. The final condition occurs if the twitcher doesn't reach its pilus within $t_{max} = 70$ STUs. Unobstructed twitchers typically reach their pilus in 10 STUs. At higher densities, a low t_{max}

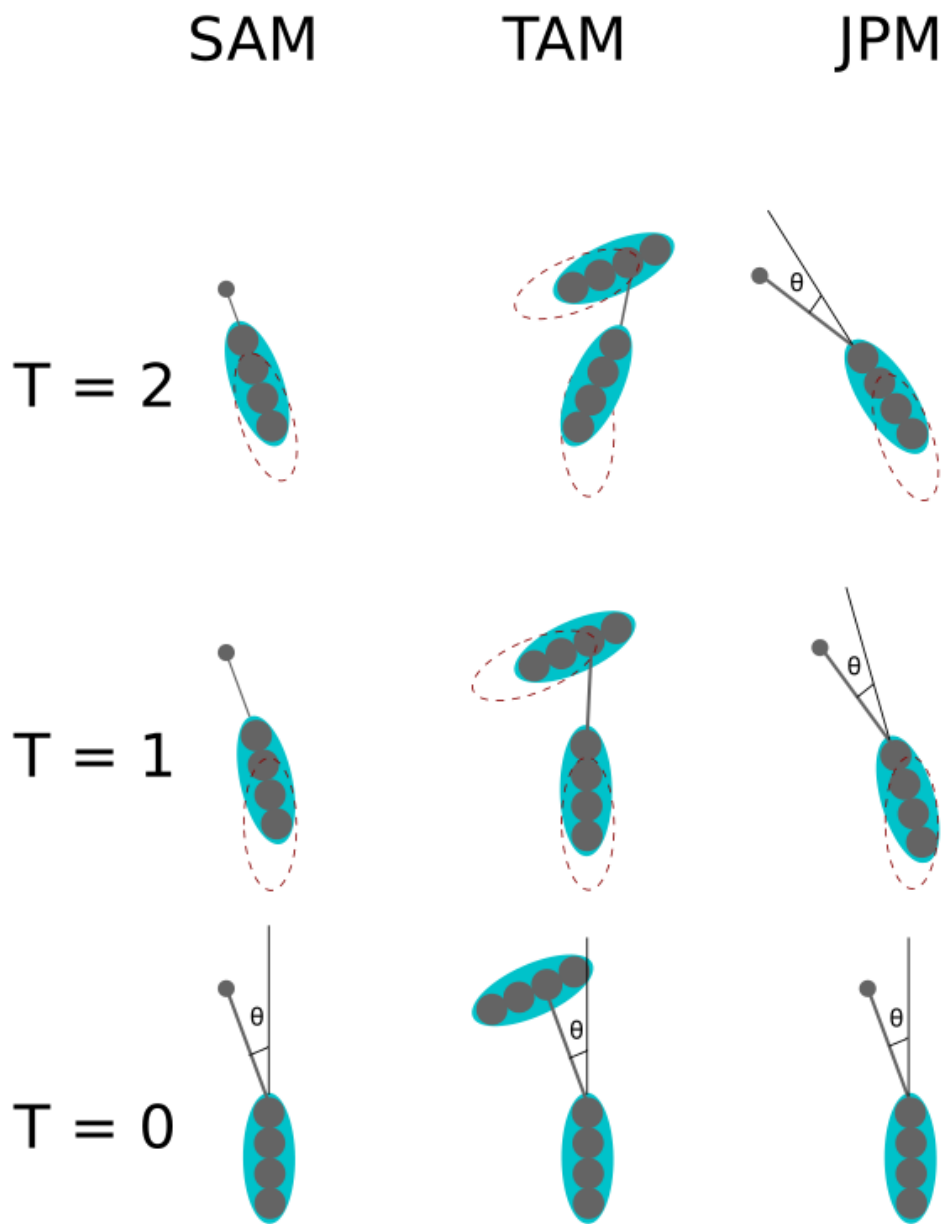


Figure 4.4: Motility Phase of SAM, TAM, and JPM Twitchers over two STUs. Time increases from bottom to top. Red outlines show where the twitcher was during the previous STU

results in log-jams, while high t_{max} results in swimming motility. A t_{max} of 70 was selected to prevent the occurrence of log-jams and swimming motility.

4.3.6.2 Twitcher Attachment Model (TAM) Twitchers

The second model is the Twitcher Attachment Model (TAM). As more twitchers are added to the system, less space is available for twitchers to attach directly to the surface. If a twitcher is not able to attach to the surface, it would be able to attach to another twitcher.

To facilitate attachment, TAM twitchers have a second dummy particle that has a short-ranged attraction with twitcher body particles. When a surface attaching dummy lands on another twitcher, it is replaced with a twitcher attaching dummy. The twitcher attaching pilus is attracted to the body particle of the twitcher it lands on. The attaching twitcher makes its way over to the twitcher attaching dummy as normal, moving towards the twitcher it has attached to. TAM twitchers have the same conditions as SAM twitchers for entering the rest phase from motility phase. However, when a TAM twitcher attaches to another twitcher, it is unable to move within L_{reach} units of its dummy. The WCA potential prevents twitchers from passing through each other, preventing the attaching twitcher from reaching its dummy. Instead, when a TAM twitcher attaches to another twitcher, it goes to rest when it reaches within $L_{detach} = 1.2$ spatial units of its dummy. This is equivalent to 0.2 spatial units from the twitcher body part that it has attached to. This modified distance does not apply when a TAM twitcher attaches to the surface.

4.3.6.3 Jetpack Model (JPM) Twitchers

The final model is the jetpack model (JPM). This is a simple model used to provide contrast with the previous models. Of the models outlined in this thesis, the JPM model is the most similar to models of rod-like swimmers discussed in

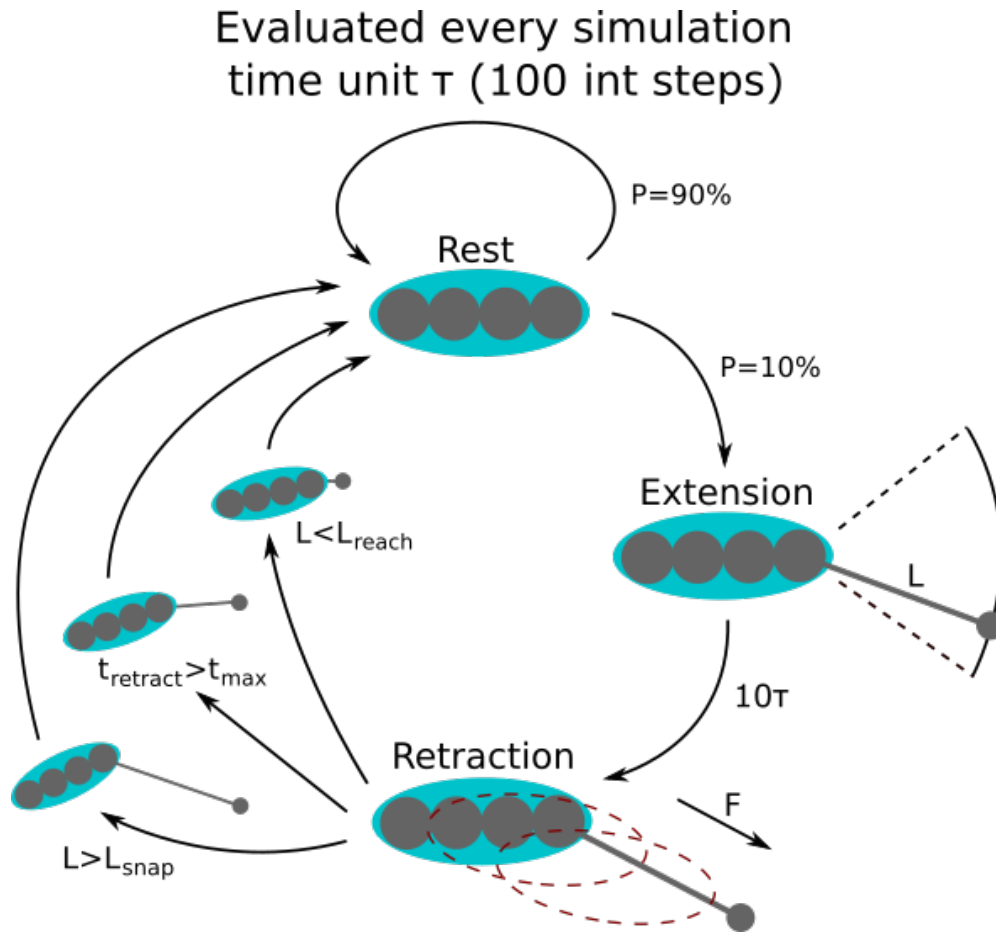


Figure 4.5: Twitching motility cycle of a single Surface Attachment Model (SAM) Twitcher - made by Andrew Nagel (permission form to use this figure can be seen on pg 5).

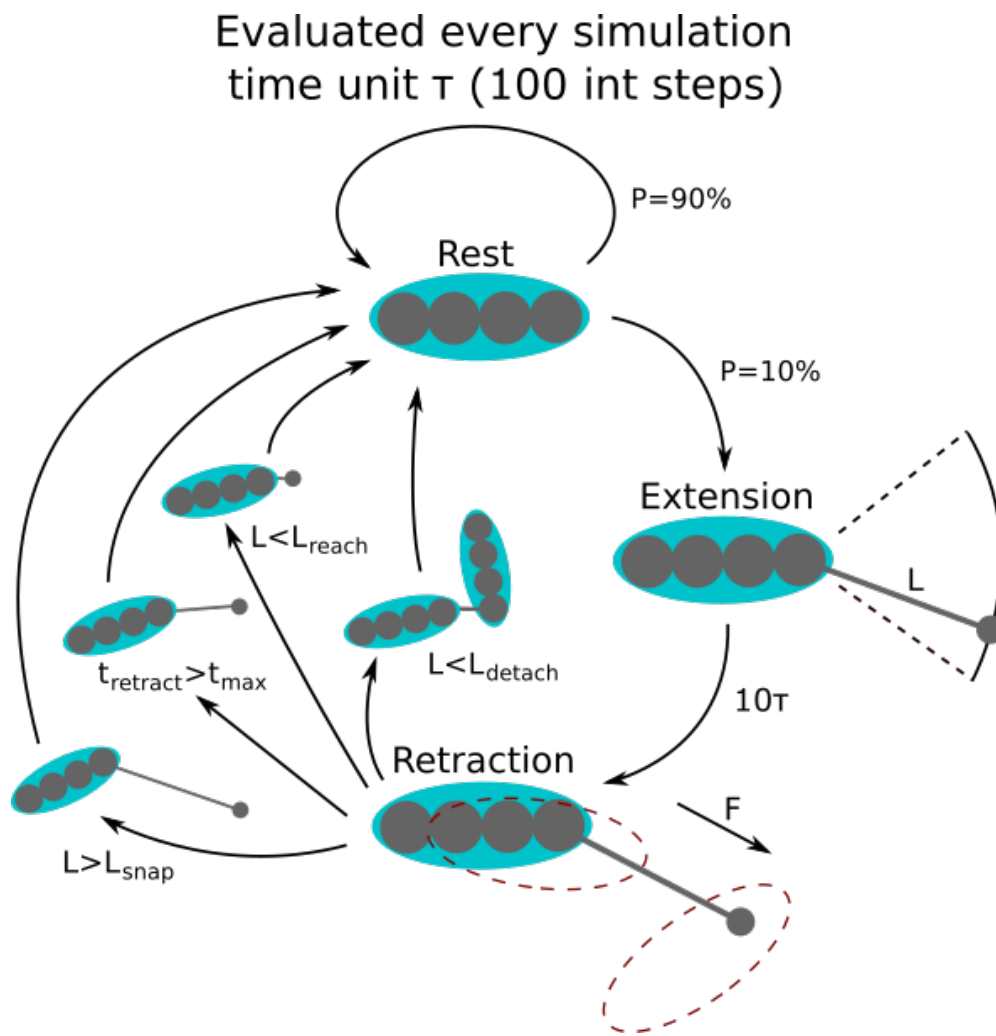


Figure 4.6: Twitching motility cycle of a single Twitcher Attachment Model (TAM) Twitcher

Table 4.1: List of Twitcher Variables. While all of these can be modified, the following variables have been set to the following for the content of this document

Variables	Value
Number of Body Particles	4 particles
Extension Length	2.4 spatial units
Cone Width	$\pi/4$ radians per side
Chance to Leave Rest	10% per time step
t_{max}	70 STUs
Extension Time	10 STUs
L_{reach}	0.2 spatial units
t_{jp}	10 STUs
L_{snap}	3.0 spatial units
Attachment Distance	0.5 spatial units
L_{detach}	1.2 spatial units
Reversal Probability	0% per motility cycle initiation
t_{sim}	1,000,000 STUs

Section 2.1.4. JPM twitchers make use of a constant force to propel themselves forward. Rather than using a grappling hook to pull the twitcher to a specific point, the twitcher pushes itself forward as if it were using a jetpack. JPM twitchers use the dummy particle to guide its motion. At the start of each STU, the dummy particle is replaced 2.4 spatial units away at the same angle that was selected during the extension phase. This is unlike the attachment models, which only place their dummy at the end of the extension phase. JPM twitchers move for $t_{jp} = 10$ STUs before going into rest.

4.3.7 Analysis of Collective Motion

Simulations were conducted for $t_{sim} =$ one million STUs. One million STUs is necessary for twitchers to achieve diffusive motion (explained in the results section). The following methods were used to analyse twitcher trajectories to determine the presence or absence of collective motion.

Evaluated every simulation time unit τ (100 int steps)

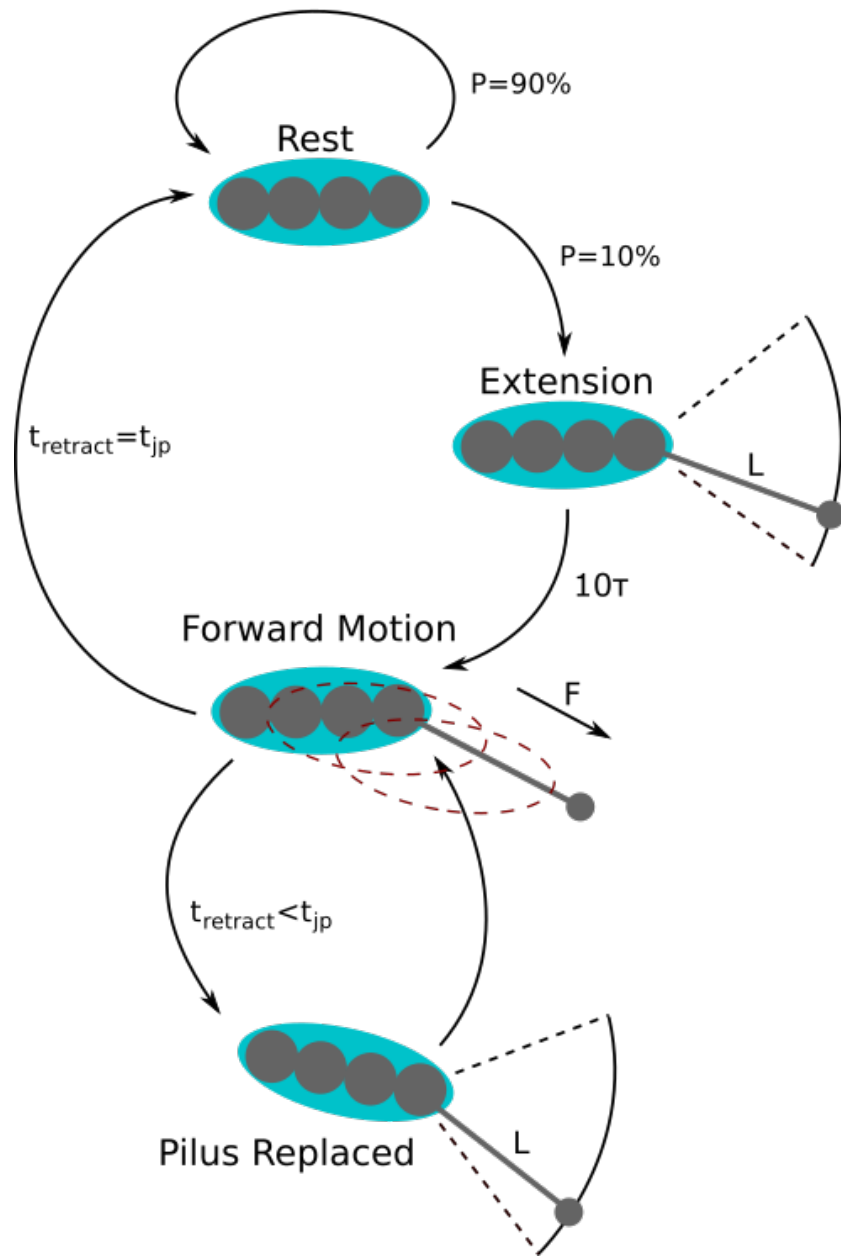


Figure 4.7: Twitching motility cycle of a single Jetpack Model (JPM) Twitcher

4.3.7.1 Mean Squared Displacement (MSD) and Diffusion

Mean Squared Displacement (MSD) was measured for all of the twitchers over one million STUs. MSD can be used to measure the rate at which a twitcher spreads across a surface over short and long periods of time. For example, the MSD over a time interval of 1 measures a twitcher's displacement over a period of 1 STU. MSD over a time interval of 100 measures a twitcher's displacement over a period of 100 STUs. MSD increases as the time interval increases, but by investigating the rate at which MSD increases, we gain insight into the behaviour of the collective behaviour of the twitchers.

MSD is expressed with the following formula:

$$MSD(dt) = \langle \Delta r(dt)^2 \rangle = \frac{1}{t_{sim} - dt} \sum_{t=1}^{t_{sim}-dt} \left(\frac{1}{N} \sum_{n=1}^N (r_n(t+dt) - r_n(t))^2 \right) \quad (4.15)$$

where $r(t)$ is the position of a twitcher at time t , t is a point of reference, dt is a time interval, N is the number of twitchers in the system, and n covers each twitcher in the system.

By calculating MSD, we were also able to extract a long time diffusion coefficient. The diffusion coefficient can be measured using the Einstein relation [50]:

$$\langle \Delta \vec{r}^2(dt) \rangle = 2dDt \quad (4.16)$$

where D is the diffusion coefficient, and d is the dimensionality of the system. In this instance, simulations are conducted in 2D, so d is set to 2. The diffusion coefficient is a measure of how quickly the twitchers can spread across a surface over a large period of time. A higher diffusion coefficient means that the collective of twitchers can spread across a surface more quickly.

4.3.7.2 Velocity Autocorrelation (VAC)

Velocity Autocorrelation (VAC) is also useful in measuring the collective behaviour of twitchers. VAC compares the velocity of twitchers to measure consistency with itself at later times. It is calculated with the following equation:

$$VAC(dt) = \langle (v(t) \cdot v(t+dt)) \rangle = \frac{\frac{1}{t_{sim}-dt} \sum_{t=1}^{t_{sim}-dt} \frac{1}{N} \sum_{n=1}^N (v_n(t) \cdot v_n(t+dt))}{\langle v(t) \cdot v(t) \rangle} \quad (4.17)$$

High VAC means that a twitcher's velocity is highly correlated with itself within a set period of time. A decrease in VAC suggests that the direction of a twitcher is uncorrelated with itself. Correlation decreases as a result of twitchers moving in different directions and at different speeds as time progresses.

The next section outlines the methodology used to study phytoglycogen nanoparticles. Analysis of twitching bacteria can be seen in the following chapter.

4.4 Phytoglycogen Nanoparticles

Simulations outlined below are conducted in fully atomistic detail using molecular dynamics. The techniques used to conduct atomistic MD simulations will be outlined below.

4.4.1 AMBER MD

Phytoglycogen simulations are made using AMBER MD [51]. AMBER MD is used to set up, run, and analyse MD simulations for the purpose of studying biochemical systems [51]. MD is applied through the use of a force field, which

has the following generic form [52]:

$$\begin{aligned}
U = & \sum_{\text{bonds}} \frac{1}{2} k_b (r - r_0)^2 + \sum_{\text{angles}} \frac{1}{2} k_a (\theta - \theta_0)^2 + \sum_{\text{torsions}} \frac{V_n}{2} (1 + \cos(n\Phi + \delta)) \\
& + \sum_{\text{improper}} \frac{k_{imp}}{2} (\omega - \omega_0)^2 + \sum_{\text{LJ}} 4\epsilon \left(\left(\frac{\sigma}{r} \right)^{12} - \left(\frac{\sigma}{r} \right)^6 \right) + \sum_{\text{coulomb}} k_\epsilon \frac{q_i q_j}{r}
\end{aligned} \tag{4.18}$$

where U is potential energy, k_b , k_a , and k_{imp} are harmonic spring constants for bonds, angles, and improper torsional configurations respectively, r is the distance between two particles and r_0 is the equilibrium length of a bond between two particles, θ is the angle of three particles and θ_0 is the equilibrium angle of three bonded particles, n is the number of maxima or minima between 0 and 2π , Φ is the equilibrium torsional angle, δ is the phase, V_n is the magnitude constant for torsional configurations, ω is an improper torsional angle corresponding to deviations from the plane, ϵ is the strength constant for LJ, σ is the size of the particles, k_ϵ is the dielectric constant ($9.0 \cdot 10^9 Nm^2 C^{-2}$), q_i and q_j are the charge of a particles i and j .

Torsional angles are defined between 4 particles bonded together in a sequence. Torsion is associated with bond rotations, and is typically represented as a cosine function given that rotational configurations can be repeated. In most cases, torsion is not as rigid as bonds. However, there are instances (such as with aromatic rings) where the torsional potential is not strong enough to maintain a particular rotational configuration. In these instances, an additional term is used to prevent improper configurations. This term is included in the above formula as \sum_{improper} .

Phytoglycogen simulations covered in this thesis make use of the GLYCAM_6J-1 force field [53]. The GLYCAM_6 force field is specifically designed to implement carbohydrates in AMBER MD [53], and contains parameters for bonds, angles,

torsions, LJ interactions and charges involved in carbohydrate structures.

4.4.2 The Repeatable Branching Unit

Given that the PhytoSpherixTM nanoparticle consists of approximately 22000 monomers of glucose, it is not practical to model an entire phytoglycogen compound solvated with water on the atomistic scale. Rather than simulating the entire compound, atomistic simulations were conducted using a series of amylopectin branches, referred to as repeatable branching units (RBU). These RBUs consist of 30 glucose monomers, beginning with a chain of 10 glucose monomers, and branching out into 2 new chains of 10 glucose monomers each. Each glucose monomer is modelled in fully atomistic detail, with each sphere acting as an atom. In total, each RBU consists of 633 atoms. A single RBU in atomistic detail can be seen in Figure 4.8.

A single RBU was made using Glycam Builder [54] in order to build a protein database (PDB) file. Multiple RBUs were made using C code written in the cNAB.LAB to clone and translate additional RBUs.

4.4.3 Water

Water is explicitly included in the system through the use of the TIP3P Model [55]. Transferable Intermolecular Potential 3P (TIP3P) is a model of water consisting of LJ and Coulombic potentials [55]. While present, water is not visible in most visualizations of the system. By making the water invisible, it is easier to see the structural features of the RBUs.

4.4.4 Simulation and Analysis of RBUs

Simulations consist of as few as 9 RBUs in a configuration of 3 by 3 (Figure 4.9) to as many as 50 RBUs in a configuration of 5 by 5 by 2 (Figure 4.10).

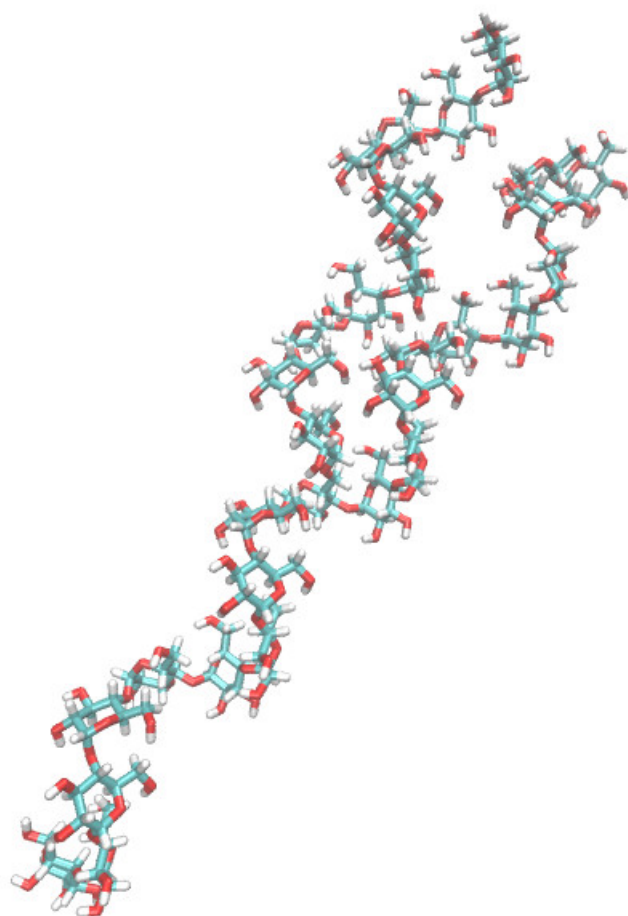


Figure 4.8: Initial configuration of 1 RBU - amylopectin

Table 4.2: Number of Atoms in a 9 RBU and 50 RBU system

Number of RBUs	Total Number of Atoms	Total Atoms in RBUs	Total Atoms in Water Molecules
9	28,342	5,697	22,645
50	602,766	31,650	571,116

These RBUs are solvated in water before the simulation begins, as discussed in the previous section. Table 4.2 lists the number of atoms in simulations with 9 and 50 RBUs. Simulations of these systems are conducted for a length of 20 nanoseconds of real time.

Some set-up was required before the simulation could be conducted. All of these steps are implemented in order to eliminate bad contacts (overlapping particles) and high energy effects, thus preventing them from causing the simulation to crash. First, energy minimization is implemented in order to prevent the occurrence of large forces as a result of adding water [44]. Next, the temperature of the system is increased from 0 Kelvin to 300 Kelvin over time. This is to prevent effects resulting from sudden temperature change. Lastly, the system is equilibrated to prevent bad contacts resulting from overlapping particles. Equilibrating the system is important to distribute kinetic energy added to the system during the previous heating step. During set-up, the position of RBUs was restrained in order to maintain the initial configuration for the production run. These restraints hold particles in position using a SHO potential (Figure 4.2).

Upon completion of the set-up phase, the position restraints on the RBUs were removed, and the production run began. Observation and analysis was conducted on the production run once it was complete.

In order to reveal interesting features of the resulting structure, visualization techniques using Visual Molecular Dynamics (VMD) software were used to better show individual RBUs and their features. Each RBU is coloured differently to distinguish it from other RBUs. RBUs are shown so that the surface of

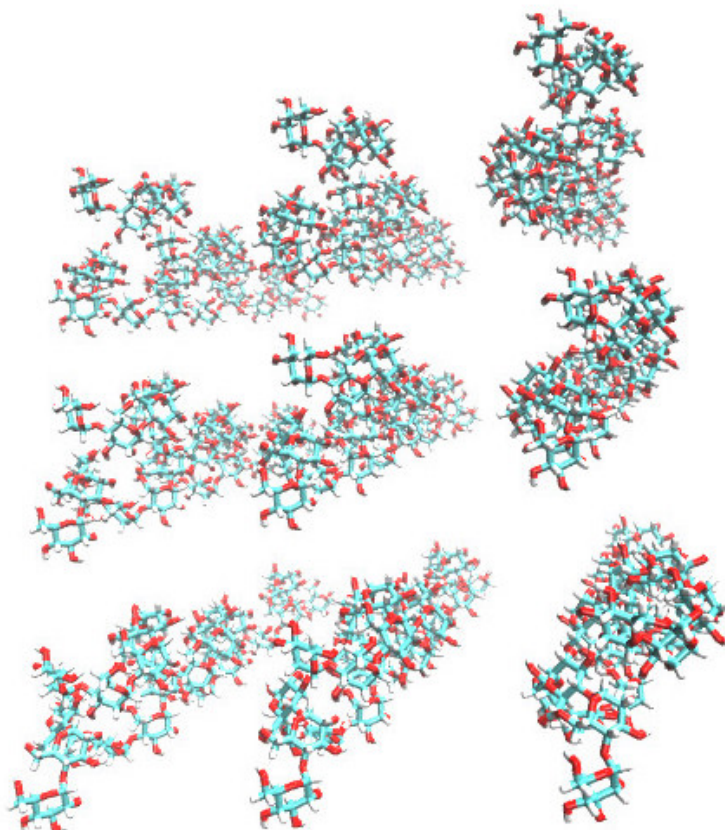


Figure 4.9: Initial configuration of 9 RBUs

the structure can be seen, as per Figure 4.11 and Figure 4.12. As RBUs come closer together, their atomistic structure is revealed beneath the surface. Also, hydrogen atoms connected to carbon atoms are shown as blue spheres, while hydrogen atoms connected to oxygen atoms are shown as red spheres.

As shown, each of these models make use of molecular dynamics. Each uses MD differently to account for the differences in scale. The following two chapters will cover the results obtained through analysis of the above two systems.

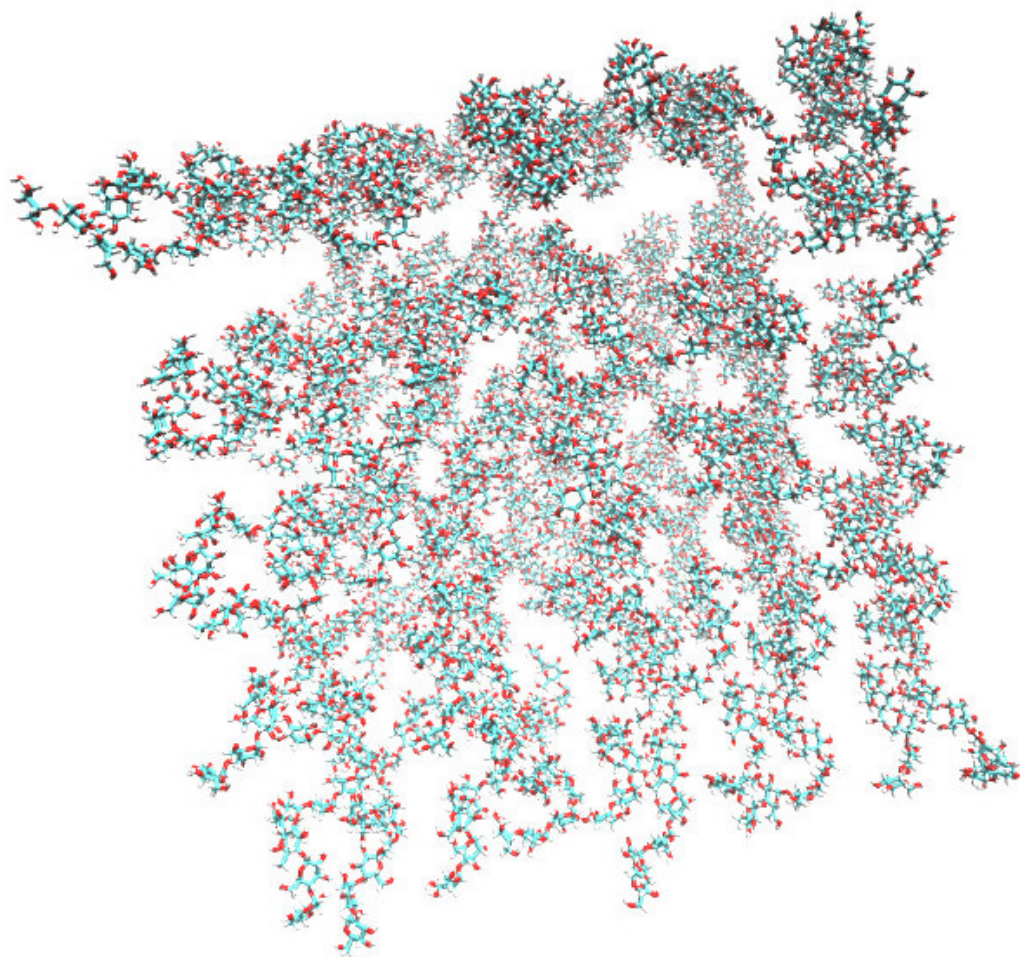


Figure 4.10: Initial configuration of 50 RBUs

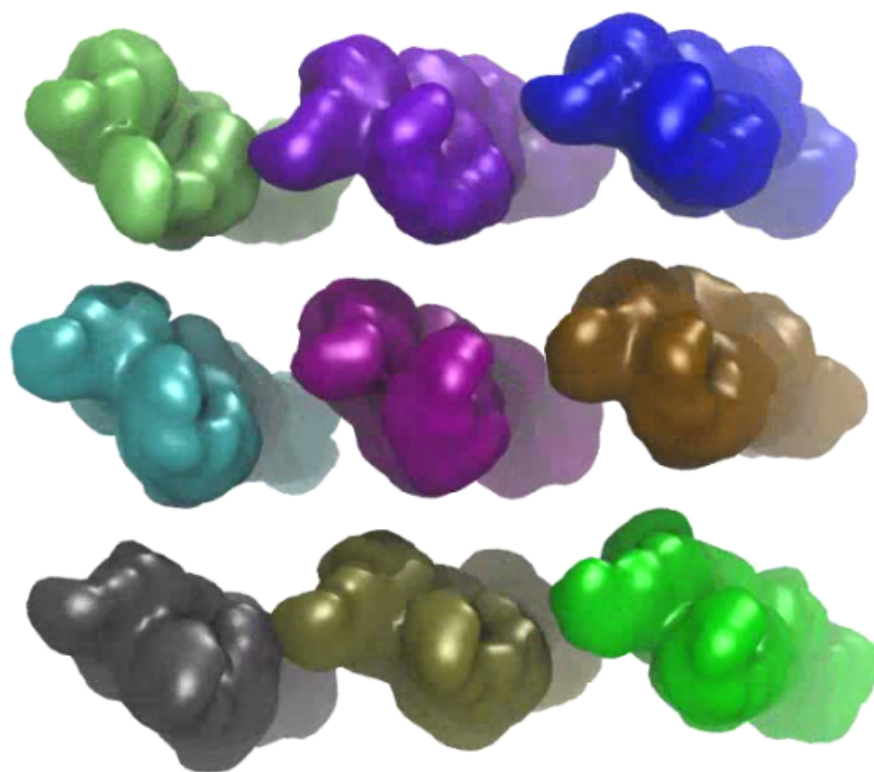


Figure 4.11: Surface structure of the initial configuration of 9 RBUs

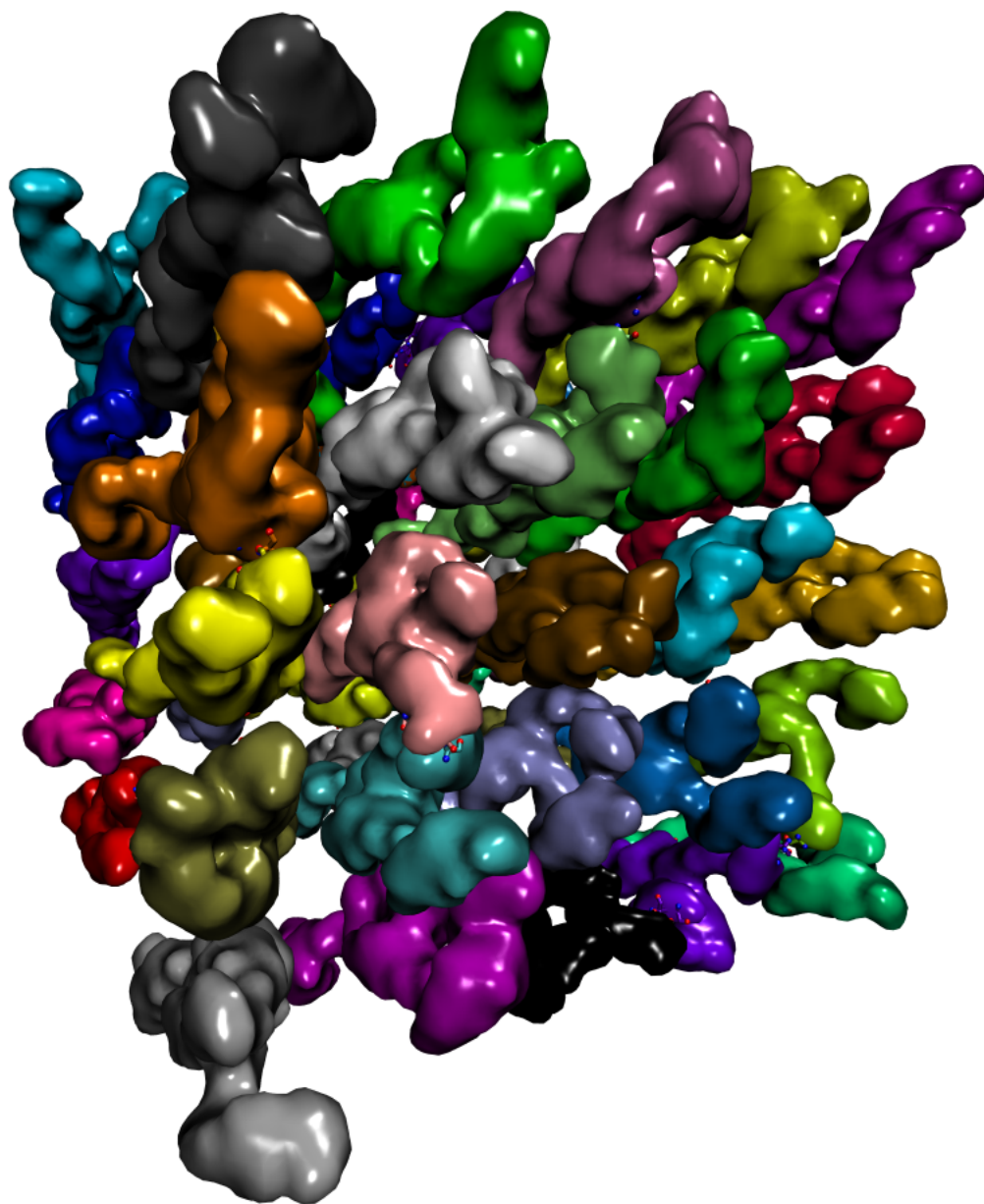


Figure 4.12: Surface structure of the initial configuration of 50 RBUs

4.4.5 Adding Beta-Carotene to RBU Simulations

The structure of beta-carotene was obtained from the protein data bank [56]. Once the structure was obtained, the GLYCAM06 force-field was applied to it using Antechamber [51] - a built-in feature of AMBER MD that can be used to apply a force field to new structures.

Chapter 5

Results - Twitching

Bacteria

5.1 Collective Motion of SAM Twitchers

Surface attachment twitchers simulate twitching motility through the use of a guiding dummy particle. This model is made to simulate motion through the use of a grappling hook-like structure like T4P. Figure 5.1 shows a comparison between the individualistic motion exhibited by 500 twitchers, and the collective motion exhibited by 2000. The left side shows 500 twitchers. These twitchers have access to space to move around freely, although they do sometimes collide with each other. In contrast, 2000 twitchers are shown to be tightly packed. These twitchers move in collective packs, as their direction is restricted by their neighbours.

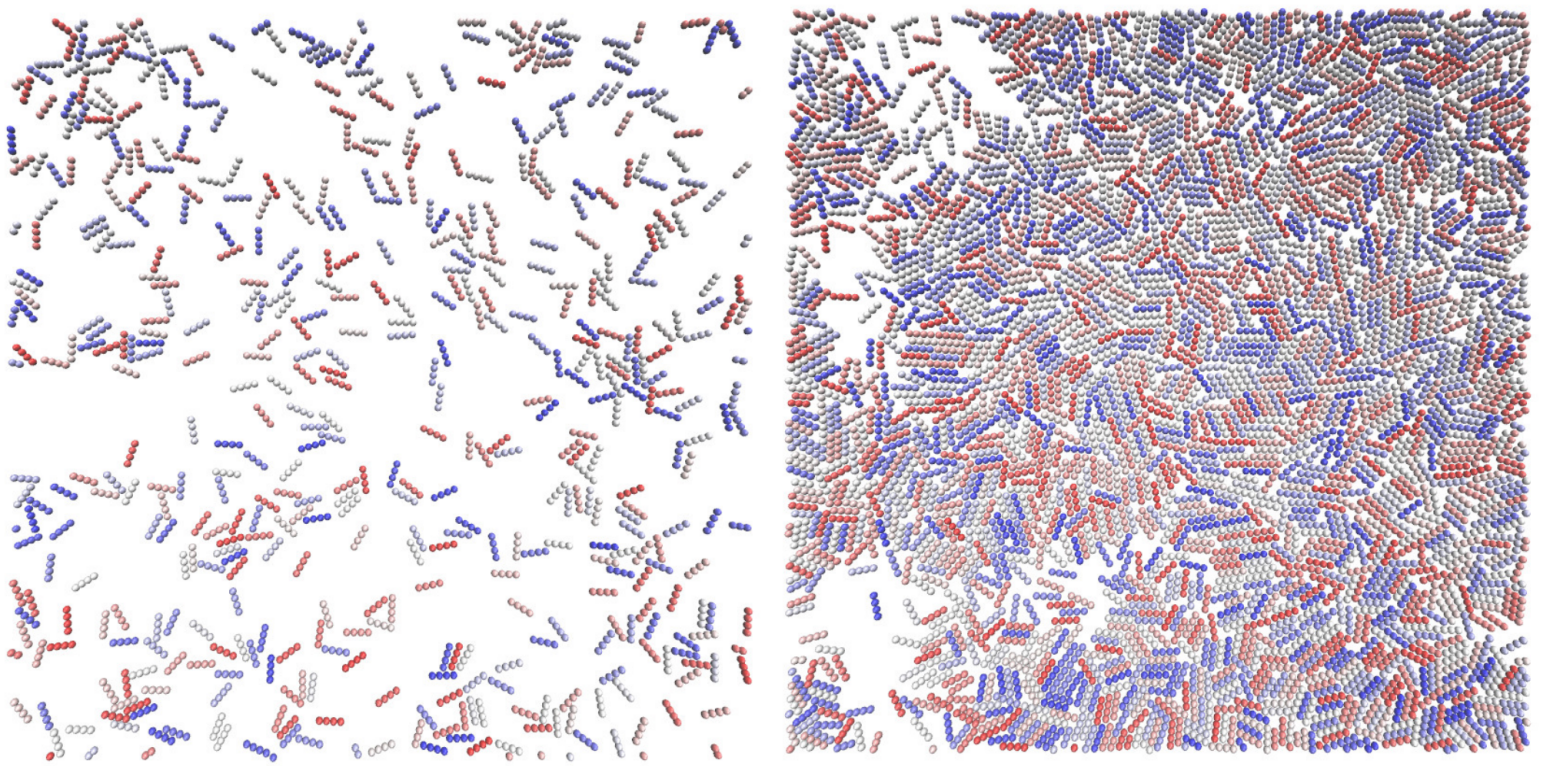


Figure 5.1: 500 and 2000 surface attachment twitchers in an area of 100 by 100 squared spatial units

5.1.1 Mean Squared Displacement

5.1.1.1 Interpreting MSD

Figure 5.2 shows an example plot outlining the MSD of 500 SAM Twitchers (blue). As the timescale increases, MSD also increases. However, there are regimes where the rate of increase changes. Between 10^0 and 10^1 , the twitchers are moving ballistically. A twitcher that moves ballistically is one is moving directly towards its dummy, as if it were alone in the universe and without obstacles to block its way. This is because it is moving under its own power through the use of twitching motility. In an MSD plot, the ballistic regime is shown when MSD increases quadratically. Ballistic motion occurs when MSD is proportional to t^2 . On a loglog plot, ballistic motion occurs when MSD increases with a linear slope of 2. This is due to the following relationship:

$$\begin{aligned}MSD_{\text{ballistic}} = \langle \Delta r^2 \rangle &\sim t^2 \\ \log(\langle \Delta r^2 \rangle) &\sim \log(t^2) = 2\log(t)\end{aligned}\tag{5.1}$$

Around 10^1 , there is a decrease in the rate of change of MSD. This is because twitching motility is inconsistent, occurring in short jumps. Between 10^2 and 10^3 is a return to more driven behaviour. As the timescale increases, the periods of rest have less influence on the overall behaviour. Between 10^4 and 10^5 , we enter the diffusive regime. Particles in the diffusive regime appear to be moving at random. This occurs in simulated twitchers because they move within a 90 degree cone - 45 degrees to either side. At short timescales, this 90 degree allowance does not make a big difference in squared displacement, as twitchers move mostly forward and continue to face the same direction over a short timeframe. However, over long timescales, twitchers can be moved in various directions. Over long timeframes, a twitcher makes considerable progress

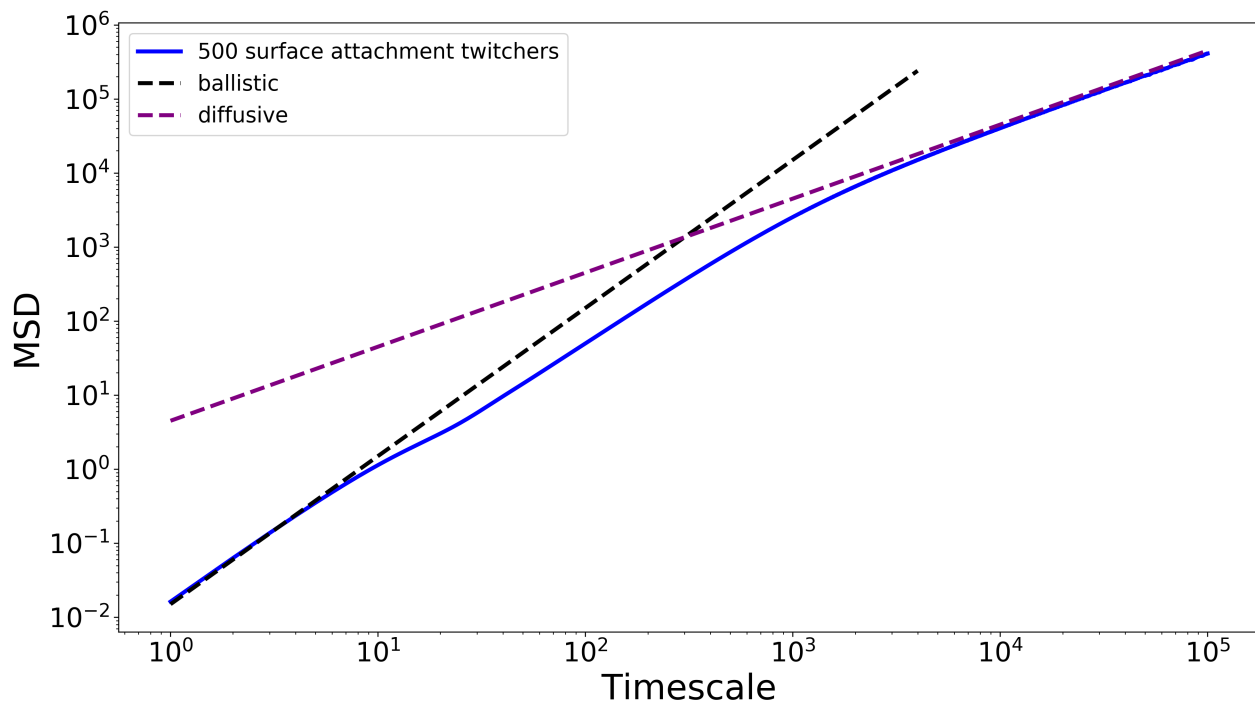


Figure 5.2: Mean Squared Displacement of 500 SAM Twachers

in displacement. An example and explanation of this can be seen in Figure 5.3. On an MSD plot, diffusive motion is shown as the MSD increases linearly with timescale, as MSD is proportional to t . On a loglog plot, diffusive motion occurs when MSD increases with a linear slope of 1.

$$MSD_{\text{diffusive}} = \langle \Delta r^2 \rangle \sim t \tag{5.2}$$

$$\log(\langle \Delta r^2 \rangle) \sim \log(t)$$

5.1.1.2 Analysing MSD

Figure 5.4 shows the MSD of SAM Twachers at various densities as they move within a box of 100 spatial units by 100 spatial units. There is a subtle effect at

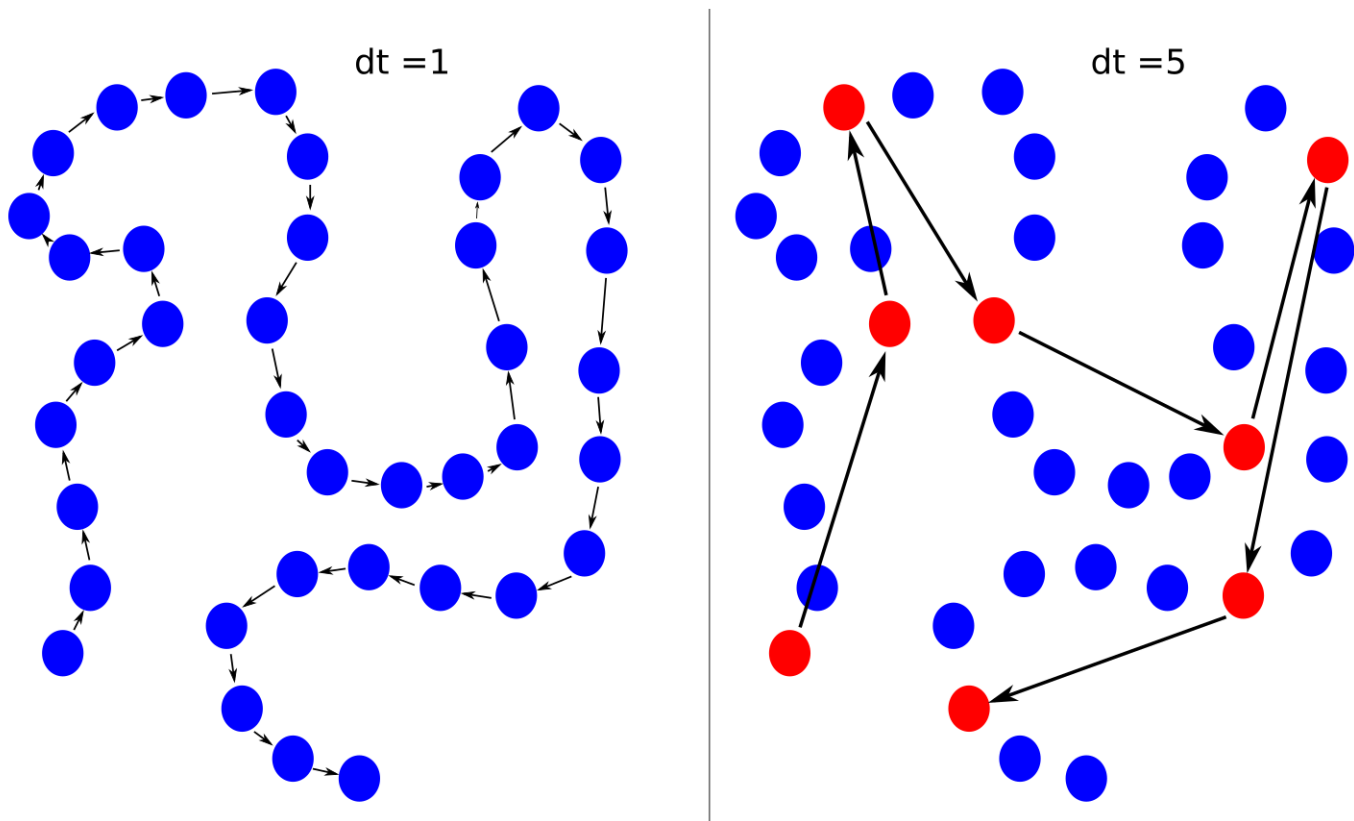


Figure 5.3: A particle moving across a surface. **left:** the particle progresses a short distance in a direction that is consistent with the direction it moved in the prior step. Small arrows show the progress that the particle makes over time. **right:** by following the red particles, it is possible to measure the displacement of a particle over a longer time window. Displacement over a long time window is considerably greater than displacement over a shorter time window. It is also less consistent in magnitude and directionality. While the particle is not moving diffusively, there is an appearance of random behaviour as the time scale increases

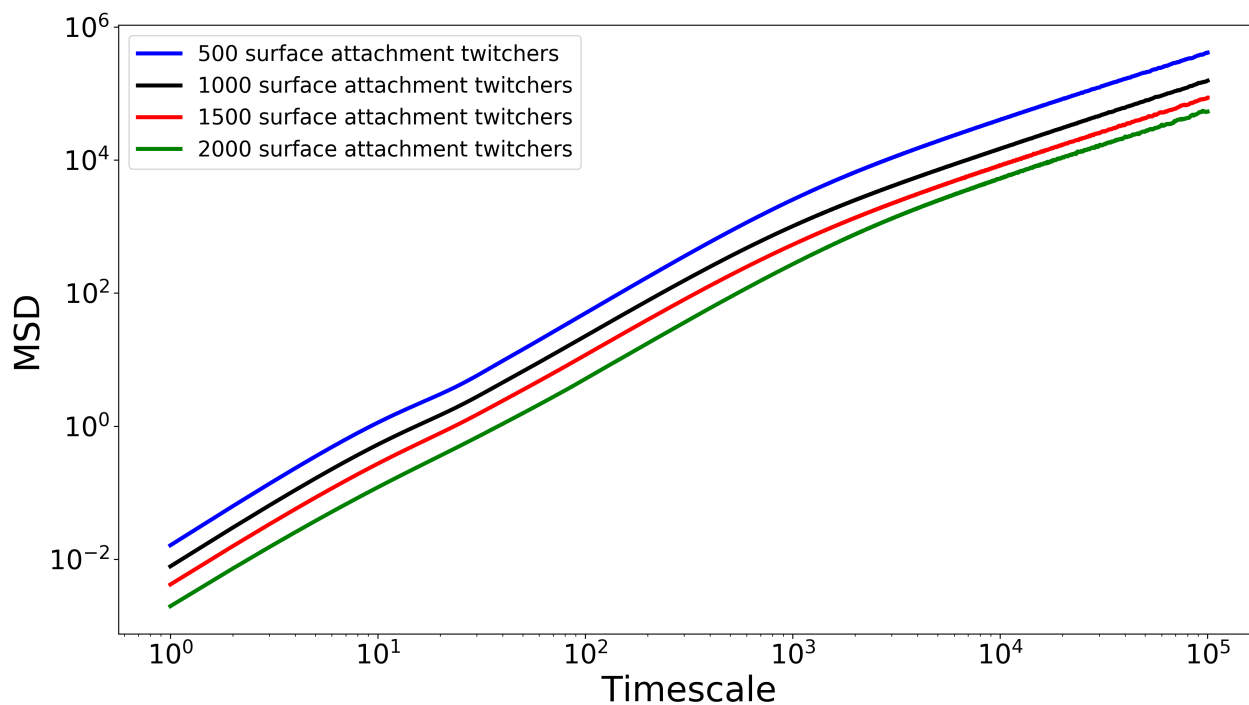


Figure 5.4: Mean Squared Displacement of 500, 1000, 1500, and 2000 SAM Twitchers. Density of twitchers increases following graph lines from top to bottom.

long timescales. As density increases, the difference in MSD from one density to another decreases. For example, the difference in long-time MSD between 2000 and 1500 is smaller than the difference in long-time MSD between 1500 and 1000.

In order to better illustrate the long-time effect, MSD results were normalized by the MSD at a timescale of 1. The differences between each density at a timescale of one is due to interactions between twitchers. At low densities, a twitcher has more room to move around freely. At higher densities, twitchers are colliding with each other and obstructing each other. By normalizing the data by the MSD at a timescale of one, the immediate short term effects are cancelled out. This makes it easier to analyse the long term effects of the sys-

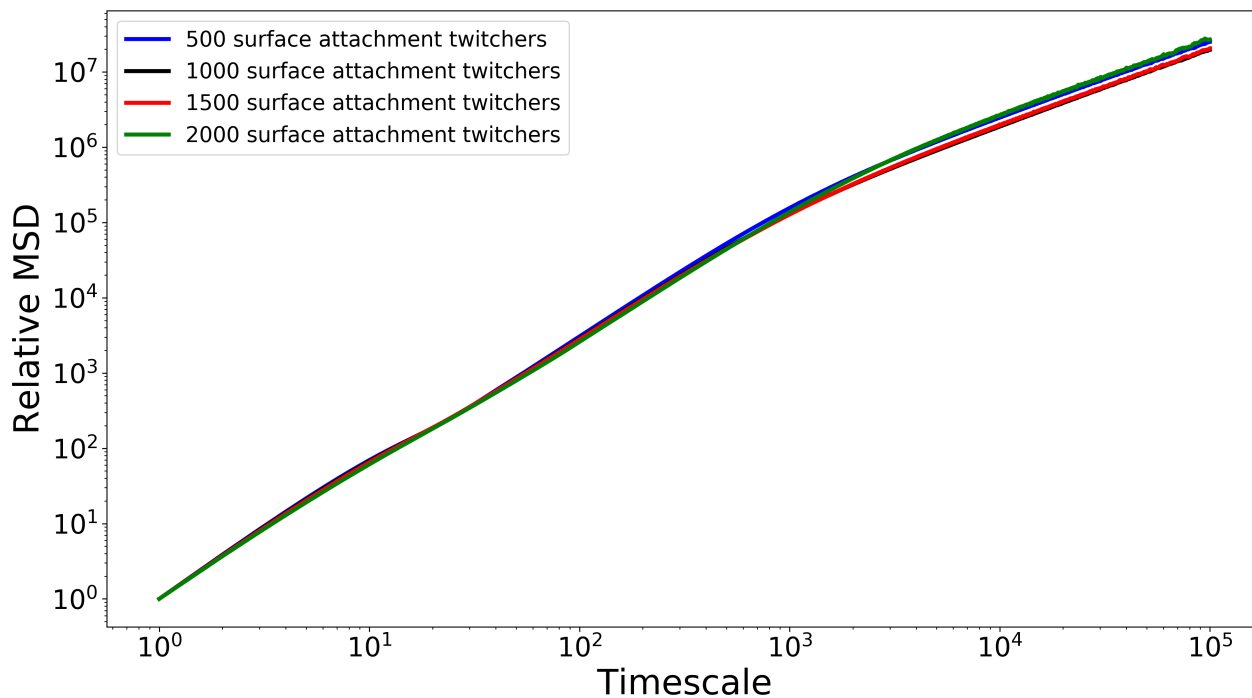


Figure 5.5: Relative Mean Squared Displacement of 500, 1000, 1500, and 2000 SAM Twitchers

tem. The long term effect is better illustrated in Figure 5.5, where the MSD measurements have been normalized.

When the short term effect is removed, the results are mostly consistent up to a timescale of 10^3 . However, there is a subtle effect between 10^1 and 10^2 that suggests the occurrence of collective motion. This can be seen in Figure 5.6.

Between 10^1 and 10^2 , the increase rate of MSD is reduced for lower densities of twitchers. At low densities, twitchers cycle between motion and rest. However, at higher densities, the increase rate of MSD is much more consistent. Twitchers at high densities start packing up and forming pockets of collective motion. By moving within a collective, an individual twitcher moves more consistently, as it is pushed along by its neighbours even while at rest.

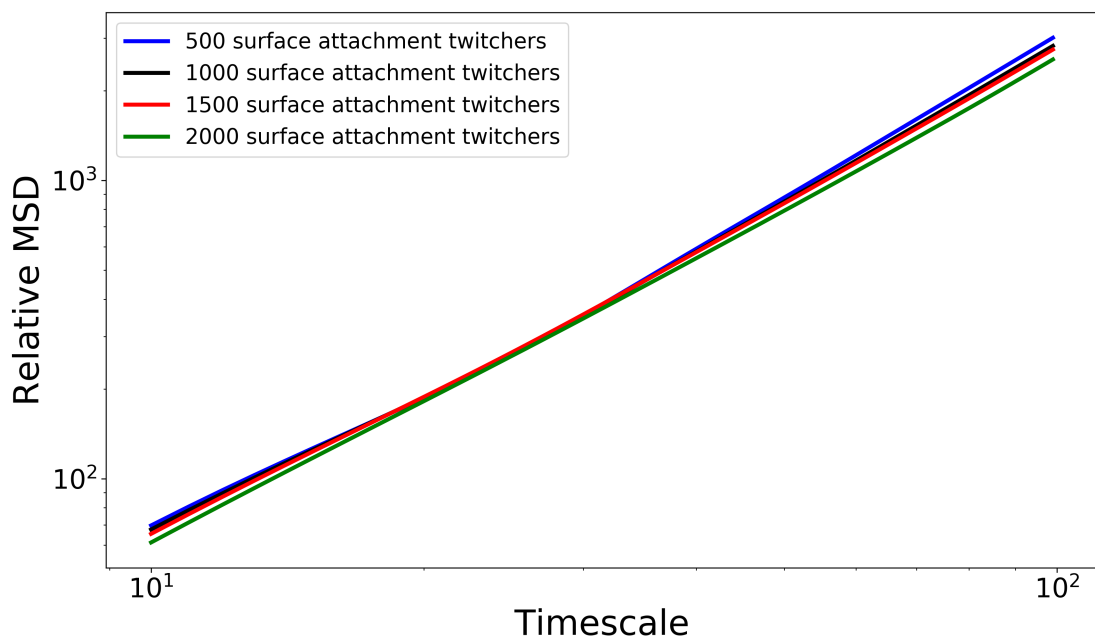


Figure 5.6: Relative Mean Squared Displacement of 500, 1000, 1500, and 2000 SAM Twitchers between Timescales of 10^1 and 10^2 . Density increases following graph lines from top to bottom.

At a timescale of 10^3 and greater, the differences are much more noticeable. This can be seen more easily in Figure 5.7, which shows the MSD of SAM twitchers between timescales of 10^3 and 10^5 . In this domain of time scales, the MSD of 500 twitchers is similar to the MSD of 2000 twitchers. Likewise, the MSD of 1000 twitchers is similar to, but slightly lower than the MSD of 1500 twitchers. This result is further evidence of collective motion. At first, increasing density results in lower MSD, as collisions knock twitchers around. These collisions slow individual twitchers down, and disrupts directed motion as one twitcher may push another to face a different direction. As the density of twitchers increases beyond 1000, collisions become less frequent, and collective motion enhances the motion of single twitchers and allows them to move more quickly. This collective motion is a result of nematic alignment, as aligned twitchers are restricted in their direction of motion.

5.1.2 Diffusion

Diffusion coefficients can be extracted by taking advantage of the following relationship [50]:

$$\langle \Delta r^2 \rangle = 2dDt \tag{5.3}$$

where d is the dimensionality of the system, D is the diffusion coefficient, and t is time. These simulations are conducted in 2D, so d is set to 2. The diffusion coefficient is determined by placing a line of best fit over the diffusive regime between 10^4 and 10^5 . This line is extended all the way to a timescale of 1, and the y-intercept is measured, at which case the diffusion coefficient can be extracted:

$$y_{intercept} = 4D \tag{5.4}$$

The diffusion coefficients of SAM twitchers can be seen in Figure 5.8. The

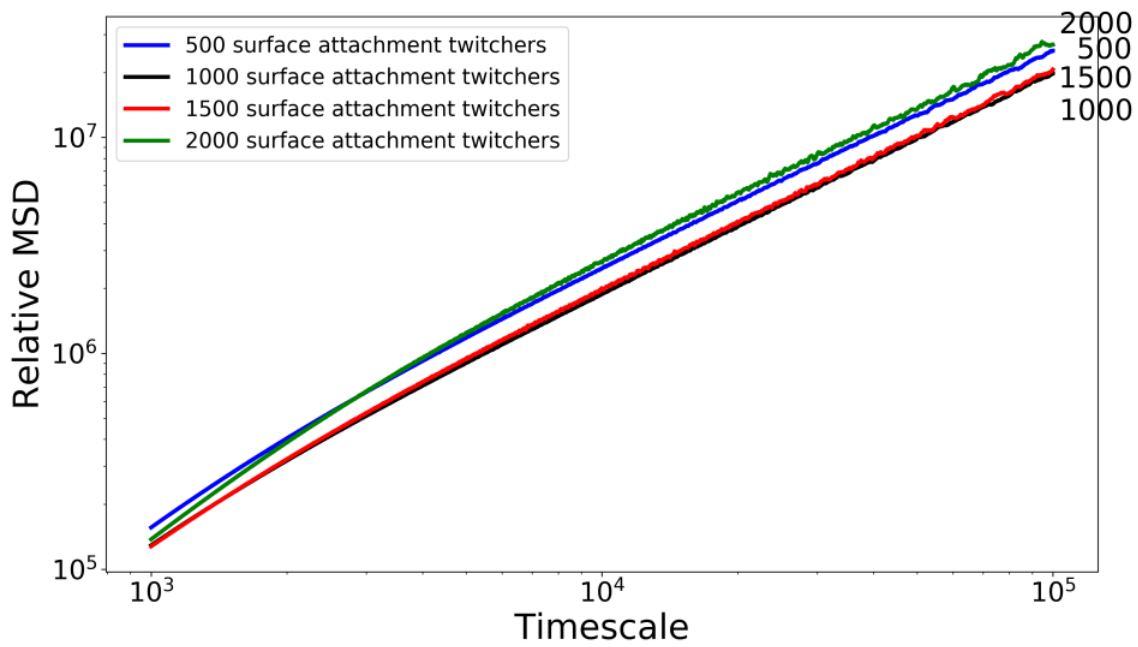


Figure 5.7: Relative Mean Squared Displacement of SAM Twitchers at time scale from 10^3 to 10^5 .

non-monotonic behaviour shown here is consistent with the relative MSD at long timescales. At low densities (500), twitchers are free to move around without colliding too much. Free space allows for the twitchers to spread out more quickly. As the density increases to 1000, the likelihood of collision increases, slowing twitchers down and reducing diffusion as compared with smaller density systems. 1000 twitchers is not enough for collective motion to dominate the system and increase relative diffusion. As such, the diffusion coefficient is minimized. As the density increases to 1500, diffusion increases. This increase in diffusion is a result of collective motion, which occurs because of nematic alignment. The alignment of twitchers allows for the formation of collective pockets where individual twitchers move together in the same direction (Figure 5.1). With even more twitchers, it is easier for individual twitchers undergo collective motion, and more collective pockets emerge as free space is taken up.

To confirm that the non-monotonic behaviour shown through analysis of MSD and diffusion is the result of collective motion, the velocity autocorrelation (VAC) of twitchers in the system was also analysed. The impact of the direction of motion is easier to detect through analysis of VAC, as the squared component of MSD masks the directional component.

5.1.3 Velocity Autocorrelation

5.1.3.1 Interpreting VAC

Figure 5.9 shows an example of velocity autocorrelation for 500 SAM Twitchers. When t is 0, VAC is 1, as the velocity of a twitcher is perfectly correlated with itself with no change in time. Over time, the VAC of a twitcher decays.

There are two noticeable regimes in VAC plots involving twitchers. Over a short period of time, VAC oscillates between high and low values. The oscillations are a result of the inconsistent motion that is a feature of twitching

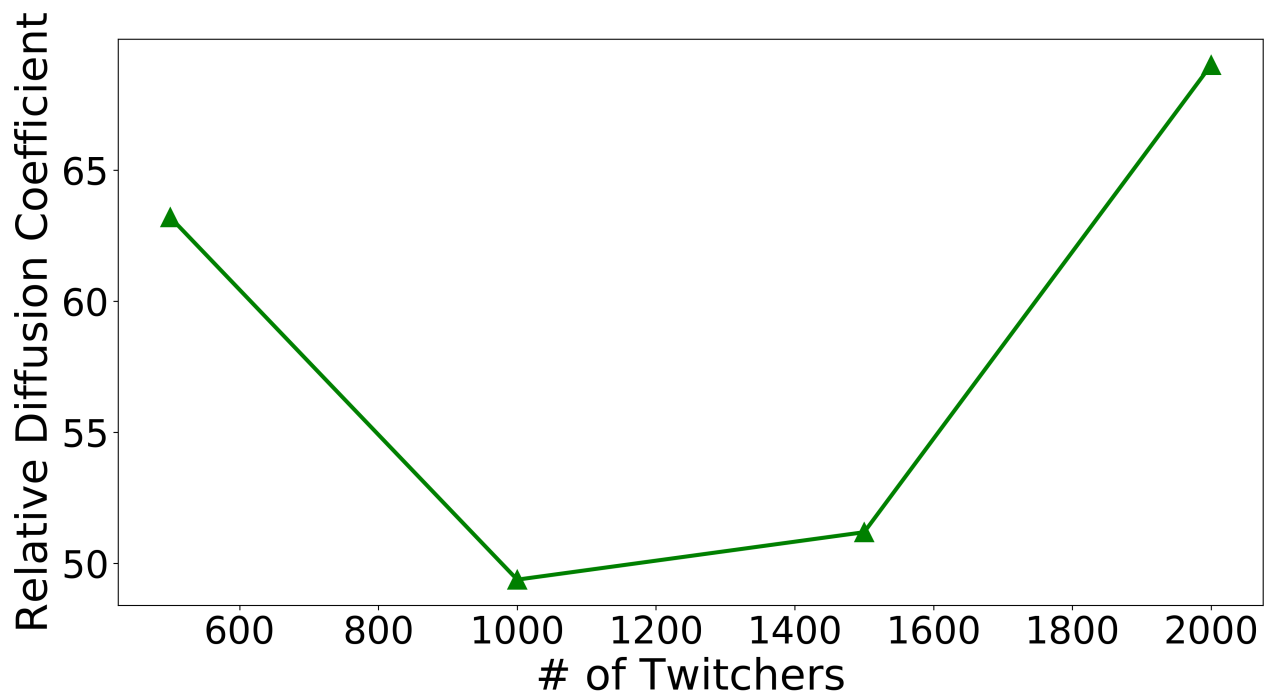


Figure 5.8: Relative Diffusion Coefficients of SAM Twitchers

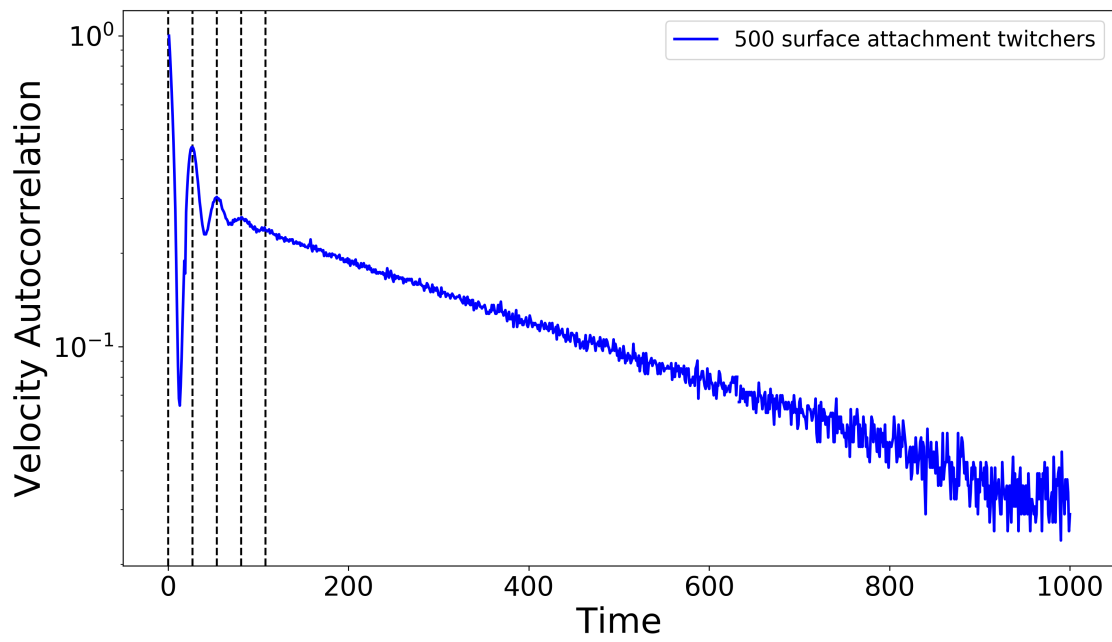


Figure 5.9: Example of Velocity Autocorrelation Plot - 500 SAM twitchers

motility. These early fluctuations have a period of 27 STUs, as shown by the dotted vertical lines. This period is consistent with the motility cycle of SAM twitchers, as each motility cycle involves 10 STUs of extension, at least 10 STUs of retraction, and approximately 10 STUs of rest.

Over longer periods of time, the VAC decays exponentially. On a semilog plot as shown in Figure 5.9, VAC decay is linear. This is due to the following relationship:

$$\begin{aligned} VAC &\sim e^{-t/\tau_d} \\ \ln(VAC) &\sim \frac{-t}{\tau_d} \end{aligned} \tag{5.5}$$

where t is time and τ_d is the characteristic decay time. Characterizing the decay in VAC is useful in order to analyze the collective behaviour of the twitchers. The characteristic decay time τ_d is the amount of time it takes for the VAC of a twitcher to decay to half of its value starting at $t = 200$. $t = 200$ was chosen as the starting point because the region of 200-500 showed an exponential decay (linear decay in a semi-log plot) for all VAC measurements, allowing for consistent means of calculating the characteristic decay time. A higher decay time suggests that a twitcher's velocity remains correlated for a longer period of time, indicating the twitcher continues in the same direction for a long period of time. A lower decay time suggests that a twitcher's velocity changes frequently.

5.1.3.2 Analysing VAC

Figure 5.10 show the VAC of SAM twitchers. This initial trend diverges as time scale increases, and these results are consistent with the MSD and diffusion results for SAM twitchers. As the density increases from 500 to 1000 twitchers, the VAC decays more quickly as timescale increases. However, as the density increases from 1000 to 1500, the VAC decays more slowly, to the point that

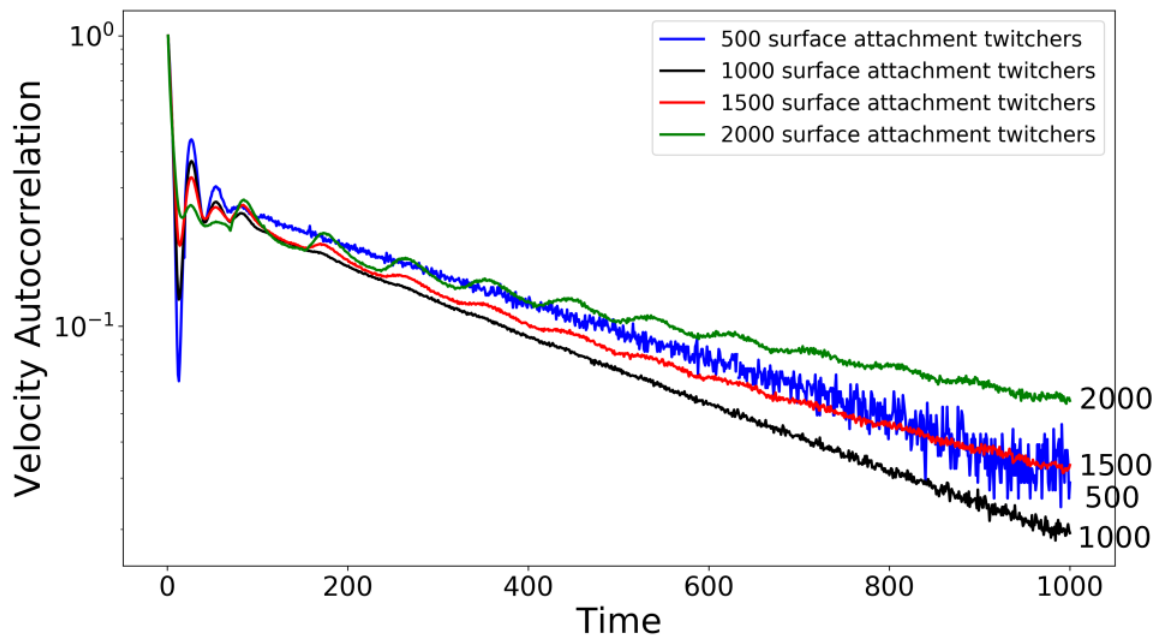


Figure 5.10: Relative velocity autocorrelation of SAM twitchers

the VAC of 1500 twitchers at a timescale of 1000 is higher than the VAC of 500 twitchers. As before, this suggests the emergence of collective motion. A twitcher aligned by other twitchers is more restricted in the direction that it can go.

As twitcher density increases, oscillations can be seen as time increases. These oscillations are the result of t_{max} , which is necessary to prevent swimming motility.

5.1.4 Characteristic Decay Time

Characteristic decay times can be extracted by placing a line of best fit over the linear region within a time domain of 200 and 500. Once this is done, the slope of the line of fit can be measured, and the characteristic decay time τ_d can be extracted:

$$Slope = \frac{-1}{\tau_d} \quad (5.6)$$

The characteristic times for SAM twitchers can be seen in Figure 5.11. As with VAC results, these decay times suggest the occurrence of collective motion after a period of time. At low densities, twitchers have more free space available to move around. Without too many neighbours to interact with, these individual twitchers move freely in any direction, and VAC decays quickly. As the density of twitchers increases from 500 to 1000, collisions become more frequent. These collisions push individual twitchers around and cause them to face different directions, thus increasing VAC decay. The reduction of free space available to 1000 SAM twitchers slows them down, but 1000 is not enough twitchers for collective motion to dominate. As such, the VAC decay is maximized, and the decay time is minimized. However, as density increases from 1000 to 1500, collective motion emerges. As free space decreases, twitchers begin to align with each other. An individual twitcher aligned by others is restricted in the direction

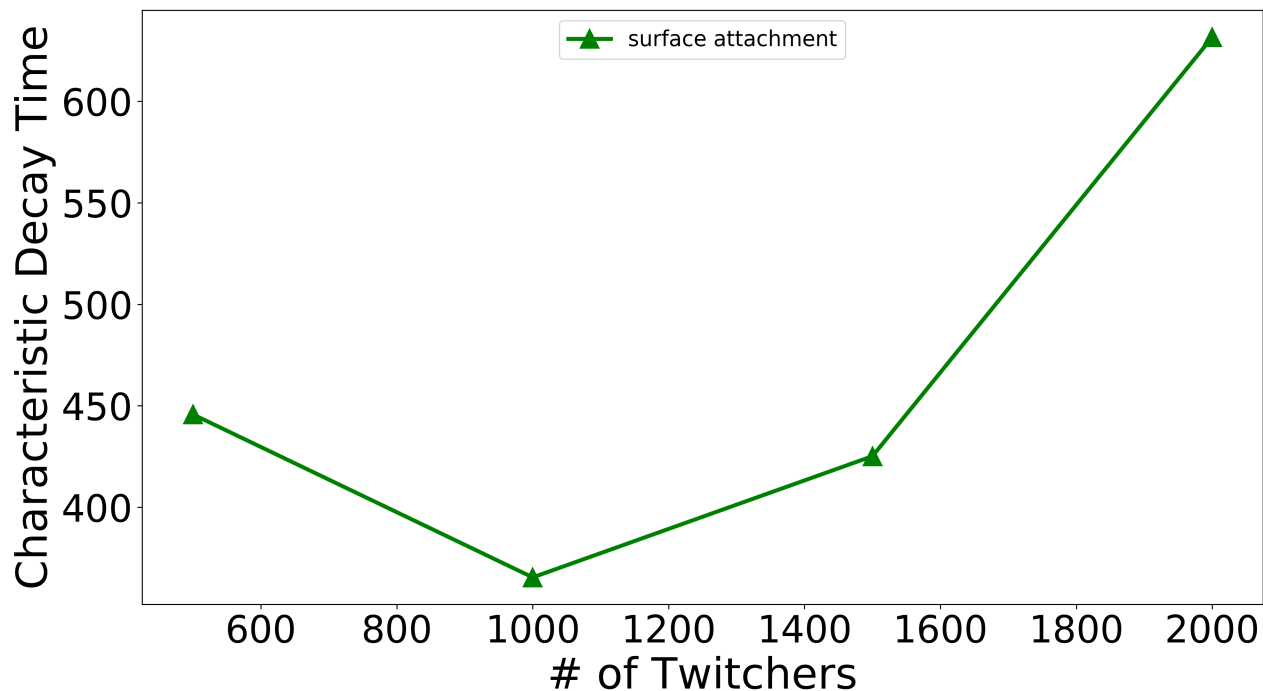


Figure 5.11: Characteristic decay times of SAM twitchers

it can go, since it cannot pass through its neighbours. As such, collective motion occurs, and the VAC decays more slowly. The effect of collective motion becomes even more noticeable as the density of twitchers increases to 2000.

5.2 Comparing Models

Three different motility models have been compared with each other in this thesis. The first (SAM) was discussed in detail above. The other two models are the Twitcher Attachment Model (TAM), and the Jetpack Model (JPM).

TAM twitchers are simulated with the consideration that in nature, it is possible for the pilus of a twitcher to attach itself to another nearby twitcher (data given to us by experimental collaborators in the John Dutcher Lab).

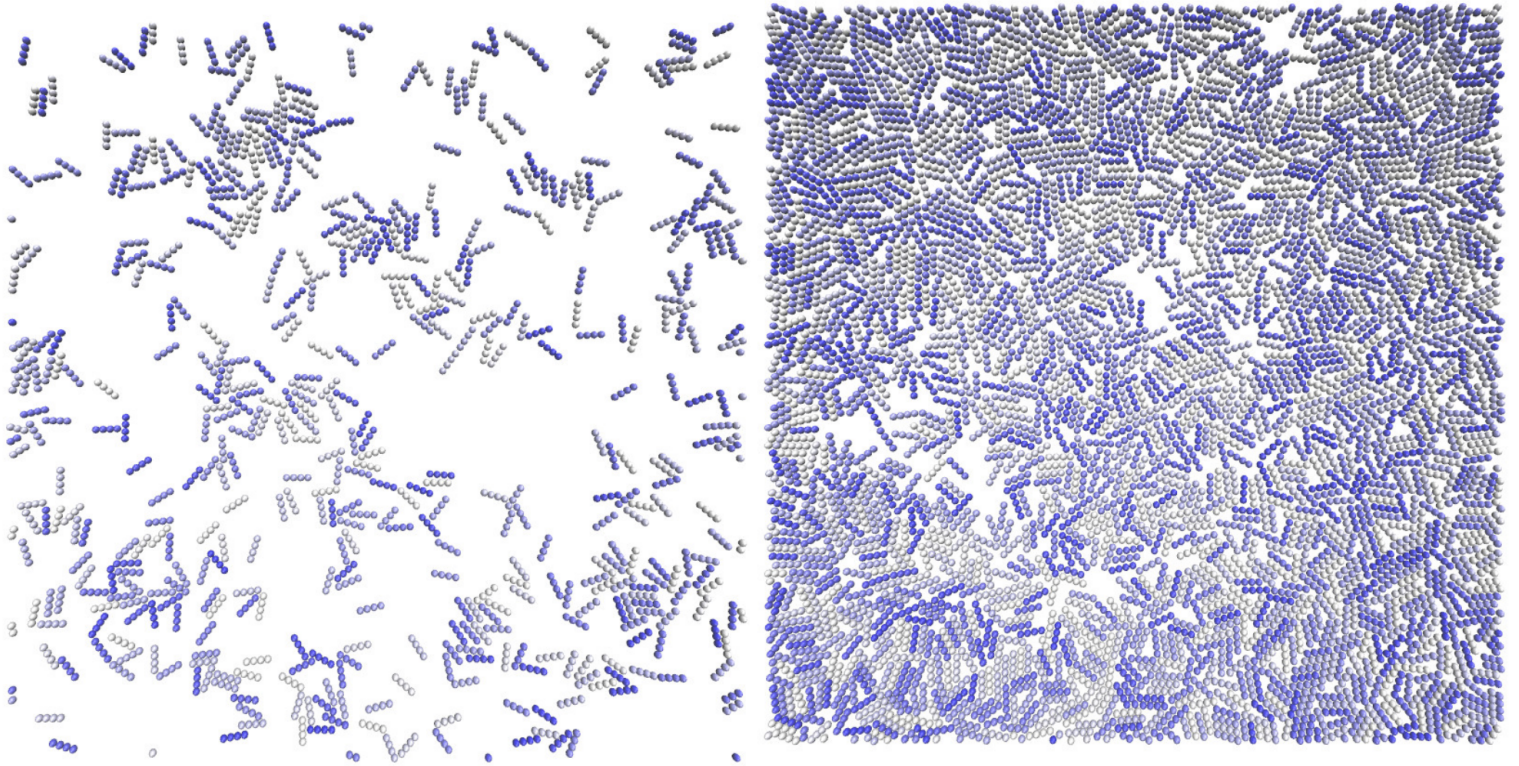


Figure 5.12: 500 and 2000 twitcher attachment twitchers in an area of 100 by 100 squared spatial units

Simulated TAM twitchers behave like SAM twitchers, except that they are also able to attach to each other. A comparison of 500 TAM twitchers and 2000 TAM twitchers can be seen in Figure 5.12. Like with SAM twitchers, TAM twitchers also exhibit collective motion as more twitchers are involved. Twitcher attachment enhances collective motion by allowing twitchers to attach to twitchers within collective packs.

JPM twitchers are conversely simplistic. Rather than using a pulling force like SAM and TAM twitchers, JPM twitchers are pushed forward with respect to the direction they face. This is unlike SAM twitchers and TAM twitchers, which move towards a specified point, and will attempt to force their way through other

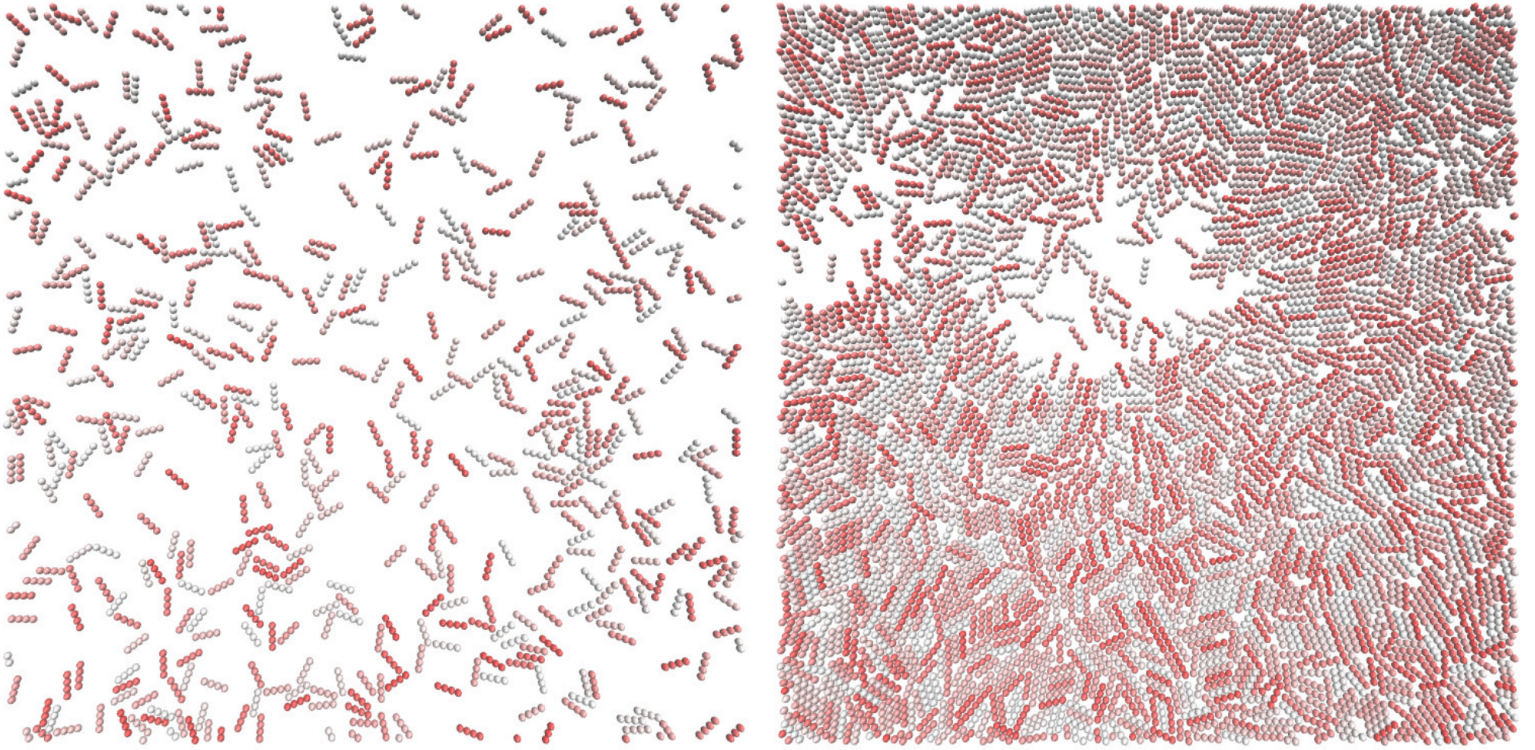


Figure 5.13: 500 and 2000 jetpack twitchers in an area of 100 by 100 squared spatial units

twitchers to do so. A comparison of 500 TAM twitchers and 2000 TAM twitchers can be seen in Figure 5.13. JPM twitchers also exhibit collective motion at high densities, but their behaviour is different from both attachment models. As JPM twitchers move with respect to the direction they face, it is possible for a twitcher to rotate quickly if space is available. More twitchers in the system results in less space for sharp turns.

5.2.1 Mean Squared Displacement Between Models

Figure 5.14 shows the relative MSD of TAM twitchers. The long term MSD shows a monotonic decreasing trend, where lower densities of twitchers are able to migrate across the surface more quickly than higher densities. These differences are more easily seen in 5.16.

Unlike with SAM twitchers (Figure 5.4), where MSD remains mostly consistent until the timescale reaches 10^3 , the MSD of TAM twitchers only remains consistent up until $3 \cdot 10^1$. This can be seen more easily in Figure 5.15.

As the number of twitchers increases, the time scale where the twitchers enters the diffusive regime increases. This is likely due to a combination of collective motion and twitcher attachment. While collective motion has a positive effect on MSD, twitcher attachment has a negative effect. This can be explained by Newton's third law - every action has an equal and opposite reaction. When a twitcher pulls at another twitcher, the two of them are pulled towards each other. The dummy acts like a rope attached to both twitchers, and the tension in the rope pulls the two twitchers together. This slows the progress of both twitchers. The attaching twitcher reaches its pilus more quickly as the twitchers are pulled towards each other. Likewise, the attached twitcher is pulled towards the attaching twitcher, slowing the attaching twitcher as it tries to move across the surface. While there is evidence of collective motion in TAM twitchers, it is not enough to increase the MSD of higher densities of twitchers beyond that of lower densities of twitchers. The effect of Newton's second law increases with the density of twitchers, as more twitchers means more chances for attachment to occur.

Figure 5.17 shows the relative MSD of JPM twitchers. Like with SAM twitchers, the JPM twitcher MSD diverges at 10^3 . It should be noted that there is an intersecting point between 10^2 and 10^3 where the behaviour changes.

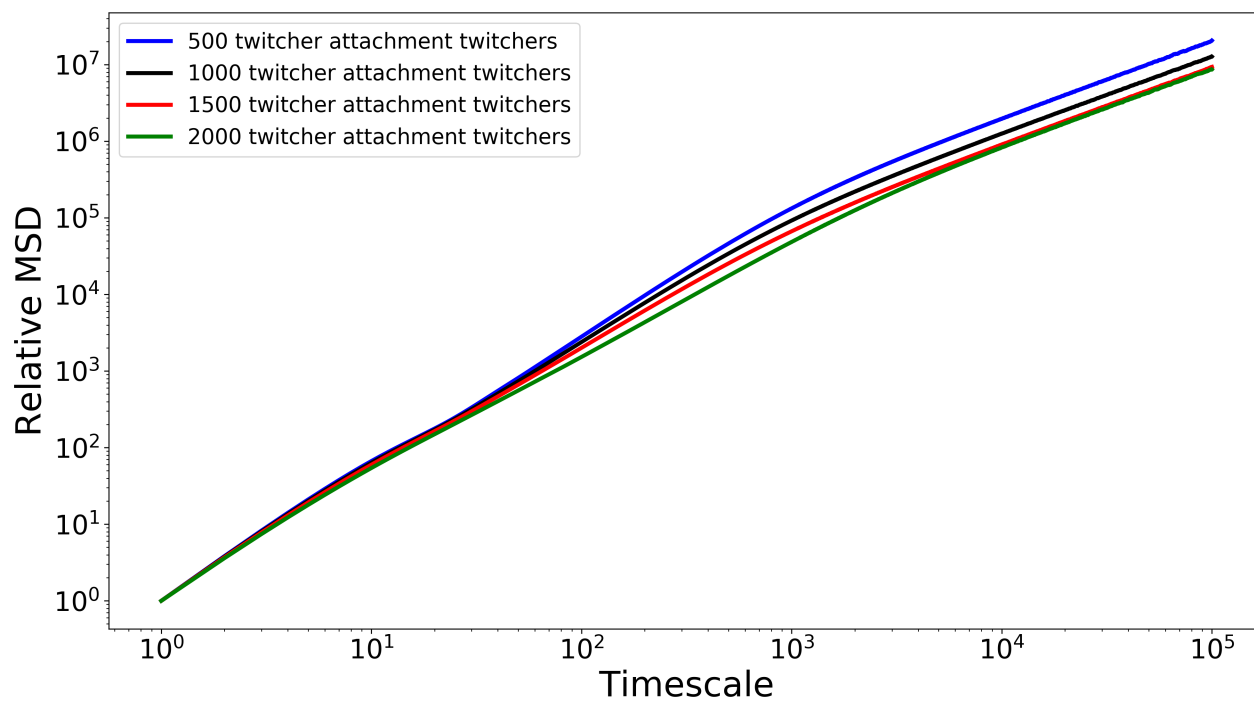


Figure 5.14: Relative mean squared displacement of TAM twitchers. Density increases from top to bottom.

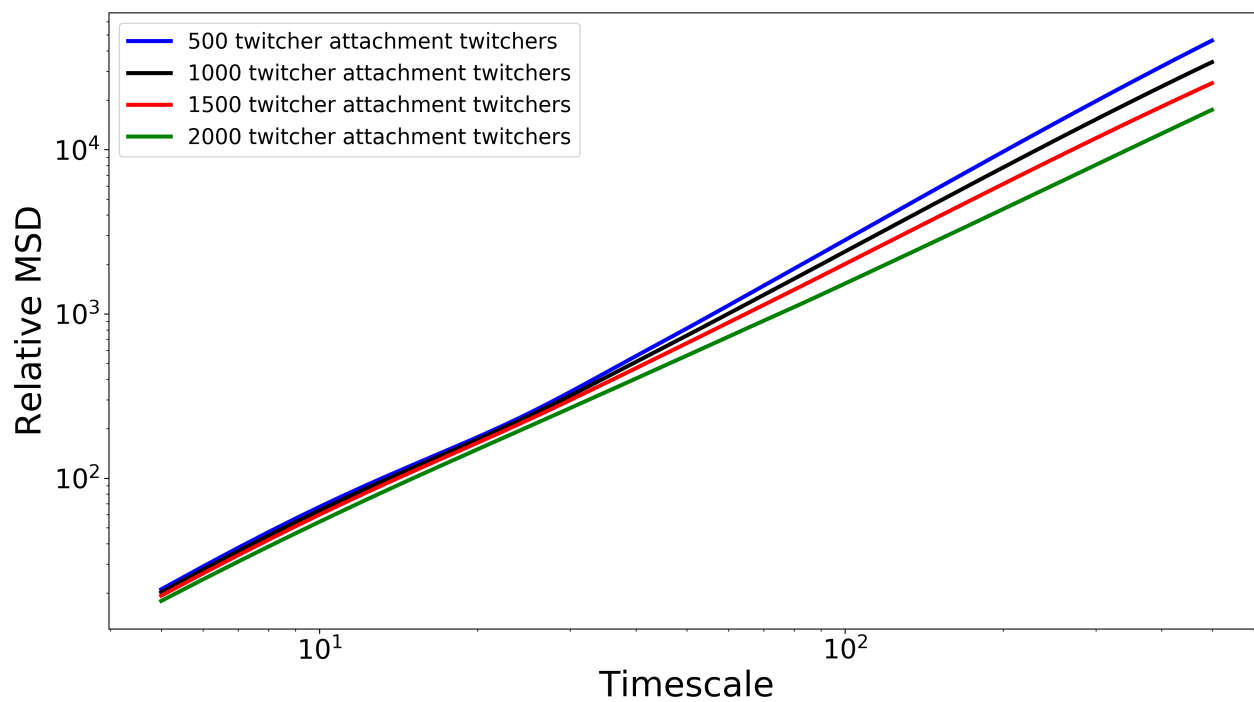


Figure 5.15: Relative mean squared displacement of TAM twitchers between timescales of $5 \cdot 10^0$ and $5 \cdot 10^2$. Density increases from top to bottom.

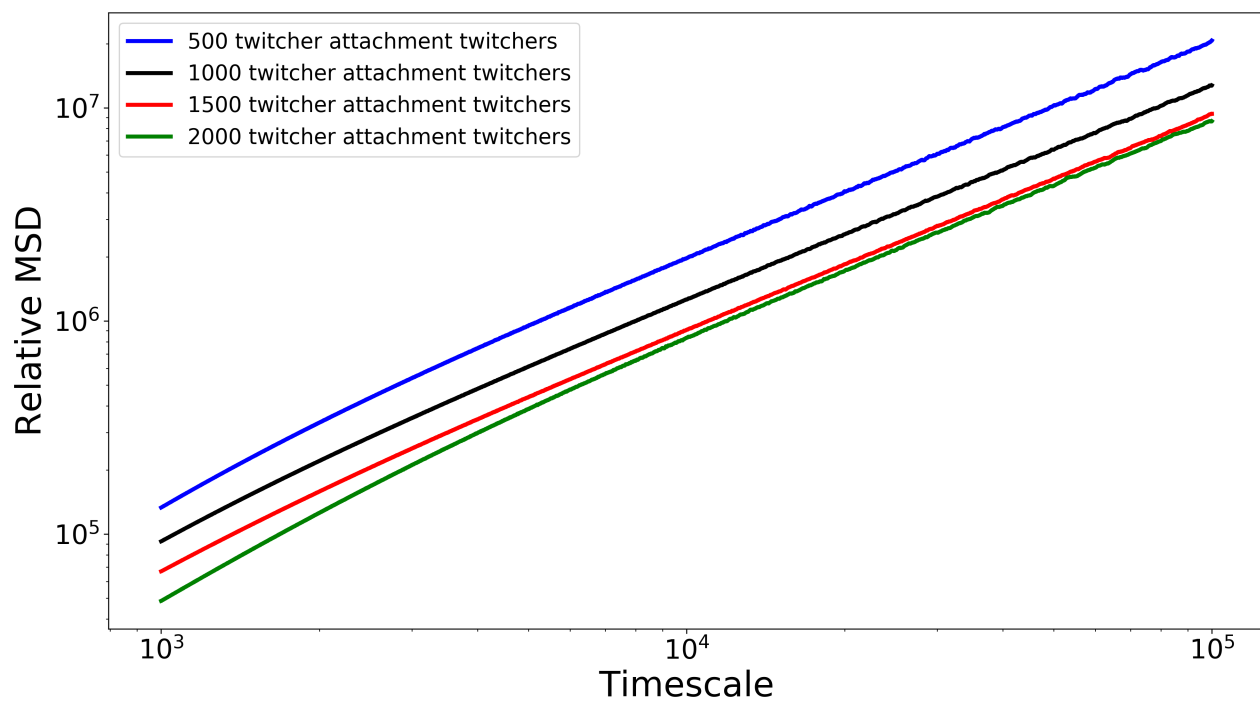


Figure 5.16: Relative mean squared displacement of TAM twitchers at time scale from 10^3 to 10^5 . Density increases from top to bottom.

This is more easily seen in Figure 5.18. At small time scales, lower densities of twitchers exhibit higher MSD. After $2 \cdot 10^2$, higher densities of twitchers begin to exhibit higher MSD. This is different from SAM twitchers, which begin to show drastic differences in their MSD a little below time scales of 10^3 .

Unlike SAM twitchers, which show non-monotonic MSD with increasing density, JPM shows monotonic increasing MSD at high time scales. This is easier to see in Figure 5.19. This is likely because jetpack motility enhances the occurrence of collective motion, as it facilitates nematic alignment. JPM twitchers always move with respect to the direction they are facing. If a twitcher is facing in the direction of other neighbouring twitchers, it will continue to move in that direction. As the density of twitchers increases, the chance of interacting with another twitcher increases as well. At higher densities, these packs of aligned twitchers occur more and more frequently. The resulting pockets of collectively moving twitchers increases the MSD of an individual twitcher. The non-monotonic behaviour exhibited by JPM twitchers occurs because JPM twitchers are capable of making sharp turns when enough space is available. These sharp turns reduce the MSD of JPM twitchers at low densities, but are less impactful as density increases.

5.2.2 Diffusion Between Models

Figure 5.20 shows the relative diffusion coefficients of all 3 tested models. SAM twitcher coefficients are shown in green triangles. The coefficients for SAM twitchers shown in Figure 5.20 match the coefficients shown in Figure 5.8. TAM twitcher coefficients are shown in blue squares. TAM twitchers exhibit monotonic decreasing diffusion as more twitchers are involved in the system. The inclusion of attachment in the model removes the non-monotonic behaviour present in SAM twitchers. While collective motion is present, the effect of New-

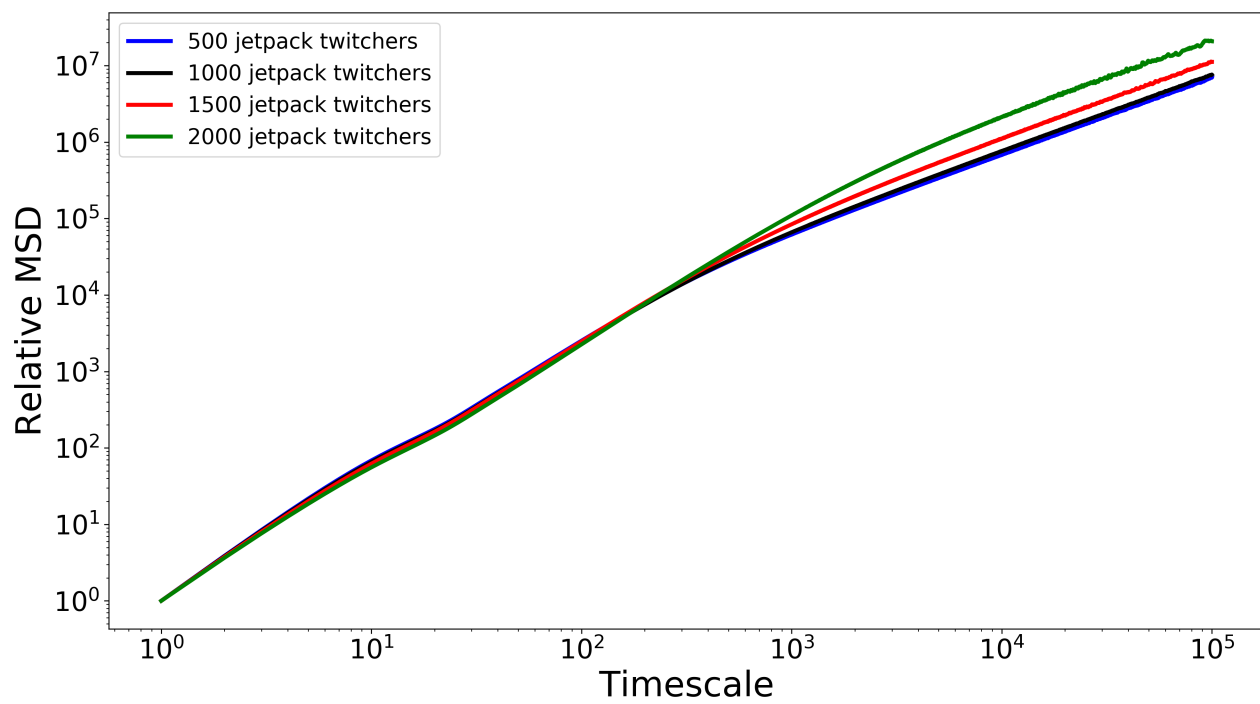


Figure 5.17: Relative mean squared displacement of JPM twitchers. Density increases from bottom to top.

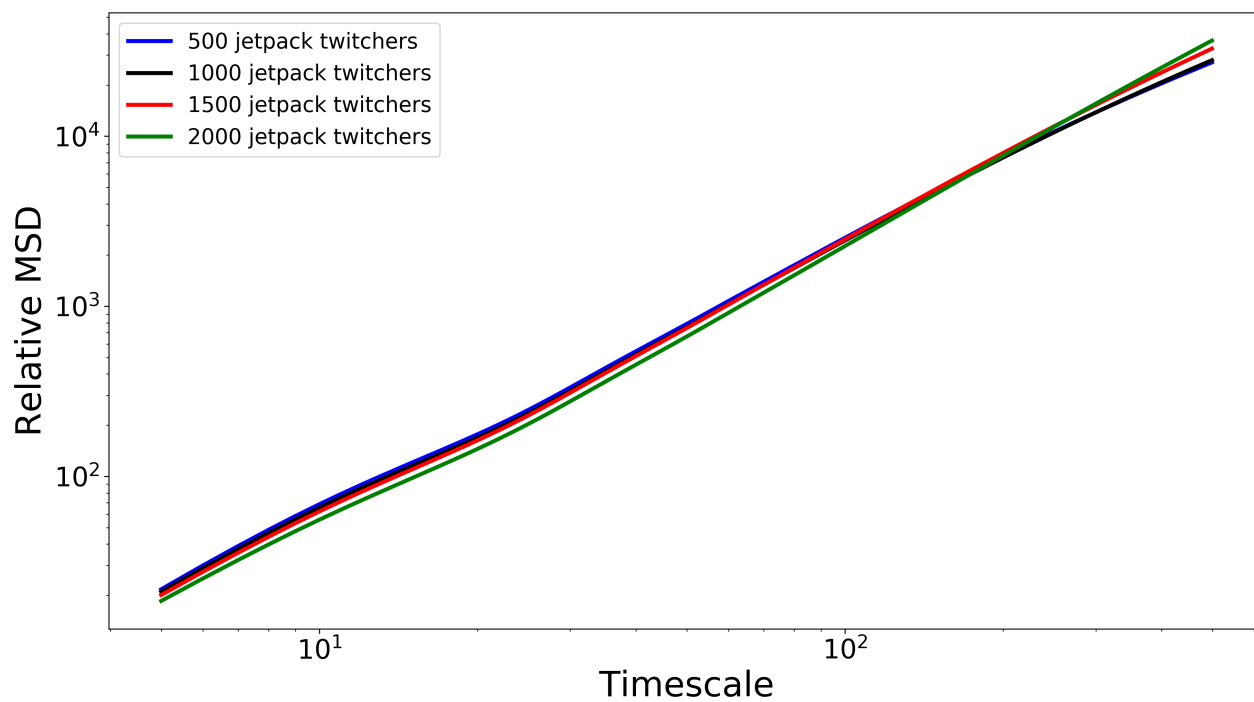


Figure 5.18: Relative mean squared displacement of JPM twitchers between timescales of $5 \cdot 10^0$ and $5 \cdot 10^2$. Density increases from bottom to top.

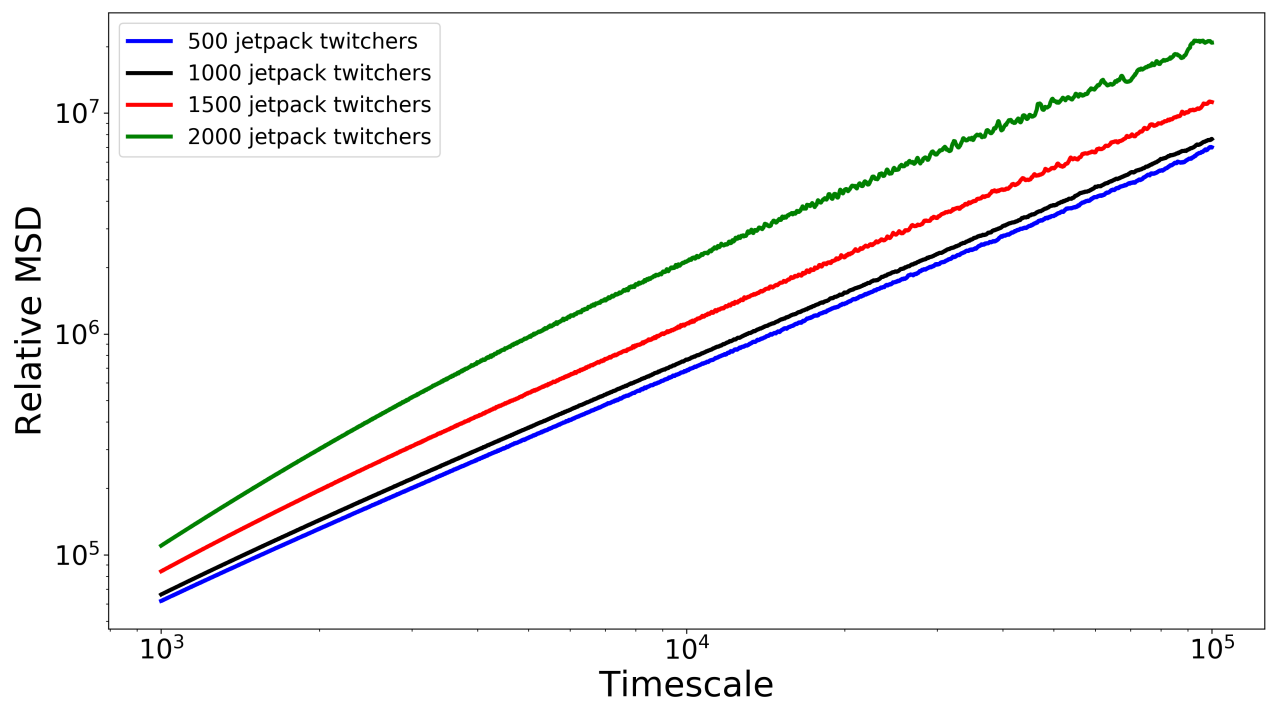


Figure 5.19: Relative mean squared displacement of JPM twitchers at time scale from 10^3 to 10^5 . Density increases from bottom to top.

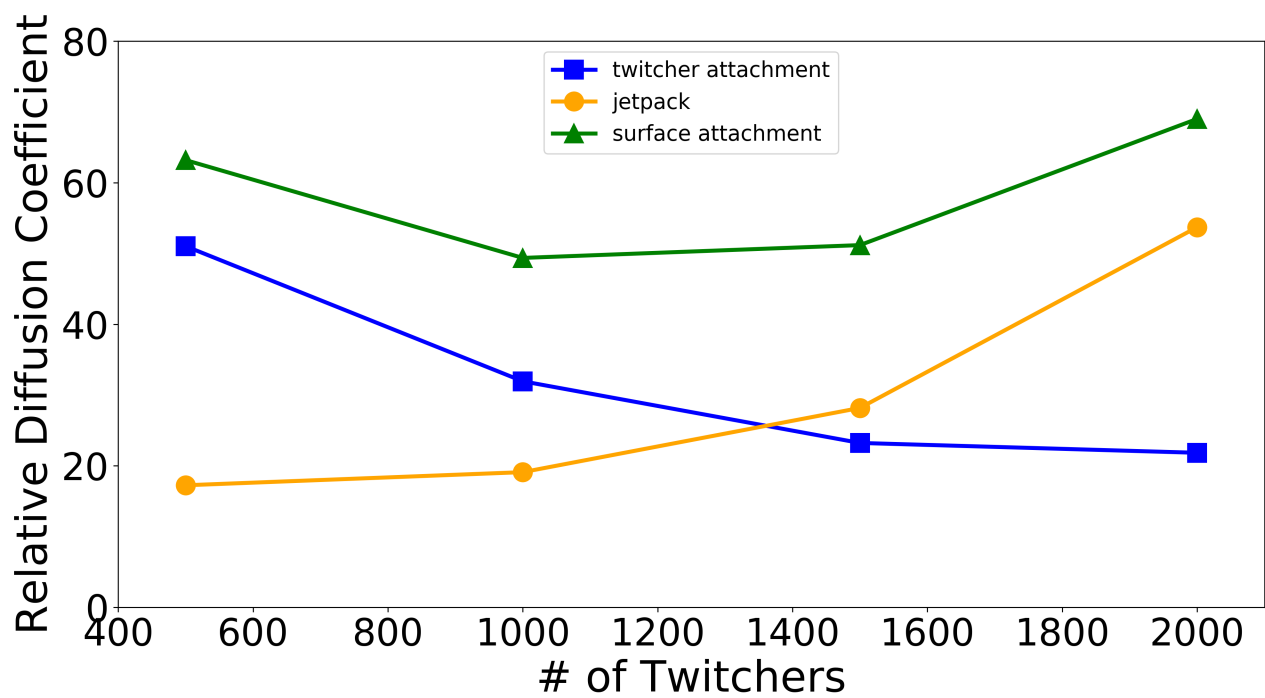


Figure 5.20: Relative diffusion coefficients of SAM twitchers, TAM twitchers, and JPM twitchers

ton's third law has a stronger effect on the diffusion of TAM twitchers, resulting in monotonic decreasing behaviour.

JPM twitchers are shown in orange circles. Unlike the other models, there is an overall increase in diffusion as more twitchers are included in the system. This is an effect of collective motion, and of the way that jetpack motility allows for sharp turns when space is available. As twitcher density increases, less space is available for sharp turns.

These results suggest collective motion in all three tested models. Analysis of VAC will further confirm this, as the direction of motion is more easily measured and analysed through VAC, rather than MSD and diffusion which measure the squared distance.

5.2.3 Velocity Autocorrelation of TAM and JPM Twitchers

Looking at the VAC of TAM twitchers (Figure 5.21) suggests the appearance of collective motion. At low densities (500), the VAC decays fairly quickly. These twitchers have access to the most free space, making it difficult for them to form collective units. The VAC decays more quickly as the density of twitchers increases to 1000 twitchers. More twitchers results in more collisions, which pushes a twitcher to face in another direction.

However, it is starting at a density of 1000 twitchers that something interesting becomes noticeable between 400 and 800 STUs. As time increases, the VAC decay decreases. This suggests that collective motion is enhanced by twitcher attachment, and that this effect is stronger after 400 STUs. Once collective units form, it is easy for a twitcher to attach itself to another member of a collective unit, enhancing collective motion and resulting in the change of decay rate. It is also possible for twitchers to join a collective unit by attaching them-

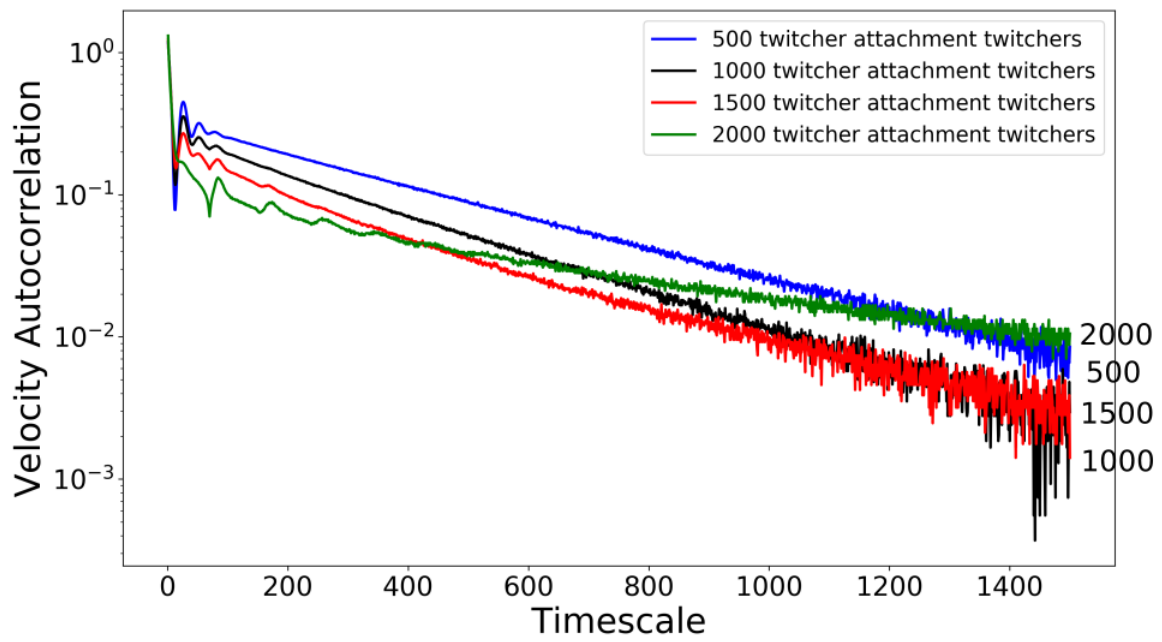


Figure 5.21: Relative Velocity Autocorrelation of TAM Twitchers

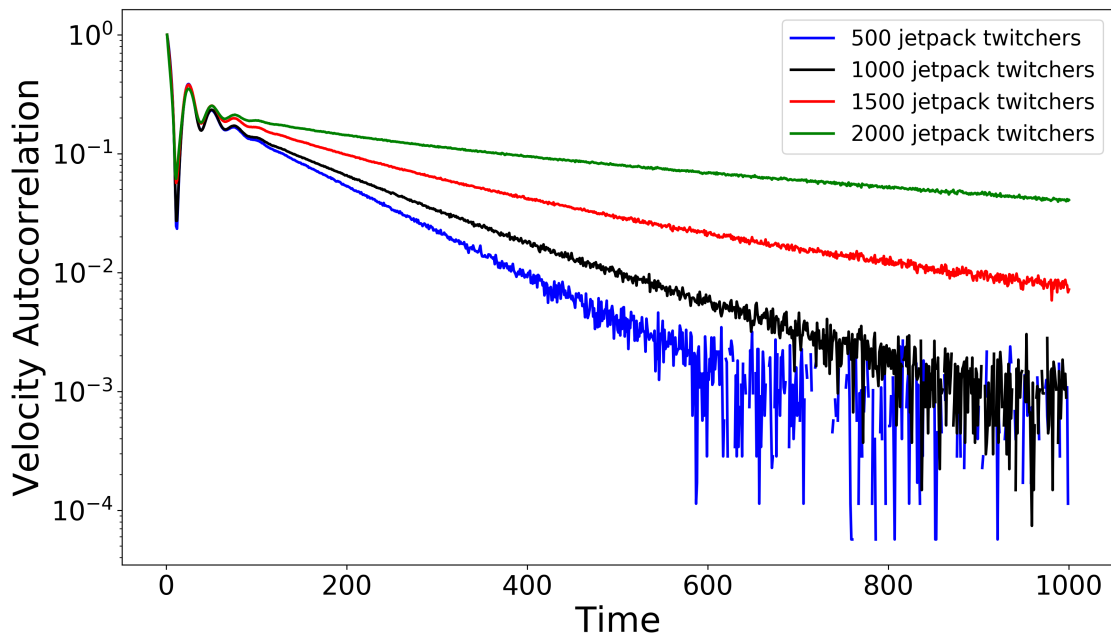


Figure 5.22: Relative velocity autocorrelation of JPM twitchers. Density increases from bottom to top.

selves to a twitcher in a collective unit and following that twitcher. This effect is more strongly noticed at higher densities of twitchers. The more twitchers there are in the system, the easier it is for a twitcher to attach itself to another. A twitcher in a collective will continue to attach itself to other twitchers in the collective. As such, an individual twitcher’s motion stays correlated over time. This result expands on the trend seen in Figure 5.20. Diffusion results show the presence of collective motion in TAM twitchers, but the effect is easier to see when looking at the VAC.

Figure 5.22 shows a more consistent trend in the VAC of JPM twitchers. As the density of twitchers increases, VAC decays more slowly. As before, this suggests that JPM motility facilitates collective motion through nematic

alignment. JPM twitchers are capable of very sharp turns if there is enough space. As more twitchers are in the system, more space is taken up, and it becomes increasingly more difficult for a JPM twitcher to turn sharply.

The magnitude differences in VAC between JPM twitchers and attachment twitchers (Figures 5.10 and 5.21) suggests another effect unique to JPM motility. At low densities, JPM twitchers have space to move around. Without neighbours to restrict their direction, a JPM twitcher can propel itself forward with 45 degrees to either side of the direction it is face. Once an angle is chosen, the JPM continues to move in the chosen angle relative to the direction it faces until it enters rest. This means that if a twitcher selects a high angle, it is able to rotate very quickly. These sharp turns have a strong impact on VAC decay. This is unlike attachment twitchers, as they attach to a point on the surface or to a twitcher, and move towards that point until entering the rest phase. As the density increases, twitchers have less space to move around. Since twitchers cannot pass through each other, it becomes harder and harder for twitchers to rotate as density increases.

5.2.4 Characteristic Decay Time

Figure 5.23 shows the characteristic decay times for all three models of twitchers. This plot shares many similarities with Figure 5.20, showing non-monotonic behaviour from SAM twitchers and monotonic increasing behaviour from JPM twitchers.

The main difference is that TAM twitchers exhibit non-monotonic behaviour with respect to twitcher density. As twitcher density increases from 500 to 1500, the characteristic decay time decreases. However, when the density increases to 2000 twitchers, the decay time increases, suggesting the occurrence of collective motion at higher densities. This is quite different from Figure 5.20, where the

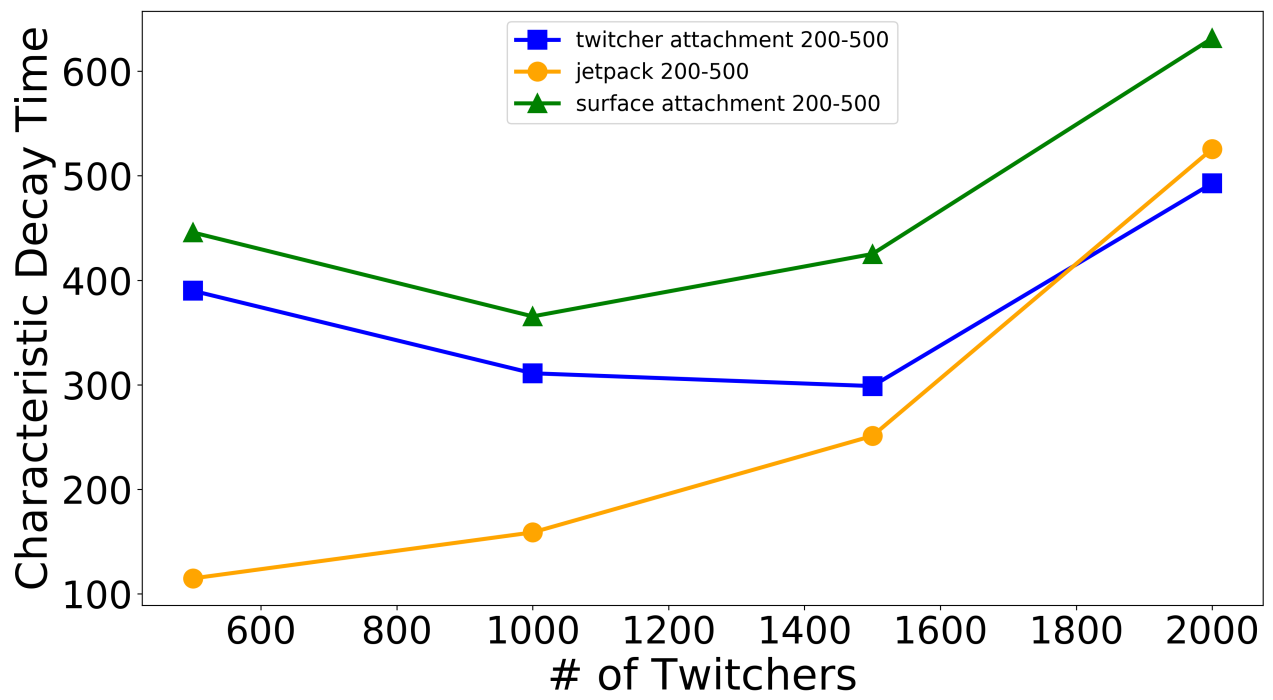


Figure 5.23: Characteristic decay times of SAM twitchers (green), TAM twitchers (blue), and JPM twitchers (orange)

diffusion coefficient of TAM decreases consistently with twitcher density. These differences are present because MSD analysis reduces the effects of changes in the direction of motion, where VAC does not. TAM twitchers inside of a collective maintain their direction of motion by attaching themselves to other twitchers inside of a collective. As more twitchers are added to the system, more opportunities for attachment occur.

The effects of changes in the direction of motion are also felt strongly when observing JPM twitchers. At low densities, the presence of free space allows for a JPM twitcher to make sharp turns. These sharp turns result in an increased decay in the VAC, resulting in a shorter decay time. As more twitchers are present in the system, less free space is available, and it becomes increasingly more difficult for twitchers to make sharp turns.

5.3 Summary

This thesis outlines and studies the behaviour of three physically relevant models. SAM twitchers use a dummy particle to simulate twitching motility using T4P. TAM twitchers include the ability for twitchers to attach to each other, making the model more relevant to living biology. TAM twitchers also take into consideration the surface available for surface attachment, as more twitchers means less surface is available. JPM twitchers most closely resemble simulations of rod-like swimmers, making for easier comparison between simulated twitchers and simulated swimmers.

The results in the above chapter suggest that all three models allow for the onset of collective motion at high twitcher densities. This collective behaviour is emergent, occurring naturally due to the effects of excluded volume. However, it is still worth noting that each model has its own distinct behaviour.

SAM twitchers exhibit non-monotonic behaviour in MSD, diffusion, and

VAC. This is the result of the competing effects of twitcher collisions at low densities and collective motion at high densities. TAM twitchers add the effects of twitcher attachment, with Newton's second law emerging as a result of twitcher attachment. While Newton's third law slows twitchers down and reduces MSD and diffusion as twitcher density increases, VAC results suggest that twitcher attachment enhances collective motion as twitchers are able to attach to each other within a collective. Twitcher attachment makes it easier for twitchers to enter collective packs, and to maintain collective motion.

JPM show consistent, monotonically increasing trends in MSD, diffusion, and VAC. JPM twitchers always move with respect to the direction they are facing. This means that JPM twitchers in a collective more easily stay in a collective, as they are restricted in the direction they are facing by their aligned neighbours. At low densities, JPM motility hinders MSD and VAC because of the sharp turns that JPM twitchers can take. As density increases, JPM twitchers have less room to make sharp turns, and collective motion emerges.

Chapter 6

Results - Phytoglycogen

Nanoparticles

6.1 Interactions between Amylopectin Chains

Simulations consist of 9 or 50 repeatable branching units (RBUs) in order to see how they will interact with each other over a 20 ns period of time. As time progresses, RBUs come closer together. This can be seen by comparing the initial and final structures (Figure 4.11 with Figure 6.1 and Figure 4.12 with Figure 6.2). Many of the interactions between RBUs appear to be long-lasting. In Figure 6.2 towards the top right corner, it is possible to see two RBUs (one red and one purple) that have formed a double-helix configuration.

Figure 6.3 shows the potential energy of the system, and demonstrates that the final structure is in a more stable configuration than the initial structure. As time passes, the potential energy of the system decreases. Lower potential energy represents a more stable system. That said, it is not possible to say if the final structure is in equilibrium.

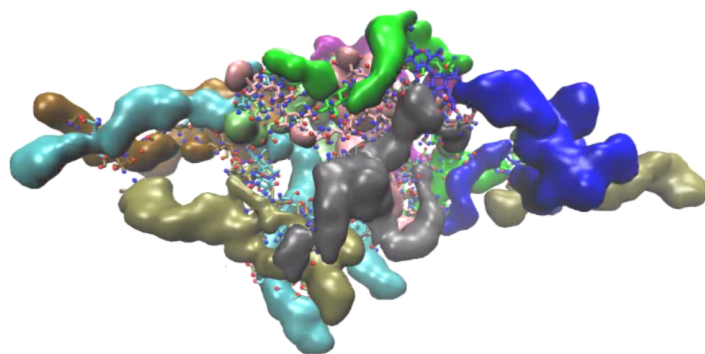


Figure 6.1: Surface plot of 9 RBUs after 20 nanoseconds

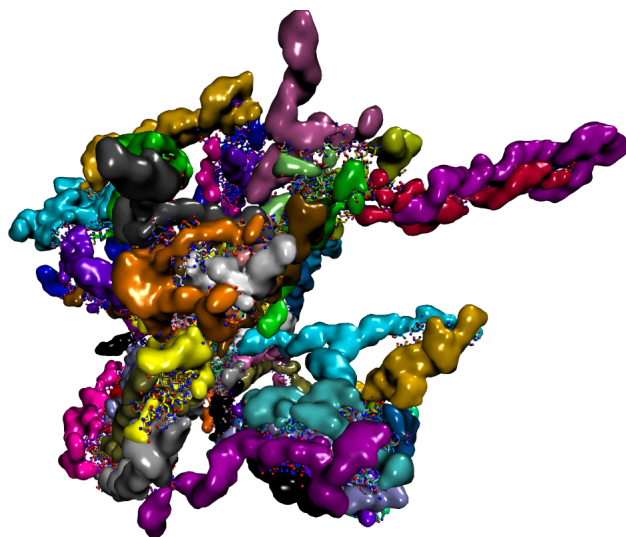


Figure 6.2: Surface plot of 50 RBUs after 20 nanoseconds

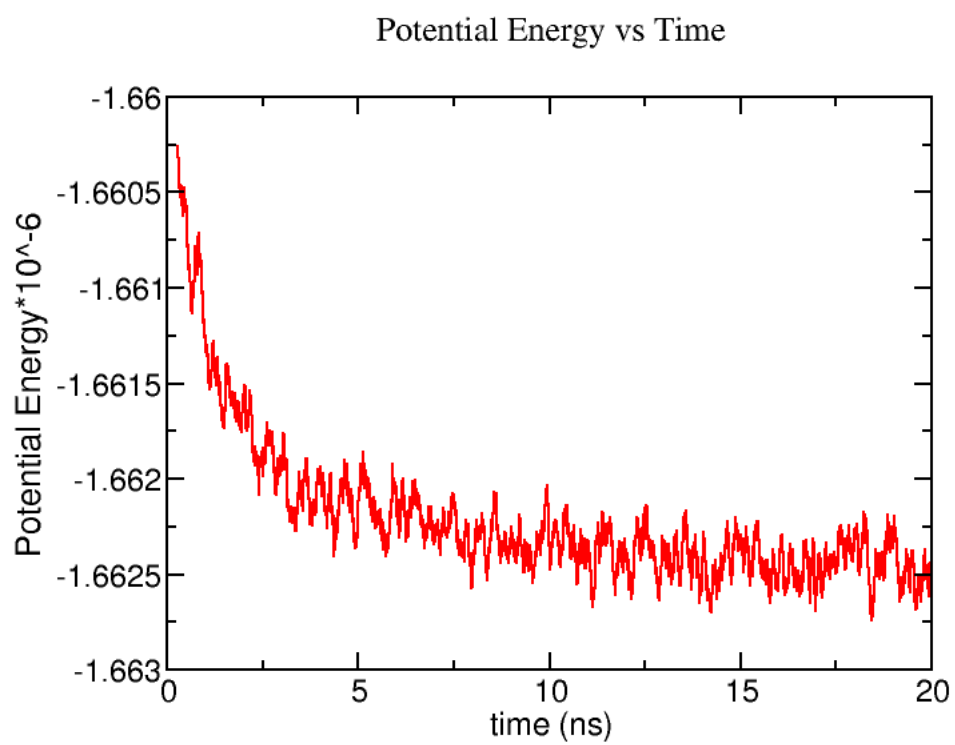


Figure 6.3: Potential Energy of the 50 RBU system over time

A zoomed in version of the 50 RBU system after 20 nanoseconds can be seen in Figure 6.4, allowing for easier observation of the interactions between chains. Hydrogen atoms bound to carbon are shown as blue, while hydrogen atoms bound to oxygen are shown as red. The interactions between chains are hydrophobic in nature, as shown by the way that the blue hydrogen atoms face each other and away from water. Red hydrogen atoms have a tendency to face outward towards water. This suggests that the entire structure is formed through a combination of hydrophobic and hydrophilic effects. While chains are held together hydrophobically, the hydrophilic nature of glucose allows for the formation of water pockets. This tendency for hydrophobic hydrogens to avoid water is called the hydrophobic effect.

The nature and extensiveness of the hydrophobic interactions can be seen when looking at isolated chains within the entire system. Figure 6.5 shows an interaction between two chains in a 9 RBU system. By isolating these chains, it is easier to see just how extensive the interactions between the two chains can be. The interactions holding these chains together appear to be hydrophobic in nature, as demonstrated by the blue hydrogen atoms facing each other.

A water pocket can be seen in Figure 6.6. The fragments come from the same chains that were shown in Figure 6.5. While the two chains are held together via hydrophobic interactions, water can be seen away from the interacting hydrophobic regions.

6.2 Hydration of 9 RBU System

We analysed the water retention of the 9 RBU system by counting the number of water molecules present within a range of distances from 1 to 20 Ångstroms away from an RBU. Figure 6.7 shows the final structure of a 9 RBU system, with visible water within 4 Ångstroms of the structure.

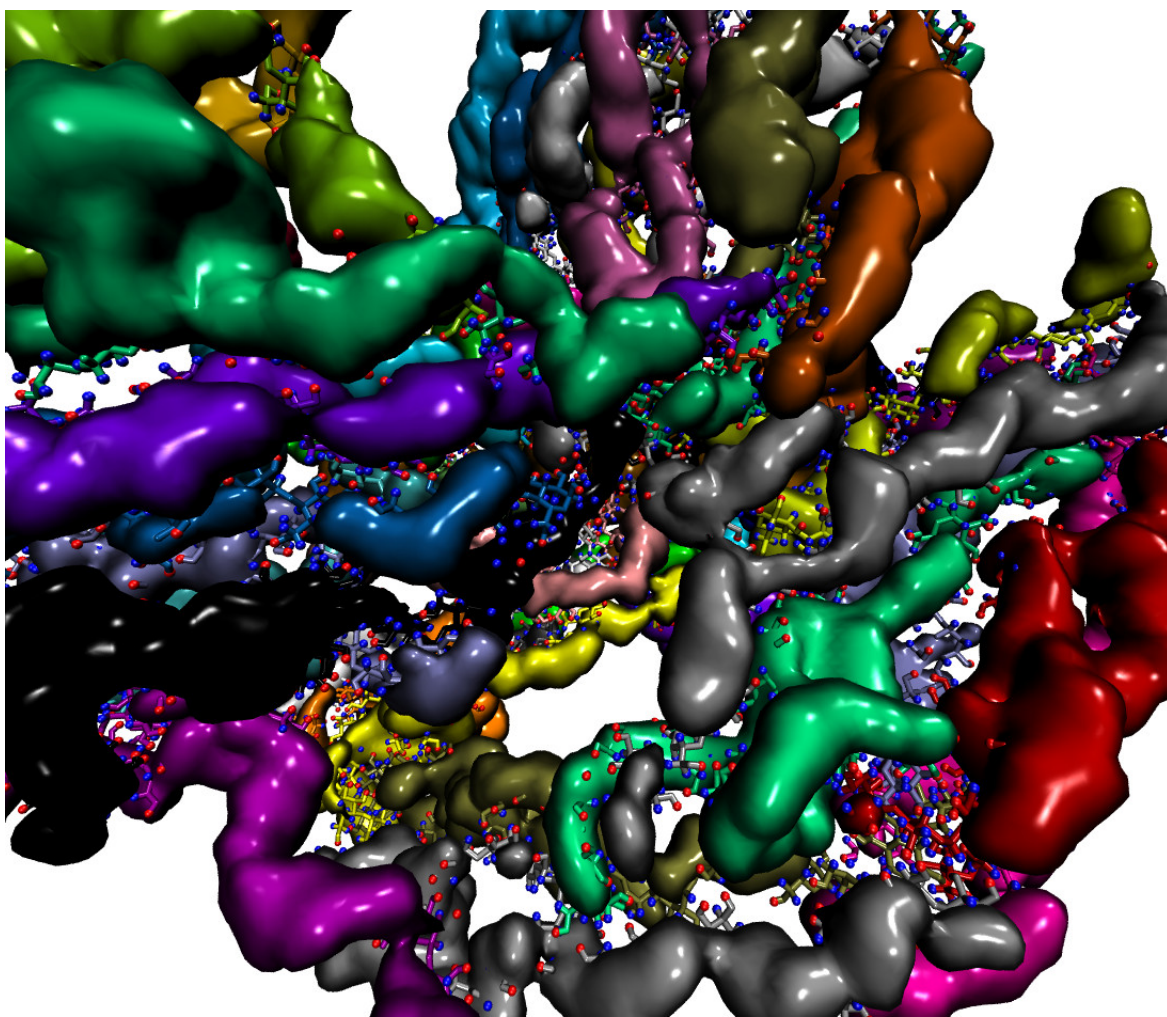


Figure 6.4: Snapshot of 50 RBU system after 20 nanoseconds



Figure 6.5: Snapshot of two chains interacting with each other - isolated from a 9 RBU system

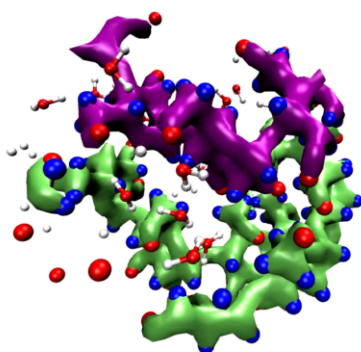


Figure 6.6: Snapshot of fragments of two chains forming a water pocket - 9 RBU system

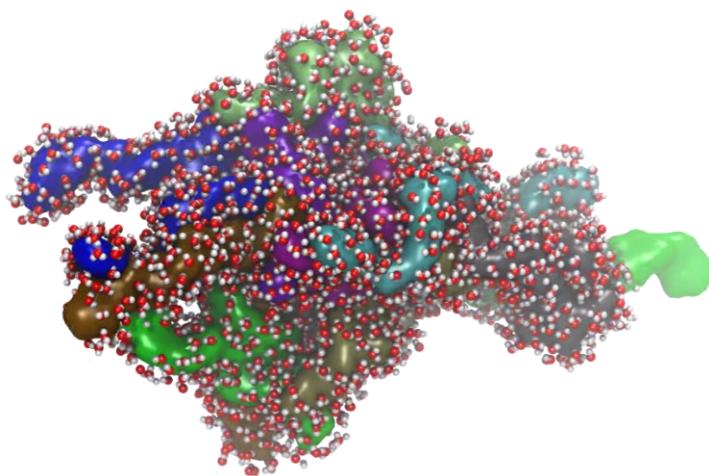


Figure 6.7: Final configuration of a 9 RBU system with visible water

The resulting number of water molecules is then normalized by 270 - this is the product of 30 glucose molecules per RBU and 9 RBUs in the system. Figure 6.8 shows the number of water molecules per glucose within the specified range. At a distance of 9 Ångstroms, a result of 21 water molecules per glucose is obtained. This result is consistent with results obtained in experiment, which suggest that the PhytoSpherixTM compound retains 22.5 water molecules per glucose [35]. However, the calculations conducted here are rough, conducted by counting oxygen molecules that make up the surrounding water. Further analysis is needed to confirm experimental results. This can be done by counting entire water molecules to potentially count water molecules that would have been missed. It is also necessary to determine how water is interacting with the RBUs by considering the conformation of water as it approaches an RBU.

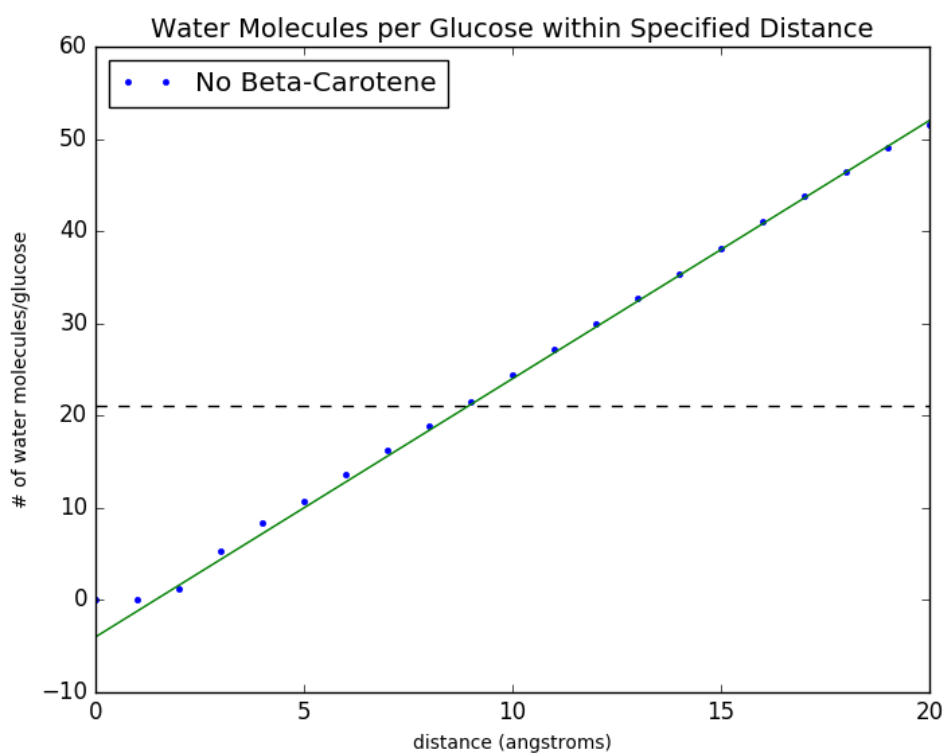


Figure 6.8: Water molecules per glucose molecule for a 9 RBU system

6.3 Beta-Carotene - Interactions Within a 9 RBU System

Mirexus is interested in determining how beta-carotene is able to interact with PhytoSpherix™, as they interact quite tightly according to their experiments. In Figure 6.9, the molecule of beta-carotene (orange) can be seen in a pocket formed by the RBUs. These interactions are hydrophobic, as the beta-carotene is interacting with hydrophobic hydrogen atoms (white bound to teal), and is hiding from water as much as possible.

Results from Mirexus are consistent with these findings, showing that beta-carotene interacts strongly with the PhytoSpherix™ compound. Mirexus is interested in using the PhytoSpherix™ compound for biomedical purposes. The idea is that PhytoSpherix™ could be used as a carrier for medicinal compounds. The results shown here suggest that PhytoSpherix™ could be used to carry beta-carotene. It is possible that these results could be extrapolated to apply to similar hydrocarbons, but further research would be required to determine if PhytoSpherix™ could be used to carry compounds with different properties.

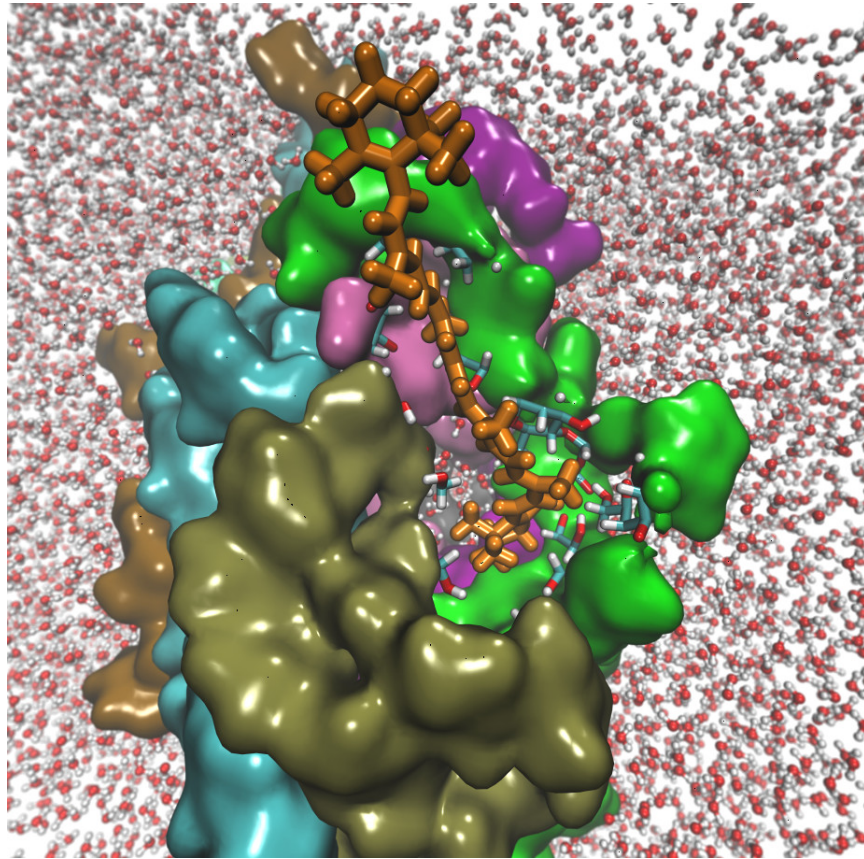


Figure 6.9: Final configuration of 9 RBUs in the presence of beta-carotene (orange)

Chapter 7

Discussion

7.1 Twitching Bacteria

This thesis outlines three distinct yet similar models of twitching bacteria, and shows that collective motion emerges naturally at high twitcher densities. As more twitchers are added beyond a certain threshold, twitchers form collective pockets and align with each other, thus facilitating collective motion. While this was already known to be the case for rod-like swimmers, confirmation was required for twitchers, as the cycle of motion and rest is a key component of twitching motility that is ignored by simulations of swimmers.

These results are comparable to rod-like swimmers studied by Balagam and Igoshin (2015) [57], who studied self-propelled rods inspired by *Myxococcus xanthus*. Here, *Myxococcus xanthus* is modelled as 7 spheres connected by springs and held in a rod-like configuration [57]. As the density of cells increases, rod-like swimmers come into alignment and form larger clusters [57]. Balagam and Igoshin have also implemented two features that we are interested in implementing. The first is the implementation of periodic reversals (discussed in section

2.1.5.2), which are reported to disrupt the formation of aligned clusters [57]. The second is the implementation of the extracellular polysaccharide trail (discussed in section 2.1.5.3), which facilitates the formation of aligned clusters even when periodic reversals are implemented [57].

The JPM would be most comparable with rod-like swimmers, but their allowance for particularly sharp turns makes comparison difficult. Conversely, the self propelled rods in simulations conducted by Peruani et al. (2008) [21] are propelled with a force that pushes the rod along the long axis. Peruani et al. suggest that these aligned rod-like swimmers are able to form clusters, and that their ability to form clusters is enhanced by increasing the number of rods and by increasing the length of rods [21].

It is important to note that the twitchers simulated here are modelled to be minimalistic in nature, and thus do not necessarily compare well with twitching bacteria. This becomes very clear when watching videos of twitching bacteria and comparing them with simulated rod-like twitchers. Twitching bacteria include various features that enhance collective motion - these features are covered in section 2.1.5. It should also be noted that since twitching motility is a highly social behaviour and dependent on cell-to-cell communication, lone bacteria do not undergo twitching motility [30]. This is unlike simulated rod-like twitchers, which continuously apply their motility cycle regardless of the presence of neighbours. The models used in this thesis can be modified to more closely resemble twitching bacteria, but this should be conducted in such a way that each new feature would be tested and implemented individually.

7.2 Phytoglycogen Nanoparticles

Results in this thesis suggest that the structure formed by interacting RBUs comes about from a mix of hydrophobic and hydrophilic interactions. Hydropho-

bic interactions allow for RBUs to form extensive interactions with each other, while hydrophilic interactions allow for the formation of water pockets. These interactions suggest that amylopectin branches are amphiphilic - able to interact with polar and non-polar compounds. These results are consistent with data provide by Mirexus, which suggests that PhytoSpherixTM is able to interact with hydrophobic and hydrophilic compounds. The way that PhytoSpherixTM interacted with beta-carotene was a surprise to Mirexus until atomistic simulations were conducted and the nature of the interactions between amylopectin was confirmed.

There is work to suggest that amylopectin could be modified to be amphiphilic [58] [59]. Both of these bodies of work suggest that polysaccharides with hydrophobic modifications can be used as a nanovehicle to deliver medicine.

It is important to note that the atomistic simulations here are not completely comparable with phytoglycogen. The PhytoSpherixTM compound is a single compound consisting of 22,000 glucose molecules. Even with 50 RBUs, simulations conducted here only reach 1500 glucose molecules separated into loose chains. This may be equivalent to the surface of the phytoglycogen structure, where loose chains may come in contact with each other.

Additional simulations of the PhytoSpherixTM have been conducted in the cNAB.LAB at a variety of different scales. These simulations range from the coarse-grained scale where individual glucose molecules are modelled as a sphere, to atomistic simulations of a smaller phytoglycogen particle. The combination of simulations at different scales will be useful in better understanding phytoglycogen nanoparticles, which will lead to new applications.

Chapter 8

Conclusion

This thesis outlines how molecular dynamics techniques were used to garner insight on two very different biological systems. Where one system functions on the microscale, studying the collective behaviour of bacteria, the other functions on the nanoscale, studying the structural features of phytoglycogen.

8.1 Summary - Twitching Bacteria

Through the implementation of simple rules, it is possible to produce rod-like twitchers that move in a collective manner. This collective behaviour enhances the motion of twitchers, allowing them to traverse across territory and colonize it at a quicker rate.

SAM twitchers exhibit the competing effects of colliding twitchers and collective motion. At first, more twitchers in the system results in collisions that disrupt individualistic motion. Beyond a certain threshold, collective motion enhances twitching motility.

TAM twitchers include the collective behaviour and collisions, but also add twitcher attachment. This attachment reduces overall progress, as Newton's

third law pulls back at the progress of leading twitchers. However, as collective packs form, collective motion is enhanced by twitcher attachment. Twitcher attachment makes it easier for twitchers to follow each other, as the attaching twitcher moves in the direction of the twitcher it attaches to.

JPM twitchers also exhibit collective motion, but in a manner that is different from the other models. In this instance, more twitchers universally leads to more collective behaviour. As twitchers form collectives, their direction of motion becomes particularly restricted as JPM twitchers always move with respect to the direction they face. This is different from attachment twitchers, which attach to a point on the surface or another twitcher, and move towards that point for a whole cycle.

8.2 Summary - Phytyglycogen Nanoparticles

Qualitative analysis of amylopectin shows that interesting structures can be formed as RBUs interact with each other. We believe this to be due to a combination of hydrophobic and hydrophilic effects, based on the orientation of hydrophobic and hydrophilic hydrogen atoms, and based on the way that these structures interact with hydrophobic structures such as beta-carotene. This hydrophobic effect explains many of the interactions that occur between the PhytoSpherixTM particles and others, as well as understanding the intermolecular interactions that occur within the compound. However, quantitative analysis will be necessary in order to gain more insight on PhytoSpherixTM. This could be done by counting the interactions between chains, and confirming the nature of these interactions by considering the orientation of the atomic structure, and by considering the distance of interacting particles. For example, hydrogen bonds occur when partially charged hydrogen faces partially charged oxygen, nitrogen, or fluorine in a linear configuration.

8.3 Future Work

Twitchers simulated in the work covered in this thesis are simple and rudimentary. These twitchers are lacking in various biological considerations that were previously covered in the literature review section. In order to gain a better insight on living bacteria, it will be necessary to model these features.

Twitcher attachment will require more tuning. As is, twitchers are able to attach to each other too easily. Too much attachment results in inhibited motion. However, it is possible that just the right amount of attachment to other twitchers can help to guide their motion and enhance collective behaviour.

Cell-to-cell communication could be modelled by implementing a feature like the Vicsek model. As it is, the Vicsek model is insufficient, as it applies to point particles. Modifications will be required in order to apply Vicsek-like motility to rods, as their directionality must be properly considered. Vicsek model particles are point particles with no inherent directionality. If something like the Vicsek model is to be considered for rod-like twitchers, directional changes must be implemented so that a rod slowly turns to move in the direction that its neighbours are moving.

To simulate the effects of agar, we could use spheres attached to springs that the twitchers will have to tunnel under. These springs inhibit the motion of spheres, and the thickness of the agar can be modelled by increasing the spring constant.

A surfactant trail could be implemented by using a list to keep track of each position of the system. Modifications can be made to variables that relate to motility, or new checks can be added in order to make twitching easier across already visited surface. For example, a surface attachment probability could be included, with a higher chance of attachment occurring when the dummy lands on already visited terrain.

Regarding research on PhytoSpherix™, more thorough quantitative analysis is required in order to better understand the interactions occurring between RBUs. This can be done by analysing the proximity and orientation of hydrogen atoms of distinct RBUs with respect to each other. Hydrophobic hydrogen atoms of nearby RBUs should be in close proximity. At the same time, analysis would be conducted on RBU hydrogen atoms with respect to water. Hydrophilic hydrogen atoms should be in close proximity to water, while hydrophilic RBUs should be farther away from water.

Similar analysis could be conducted on medicinal and supplemental compounds like beta-carotene. If beta-carotene is interacting via hydrophobic interactions, it should be close to hydrophobic hydrogen atoms.

Bibliography

- [1] R Marathe, C Meel, NC Schmidt, L Dewenter, R Kurre, L Greune, AM Schmidt, MJI Muller, R Lipowsky, B Maier, S Klumpp “Bacterial twitching motility is coordinated by a two-dimensional tug-of-war with directional memory.” *Nature Communications*, 5, 3759, 1-10 (2014)
- [2] B Maier, L Potter, M So, HS Seifert, MP Sheetz “Single pilus motor force exceed 100pN.” *Proceedings of the National Academy of Science of the United States of America*, 99, 25, 16012-16017 (2002)
- [3] W Wu, Y Jin, F Bai, S Jin “Chapter 41 - *Pseudomonas aeruginosa*” *Molecular Medical Microbiology (Second Edition)*, 2, 753-767 (2015)
- [4] K Poole “*Pseudomonas aeruginosa*: resistance to the max” *Frontiers in Microbiology*, 2, 65, 1-13
- [5] RN Jones, MG Stilwell, PR Rhomberg, SH Sader “Antipseudomonal activity of piperacillin/tazobactam: more than a decade of experience from the SENTRY Antimicrobial Surveillance Program (1997-2007)” *Diagnostic Microbiology and Infectious Disease*, 65, 3, 331-334 (2009)
- [6] A Kainuma, K Momiyama, T Kimura, K Akiyama, K Inoue, Y Naito, M Kinoshita, M Shimizu, H Kato, N Shime, N Fujita, T Sawa “An outbreak

- of fluoroquinolone-resistant *Pseudomonas aeruginosa* ST357 harboring the *exoU* gene” *Journal of Infection and Chemotherapy*, 24, 615-622 (2018)
- [7] W Chiang, M Nilsson, P Jensen, N Hiby, TE Nielsen, M Givskov, T Tolker-Nielsen “Extracellular DNA shields against aminoglycosides in *Pseudomonas aeruginosa* Biofilms” *Antimicrobial Agents and Chemotherapy*, 57, 5, 2352-2361 (2013)
- [8] D Landman, S Bratu, M Alam, J Quale “Citywide emergence of *Pseudomonas aeruginosa* strains with reduced susceptibility to polymyxin B” *Journal of Antimicrobial Chemotherapy*, 55, 954-957 (2005)
- [9] HK Johansen, SM Moskowitz, O Ciofu, T Pressler, N Hiby “Spread of colistin resistant non-mucoid *Pseudomonas aeruginosa* among chronically infected Danish cystic fibrosis patients” *Journal of Cystic Fibrosis*, 7, 391-397 (2008)
- [10] S Campana, G Taccetti, N Ravenni, I Masi, S Audino, B Sisi, T Repetto, G Do ring, M de Martino “Molecular epidemiology of *Pseudomonas aeruginosa*, *Burkholderia cepacia* complex and methicillin-resistant *Staphylococcus aureus* in a cystic fibrosis center” *Journal of Cystic Fibrosis*, 3, 159-163 (2004)
- [11] S Moreau-Marquis, BA Stanton, GA O’Toole “*Pseudomonas aeruginosa* biofilm formation in the cystic fibrosis airway” *Pulmonary Pharmacology and Therapeutics*, 21, 595-599 (2008)
- [12] P Stoodley, K Sauer, DG Davies, JW Costerton “Biofilms as complex differentiated communities” *Annual Review of Microbiology*, 56, 187-209 (2002)
- [13] KM Colvin, Y Irie, CS Tart, R Urbano, JC Whitney, C Ryder, PL Howell, DJ Wozniak, MR Parsek “The Pel and Psl polysaccharides provide *Pseu-*

- Pseudomonas aeruginosa* structural redundancy within the biofilm matrix.” Environmental Microbiology, 14, 8, 1913-1928 (2012)
- [14] SS Pedersen, N Hoiby, F Espersen, C Koch “Role of alginate in infection with mucoid *Pseudomonas aeruginosa* in cystic fibrosis” Thorax, 47, 6-13 (1992)
- [15] GA O’Toole and R Kolter. “Flagellar and twitching motility are necessary for *Pseudomonas aeruginosa* biofilm development.” Molecular Microbiology, 30, 2, 295-304 (1996)
- [16] J Taktikos, YT Lin, H Stark, N Biais, V Zaburdaev “Pili-Induced Clustering of *N. gonorrhoeae* Bacteria” PLoS ONE, 10, 9, 1-16 (2015)
- [17] D Krishnamurthy and G Subramanian “Collective Motion in a suspension of micro-swimmers that run and tumble and rotatory diffuse” Journal of Fluid Mechanics, 781, 422-466 (2015)
- [18] F Ginelli, F Peruani, M Bar, H Chate “Large-Scale Collective Properties of Self-Propelled Rods” Physical Review Letters, 104, 184502 (2010)
- [19] A Peshkov, IS Aranson, E Bertin, H Chate, F Ginelli “Nonlinear Field Equations for Aligning Self-Propelled Rods” Physical Review Letters, 109, 268701 (2012)
- [20] T Vicsek, A Czirok, E Ben-Jacob, I Cohen, O Shochet “Novel Type of Phase Transition in a System of Self-Driven Particles” Physical Review Letters, 75, 6, 1226-1229 (1995)
- [21] F Peruani, A Deutsch, and M Bar “Non-equilibrium clustering of self-propelled rods” Physical Review E, 74, 030904(R) (2006)
- [22] C Zachreson, C Wolff, C Whitchurch, M Toth “Emergent pattern formation in an interstitial biofilm” Physical Reviews E, 95, 012408 (2017)

- [23] W Ponisch, CA Weber, C Juckeland, N Biais, V Zaburdaev “Multiscale modeling of bacterial colonies: how pili mediate the dynamics of single cells and cellular aggregates” *New Journal of Physics*, 19, 015003 (2017)
- [24] Y Brill-Karniely, F Jin, GCL Wong, D Frenkel, J Dobnikar “Emergence of complex behavior in pili-based motility in early stages of *P. aeruginosa* surface adaptation” *Scientific Reports*, 7, 45467, 1-10 (2017)
- [25] CD Sifri “Quorum Sensing: Bacteria Talk Sense” *Healthcare Epidemiology*, 48, 1070-1076 (2008)
- [26] BK Hammer, BL Bassler “Quorum sensing controls biofilm formation in *Vibrio cholerae*” *Molecular Microbiology*, 50, 1, 101-114 (2003)
- [27] JS Mattick “Type IV Pili and Twitching Motility” *Annual Review of Microbiology*, 56, 289-314 (2002)
- [28] A Be’er, SK Strain, RA Hernandez, E Ben-Jacob, EL Florin “Periodic Reversals in *Paenibacillus dendritiformis* swarming” *Journal of Bacteriology*, 195, 12, 2709-2717 (2013)
- [29] A Ueda, TK Wood “Connecting Quorum Sensing, c-di-GMP, Pel Polysaccharide, and Biofilm Formation in *Pseudomonas aeruginosa* through Tyrosine Phosphatase TpbA (PA3885)” *PLoS Pathogens*, 5, 6, 1-15 (2009)
- [30] GM Patriquin, E Banin, C Gilmour, R Tuchman, EP Greenberg, K Poole “Influence of quorum sensing and iron on twitching motility and biofilm formation in *Pseudomonas aeruginosa*” *Journal of Bacteriology*, 190, 2, 662-671 (2008)
- [31] NC Caiazza, JH Merritt, KM Brothers, and GA O’Toole “Inverse Regulation of Biofilm Formation and Swarming Motility by *Pseudomonas aeruginosa* PA14” *Journal of Bacteriology*, 189, 9, 3603-3612 (2007)

- [32] K Zhao, BS Tseng, B Beckerman, F Jin, ML Gibiansky, JJ HARRISON, E Luijten, MR Parsek, GCL Wong “Psl trails guide exploration and microcolony formation in *Pseudomonas aeruginosa* biofilms” *Nature*, 497, 388-392 (2013)
- [33] GL Hazelbauer, JJ Falke, JS Parkinson “Bacterial chemoreceptors: high-performance signaling in networked arrays” *Trends in Biochemical Science*, 33, 1, 9-19 (2008)
- [34] HH Jeong, SH Lee, JM Kim, HE Kim, YG Kim, JY Yoo, WS Chang, CS Lee “Microfluidic monitoring of *Pseudomonas aeruginosa* chemotaxis under the continuous chemical gradient” *Biosensors and Bioelectronics*, 26, 2, 351-356 (2010)
- [35] JD Nickels, J Atkinson, E Papp-Szabo, C Stanley, S O. Diallo, S Perticaroli, B Baylis, P Mahon, G Ehlers, J Katsaras, JR Dutcher “Structure and Hydration of Highly-Branched, Monodisperse Phytoglycogen Nanoparticles” *Biomacromolecules*, 17, 735-743 (2016)
- [36] PO Powell, MA Sullivan, MC Sweedman, DI Stapleton, J Hasjim, RG Gilbert “Extraction, isolation and characterisation of phytoglycogen from su-1 maize leaves and grain” *Carbohydrate Polymers* 101, 423-431 (2014)
- [37] M Grossutti, C Miki, JR Dutcher “Phytoglycogen Nanoparticles: 1. Key properties relevant to its use as a natural moisturizing ingredient” *Household and Personal Care*, 12, 1, 47-51 (2017)
- [38] T Hamilton “Cornfield of dreams: University of Guelph spinoff Mirexus says its nanosized glycogen particles, isolated in corn, offer a safer and better alternative in a market dogged by controversy” *Canadian Chemical News*, 67.5, 34 (2015)

- [39] R Melendez, E Melendez-Hevia, EI Canela “The Fractal Structure of Glycogen: A Clever Solution to Optimize Cell Metabolism” *Biophysical Journal*, 77, 1327-1332 (1999)
- [40] R Melendez, E Melendez-Hevia, EI Canela “How Did Glycogen Structure Evolve to Satisfy the Requirement for Rapid Mobilization of Glucose? A Problem of Physical Constraints in Structure Building” *Journal of Molecular Evolution*, 45, 446-455 (1996)
- [41] M Grossutti, E Bergmann, B Baylis, JR Dutcher “Equilibrium Swelling, Interstitial Forces, and Water Structuring in Phytoglycogen Nanoparticle Films” *Langmuir*, 33, 2810-2816 (2017)
- [42] PI Hansen, FH Larsen, SM Motawia, A Blennow, M Spraul, P Dvortsak, SB Engelsen “Structure and Hydration of the Amylopectin Trisaccharide Building Blocks - Synthesis, NMR, and Molecular Dynamics”
- [43] BM Sattelle and A Almond “Microsecond kinetics in model single- and double-stranded amylose polymers” *Physical Chemistry Chemical Physics*, 18, 8119, 2014
- [44] E Lindahl “Molecular Dynamics Simulations” *Methods in Molecular Biology Molecular Modeling of Proteins*, 3-26 (2015)
- [45] JA Anderson, CD Lorenz, A Travasset “General purpose molecular dynamics simulations fully implemented on graphics processing units” *Journal of Computational Physics*, 227, 5342-5359 (2008)
- [46] J Glaser, TD Nguyen, JA Anderson, P Liu, F Spiga, JA Millan, DC Morse, SC Glotzer “Strong scaling of general-purpose molecular dynamics simulations on GPUs” *Computer Physics Communications*, 192, 97-107 (2015)

- [47] GW Slater, C Holm, MV Chubynsky, HW de Haan, A Dube, K Grass, OA Hickey, C Kingsburry, D Sean, TN Shendruk, L Zhan “Modeling the separation of macromolecules: A review of current computer simulation methods” *Electrophoresis*, 30, 792-818 (2009)
- [48] GS Grest, K Kremer “Molecular dynamics simulation for polymers in the presence of a heat bath” *Physical Review A*, 33, 3628 (1986)
- [49] JD Weeks, D Chandler, HC Andersen “Role of Repulsive Forces in Determining the Equilibrium Structure of Simple Liquids” *Journal of Chemical Biophysics*, 54, 5237-5247 (1971)
- [50] A Einstein “ber die von der molekularkinetischen Theorie der Wrme geforderte Bewegung von in ruhenden Flssigkeiten suspendierten Teilchen” *Annalen der Physik*, 32, 8, 549-560 (1905)
- [51] R Salomon-Ferrer, DA Case, RC Walker “An overview of the Amber biomolecular simulation package” *WIREs Computational Molecular Science* 1-13 (2012)
- [52] MA Gonzalez “Force fields and molecular dynamics simulations” *Collection SFN*, 12, 169-200 (2011)
- [53] KN Kirschner, AB Yongye, SM Tschampel, J Gonzalez-Outerino, CR Daniels, BL Foley, RJ Woods “GLYCAM06: A Generalizable Biomolecular Force Field. Carbohydrates” *J Computational Chemistry*, 29, 4, 622-655 (2008)
- [54] Woods Group. (2005-2018) GLYCAM Web. Complex Carbohydrate Research Center, University of Georgia, Athens, GA. (<http://glycam.org>)

- [55] P Mark, L Nilsson “Structure and Dynamics of the TIP3P, SPC, and SPC/E Water Models at 298 K” *Journal of Physical Chemistry*, 105, 9954-9960 (2001)
- [56] HM Berman, J Westbrook, Z Feng, G Gilliland, TN Bhat, H Weissig, IN Shindyalov, PE Bourne “The Protein Data Bank” *Nucleic Acids Research*, 28: 235-242 (2000)
- [57] R Balagam, OA Igoshin “Mechanism for collective cell alignment in *Myxococcus xanthus* bacteria” *PLOS Computational Biology*, 11, 8, 1-20 (2015)
- [58] HW Lu, LM Zhang, C Wang, RF Chen “Preparation and properties of new micellar drug carriers based on hydrophobically modified amylopectin” *Carbohydrate Polymers*, 83, 4, 1499-1506 (2011)
- [59] D Zeng, J Fan, Z Deng, J Tan, Z Deng, LM Zhang, L Yang “One-step synthesis of amphiphilic hyperbranched amylopectin derivatives, characterization and use as functional nanovehicles” *Carbohydrate Polymers*, 98, 1, 905-913 (2013)